EVALUATION OF INFLAMMATION AND MORPHOMETRIC PARAMETERS ASSOCIATED WITH NEURAL DEVICE IMPLANTATION IN THE SCIATIC NERVE

by

Michael Benjamin Christensen

A dissertation submitted to the faculty of
The University of Utah
in partial fulfillment of the requirements for the degree of

Doctor of Philosophy

Department of Bioengineering

University of Utah

May 2011

The Graduate School
THE UNIVERSITY OF UTAH

STATEMENT OF DISSERTATION APPROVAL

The dissertation of Michael Benjamin Christensen
has been approved by the following supervisory committee members:

Patrick A Tresco , Chair	3/17/2011 Date Approved
Richard A Normann , Member	3/17/2011 Date Approved
Vladimir Hlady , Member	3/17/2011 Date Approved
Robert Hitchcock , Member	3/17/2011 Date Approved
Bradley Greger , Member	3/17/2011 Date Approved
Marshall Smith , Member	3/17/2011 Date Approved

and by Patrick A Tresco, Chair of the Department of Bioengineering

and by Charles A. Wight, Dean of The Graduate School

ABSTRACT

Peripheral nerve electrodes offer the potential to record and stimulate nerve fibers for the control of neuroprosthetic devices or for functional electrical stimulation. For example, nerve cuff electrodes have been successfully used in clinical applications such as sacral nerve stimulation for the treatment of bladder incontinence and peroneal nerve stimulation for the treatment of foot drop. While nerve cuff electrodes function in these applications where broad stimulation of the nerve is suitable, specific recording and stimulation of small groups of nerve fibers is only possible through the use of more invasive electrodes. However, such electrodes elicit a foreign body response which can include the recruitment of macrophages to the device interface and changes in morphometric parameters in the implanted nerve which could negatively affect the performance of the electrodes. Here, we investigated the foreign body response to chronically implanted axially penetrating arrays and their associated encapsulation cuffs, as well as encapsulating cuffs in the absence of a penetrating array, in sciatic nerve. Additionally, we investigated the validity of the commonly used method of using the contralateral nerve as an internal control to an ipsilateral procedure. We found that the implantation of axially penetrating arrays and their associated cuffs elicits an inflammatory reaction, including the recruitment of macrophages to the electrode and cuff interfaces, which is accompanied by morphometric changes in the implanted nerve, similar to other penetrating arrays. Additionally, we found that the implantation of nerve

cuffs alone elicited a similar reaction which was exacerbated when using an open mesh design. These studies establish a baseline measurement of the inflammatory response to axially penetrating arrays and their associated cuffs which can be used when considering future designs. These studies also suggest that the role of encapsulating cuffs in the inflammatory response to devices which contain both a cuff and a penetrating electrode needs to be further elucidated. We also found that naturally occurring difference in morphometric parameters do exists based on nerve location, and that ipsilateral procedures can cause changes in contralateral morphometric parameters compared with naïve controls, suggesting that the use of contralateral nerves as internal controls is inappropriate.

TABLE OF CONTENTS

LIST OF FIGURES

LIST OF TABLES

LIST OF ABBREVIATIONS

Defining Term	Abbreviation
4', 6-diamidino-2-phenylindole dihydrochloride	DAPI
Analysis of variance	ANOVA
Autonomic nervous system	ANS
Blood-nerve-barrier	BNB
Brain-derived neurotrophic factor	BDNF
Central nervous system	CNS
Ciliary neurotrophic factor	CNTF
Deep brain stimulator	DBS
Electron microscopy	EM
Extracellular matrix	ECM
Flat interface nerve electrodes	FINE
Immunohistochemistry	IHC
Institutional animal care and use committee	IACUC
Interferon-γ	IFNγ
Interleukin-1	IL-1
Interleukin-6	IL-6
Interleukin-10	IL-10
Interleukin-12	IL-12

Interleukin-18 ..... IL-18

Leukemia inhibitory factor ..... LIF

Lipopolysaccharide ..... LPS

Longitudinal Intrafascicular electrode ..... LIFE

Nerve growth factor ..... NGF

Peripheral nervous system ..... PNS

Phosphate-buffered saline ..... PBS

Scanning electron microscope ..... SEM

Sprague-Dawley ..... SD

Standard deviation ..... stdev

Standard error of the mean ..... SEM

Transmission electron microscope ..... TEM

Transforming growth factor-beta ..... TGF-β

Tumor necrosis factor-alpha ..... TNF-α

Utah electrode array ..... UEA

Utah slant electrode array ..... USEA

ACKNOWLEDGEMENTS

I would like to express my appreciation to my advisor, Dr. Patrick Tresco, for giving me the chance to come into his lab and for providing me with mentoring and learning opportunities and financial support during my time at the University. I would also like to thank my committee, Drs. Bradley Greger, Robert Hitchcock, Vladimir Hlady, and Richard Normann, for providing collaborative research opportunities, input, and support. I also wish to thank those outside of my lab who provided opportunities for, or assisted with, my research including Dr. Greg Clark, Dr. David Warren, Noah Ledbetter, Creighton Petty, Eric Gibbons, and the staff at the electron microscopy core facility. Additionally, I would like to thank members of the Keck Center for Tissue Engineering for providing support and input on my research including Dr. Brent Winslow, Dr. Mike Bridge, Dr. Braden Leung, Dr. Jeff Wolchok, Dr. Xiaoyu Chen, Elena Budko, John Skousen, Fan-Wei Meng, Stewart Yeoh, and the many undergraduates who have come through the lab, particularly Serena Pearce. Finally, I would like to thank my family, especially my wife Andrea, for their support and encouragement during my schooling.

CHAPTER 1

INTRODUCTION

A Brief Review of General Peripheral Nerve Anatomy

A basic understanding of the anatomy of the peripheral nervous system (PNS) is necessary in order to describe changes that may take place therein. Fibers of the PNS can be classified in many ways, but the most common classification places fibers into one of two categories: myelinated and unmyelinated. Myelinated fibers include alpha and gamma motor fibers, which control muscle contraction and regulate the gain of the stretch reflex, respectively, and Aα, Aβ, and Aδ sensory fibers, which provide feedback on muscle length and tension and are sensitive to cold and pressure information. Myelinated fibers range in diameter from 1-20 μm. A single Schwann cell will wrap the axon of only one of these fibers with a composition of cholesterol, phospholipids, glycolipids, and proteins [1-3] termed myelin which acts as an electrical insulator and allows faster propagation of action potentials down the axon. Occasionally, part of the Schwann cell cytoplasm will become trapped in the inner layers of the myelin sheath during the myelination process forming pockets of cytoplasm termed Schmidt-Lanterman incisures (Figure 1-1:A). The distance over which the myelin sheath from a single Schwann cell extends along an axon is approximately proportional to the diameter of the fiber in a ratio that has been reported to be between 1:60 and 1:100 [4-6]. The space

between myelin sections, which is approximately 0.3 μm in length, is termed the Node of Ranvier (Figure 1-1:B), named after Louis-Antoine Ranvier who first described such interruptions in 1871 [7]. Conduction velocities in these myelinated fibers, which were first tested by Herman von Helmholtz in 1850 [8], range between 4-120 m/s[9-12]. The conduction speed in these fibers depends on the diameter of the axon, the thickness of the myelin, and the distance between nodes [13]. However, in normal mammalian nerves, the myelin thickness and the internode distance are both proportional to the axon diameter, thus making the axon diameter the main determinant of conduction velocity.

Unmyelinated fibers include C sensory fibers and some fibers of the autonomic nervous system (ANS). A single Schwann cell will normally encompass 1-20 of these fibers within its cytoplasm in formations called Remak bundles (Figure 1-1:C), being named after Roberto Remak who first described unmyelinated fibers in 1838 [14]. These fibers are generally between 0.2-2 μm in diameter [15-17] and have conduction velocities in the range of 0.5-2.5 m/s [9, 16, 18]. In mixed nerves, such as the sciatic nerve and its major branches, a combination of myelinated and unmyelinated fibers exists. However, because of their small size, unmyelinated fibers are unable to be effectively resolved using light microscopy and must be imaged using electron microscopy. Since the majority of the different classes of fibers (Aα, Aβ, Aδ, and Aγ) are myelinated and easily resolved using light microscopy, the remainder of this dissertation will focus solely on myelinated fibers.

Individual nerve fibers are bundled together in formations termed fascicles, which are surrounded by 4-10 concentric layers of modified fibroblasts [19-21] connected via tight junctions [19], termed the perineurium, which provides a diffusion barrier between

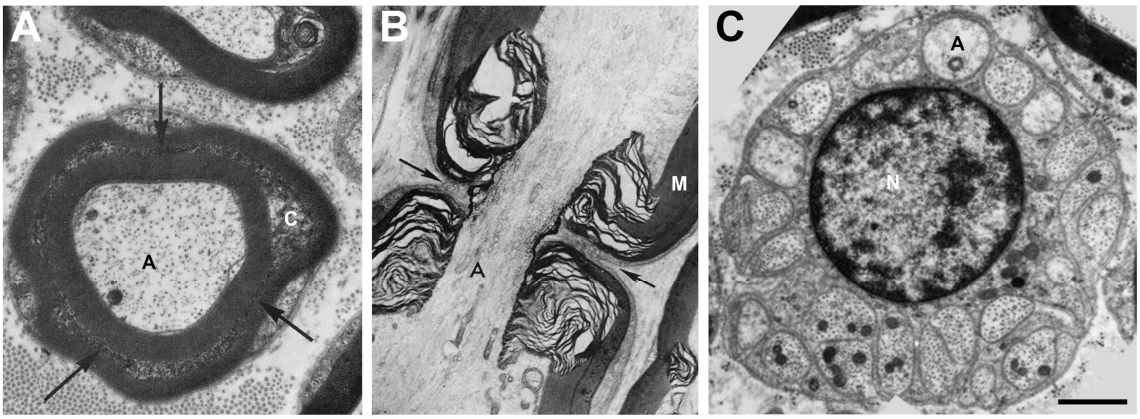

Figure 1-1: Features of the PNS shown using transmission electron microscopy (TEM). **A)** Micrograph showing a Schmidt-Lanterman incisure around a myelinated axon (A). These formations are caused by the entrapment of Schwann cell cytoplasm (C) within the myelin lamella. Adapted from Schroder [22]. **B)** TEM image of a Node of Ranvier (arrows). The Schwann cell myelin (M) will branch into finger-like projections near the node, leaving only about 0.3 µm of the axon (A) unmyelinated. Adapted from Waxman [23]. **C)** An example of a Remak bundle. A single Schwann cell (N) will encompass between 1-20 unmyelinated axons (A) within its cytoplasm. Adapted from Murinson et al. [24].

the epineurial and endoneurial spaces [25-27] and maintains a hypertonic environment within the fascicle [28] which facilitates conduction. The number of fascicles contained within a nerve can vary between one and several dozen. Types I and III collagen compose the connective tissue space within the fascicles, termed the endoneurium, endoneurial space, or intrafasciclular space, although type III collagen is the more predominant collagen present [21, 29-31]. Type I collagen is the main constituent of the connective tissue space outside of the fascicles [21, 29-31], termed the epineurium, epineurial space, or interfascicular space (Figure 1-2:A-C).

The Sciatic Nerve

The sciatic nerve, which will be the nerve of focus in this dissertation, is the largest peripheral nerve in the body. The sciatic nerve originates from the fourth lumbar

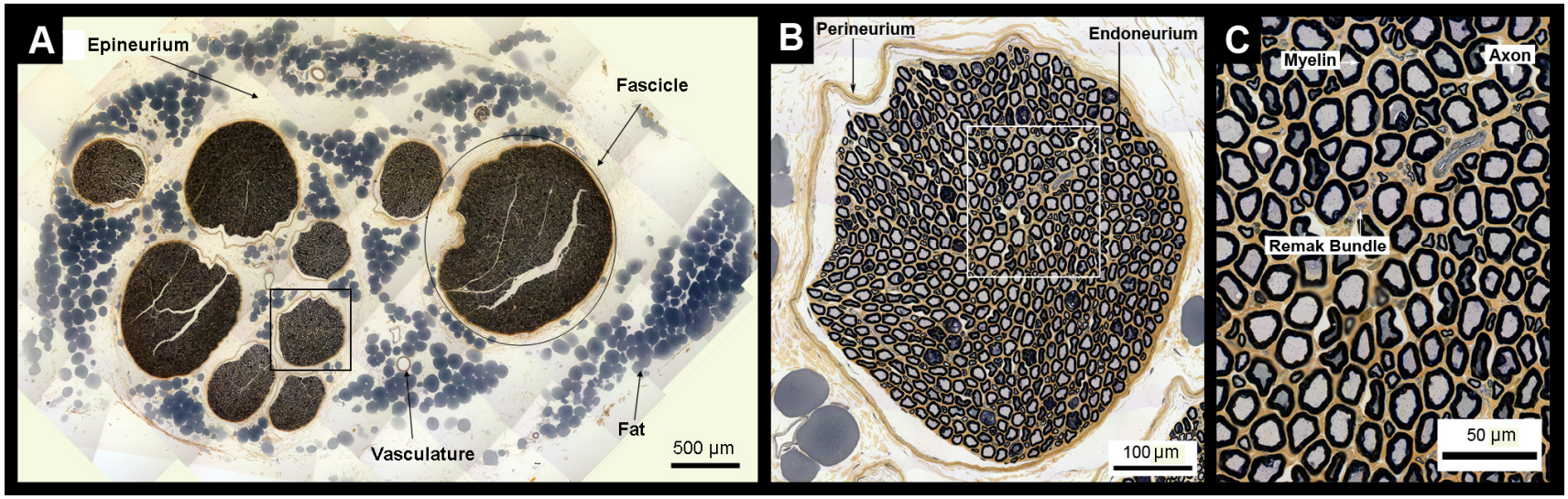

Figure 1-2: Anatomical terminology in peripheral nerves. **A)** Microscopic image of a complete cross-section of a nonimplanted cat sciatic nerve. Individual nerve fibers are bundled together to from fascicles, which are surrounded by several layers of modified fibroblasts, termed the perineurium, which creates a diffusion barrier between the intrafascicular and interfascicular spaces. The connective tissue space outside of the fascicles is termed the epineurium and is composed primarily of type I collagen. Evidence of blood vasculature and fatty deposits is also visible. **B)** Higher magnification view of boxed fascicle in A. The perineurium is more clearly visible at this magnification. The connective tissue space inside the fascicle, in between individual nerve fibers, is termed the endoneurium and is composed primarily of type III collagen. **C)** Higher magnification view from B showing individual nerve fibers. Myelinated nerve fibers are composed of the nerve axon and the surrounding myelin, which is generated by Schwann cells. Unmyelinated axons are grouped together and encased in the cytoplasm of a Schwann cell in a formation termed a Remak bundle.

segment to the second sacral segment [32, 33], leaves the pelvic area through the greater sciatic foramen, and descends under the cover of the gluteous maximus. The nerve then bifurcates into the tibial and common peroneal branches, typically behind the knee. The sciatic nerve and its tributary nerves innervate nearly all of the skin in the leg as well as the hamstring muscles in the upper leg and the muscles of the lower leg and foot. Because of its size and relative ease of accessibility, the sciatic nerve is commonly used in peripheral nerve studies.

The gross organization of the sciatic nerve varies widely depending on species and location. Rat sciatic nerves have been reported to be unifascicular in nature until splitting into distinguishable peroneal and tibial components just distal to the head of the femur [33], and contain between 6300-8500 myelinated fibers [33-41]. Cat sciatic nerves have been reported to contain between 4-28 fascicles before splitting into the peroneal and tibial branches [32] and contain 16000-21000 myelinated fibers [42, 43]. The number of fascicles in the human sciatic nerve is highly variable, with a range of 27-70 fascicles based on a limited number of samples [44]. The number of myelinated axons in the human sciatic nerve is not documented.

Peripheral Nerve Changes Following Traumatic Injury

In order to understand the changes that occur following the implantation of peripheral nerve electrodes, it is important to have a basic understanding of the common events that take place in peripheral nerves following injury. Some of these changes, such as those which occur in myelinated nerve fibers, Schwann cells, and macrophages, are detailed below. All of the following information from the literature has been obtained

from experiments using crush or transection models without the presence of a foreign material.

Nerve Fibers

Distal degeneration of axons and their associated myelin, as well as the infiltration of phagocytic cells, are the hallmark events following nerve injury. This degeneration of nerve fibers was first described by Augustus Waller in 1850 [45] and has been hence termed Wallerian Degeneration. Changes in nerve fibers distal to a traumatic injury, such as a crush or transection injury, have been observed as early as 2 minutes after injury. These changes include the retraction of myelin in the paranodal regions and the dilation of Schmidt-Lanterman incisures (Figure 1-3:A). These changes occur more rapidly in smaller axons [46].

Calcium dependant axonal breakdown also occurs rapidly following traumatic nerve injury [47]. Accumulation of mitochondria in the axon, associated with the fragmentation of neurofilaments and neurotubules, has been observed as early as 12-24 hours postinjury [48-50]. Axonal degradation is completed by about the 6^{th} day following injury [50]. Degeneration of the myelin sheath starts shortly after axonal degradation, beginning at about 24 hours postinjury [48, 49, 51] and has typically been completed within several months [52]. Since myelin degradation takes longer than axonal degradation, collapse of the myelin sheath is often observed after injury (Figure 1-3:B). Early signs of myelin degradation include the splitting of myelin lamellae and the formation of myelin ovoids (Figure 1-3:C). The process of myelin degradation by phagocytic cells is discussed in further detail below.

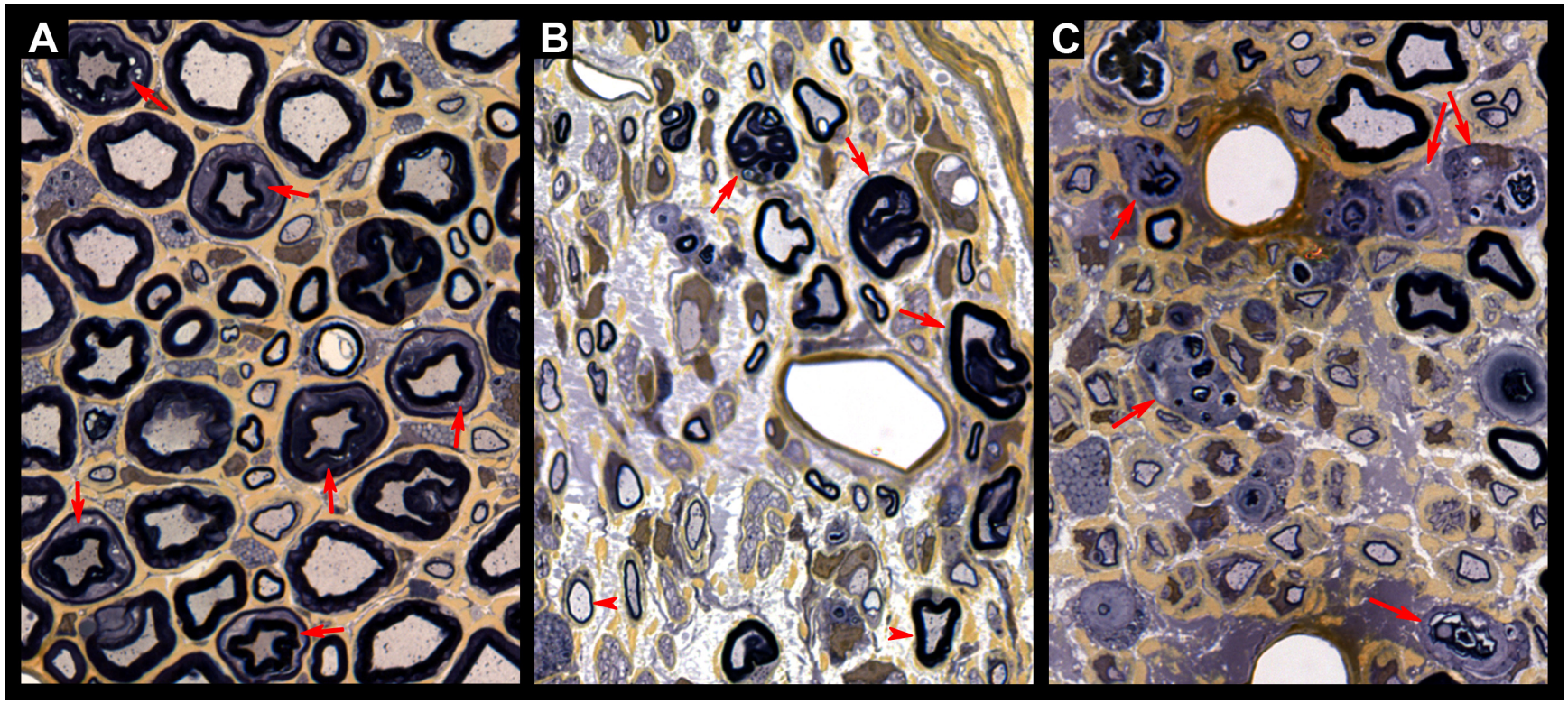

Figure 1-3: Signs of Wallerian degeneration. **A)** One of the early indications of Wallerian degeneration is the dilation of Schmidt-Lanterman incisures (arrows). **B)** Axonal degradation is also an early indicator of Wallerian degeneration. Because axons are degraded more quickly than myelin, myelin collapse is often observed (arrows). Following axon and myelin degradation, axons begin to regenerate. However, myelination around these axons is often much thinner than normally observed (compare arrowheads). **C)** Myelin clearance is primarily accomplished though infiltrating macrophages which can take up to several months to completely clear the myelin debris (arrows).

Axonal regeneration starts within days after injury. During the process of regeneration, axons will produce multiple collateral sprouts in an attempt to reinervate their distal targets [53]. Once one of these sprouts reaches an appropriate target, the other collateral sprouts will be pruned [54]. This arborization can lead to significant increases in the number of myelinated fibers found distal to an injury for several months [55-57]. The rate of elongation of regenerating axons has been shown to be faster in crush (3.2 mm/day) than transection (2.5 mm/day) injuries [12], likely due to the retention of integrity of Schwann cell basal lamina tubes following crush but not transection injuries, which help direct regenerating axons.

Following the start of the regeneration of axonal processes, Schwann cells will begin to remyelinate. Degenerated myelin components, primarily cholesterol, that were phagocytosed have been shown to be reused when new myelin sheaths are deposited around these regenerating axons [58]. This reuse of myelin cholesterol is regulated through the generation of apolipoprotein E which is produced by infiltrating macrophages [59]. However, due to the proliferation of Schwann cells following injury, the internodal spacing in these regenerated axons becomes a fairly constant 300 μm, rather than being proportional to the axon size [4]. Newly deposited myelin is also often thinner than what would normally be found (Figure 1-3:B).

Schwann Cells

For many years there was debate in the scientific community as to the origin of cells which clearly were participating in the breakdown of myelin at early time points after injury. Only in the last 30 years have scientists been able to identify these cells as resident Schwann cells [49, 60, 61]. It is now clear that, following injury, Schwann cells

will fragment their own myelin into ovoids as well as consume small whorls of myelin debris [62]. These myelin fragments are identifiable in vacuoles contained in the Schwann cell cytoplasm [51].

Starting 2-4 days postinjury, Schwann cells will also undergo active mitosis [49, 63, 64]. Divided cells will line up within the basal lamina tubes to form bands of Bünger which later provide guidance cues to regenerating fibers [65]. The increase in Schwann cell number following division also leads to decreased internode spacing on regenerated fibers as mentioned above [4].

In addition to early phagocytic and later remyelination roles, Schwann cells are also known to produce a number of trophic factors. These including nerve growth factor (NGF) [66], brain-derived neurotrophic factor (BDNF) [67], ciliary neurotrophic factor (CNTF) [68], and leukemia inhibitory factor (LIF) [69], which all have roles in promoting neuronal survival and outgrowth [70], as well as interleukin-1 (IL-1) [62] which acts primarily as a proinflammatory cytokine, but which also promotes NGF production [71, 72], interleukin-6 (IL-6) [73] which both promotes survival and outgrowth of neurons and acts as a proinflammatory cytokine [74, 75], and interleukin-10 (IL-10) [62] which is a broad spectrum inhibitor of other cytokines including IL-1, IL-6, interleukin-12 (IL-12), interleukin-18 (IL-18), and tumor necrosis factor-alpha (TNF-α) [76].

Macrophages

While endogenous macrophages do exist in the normal endoneurial space, they make up only 2-4% of the total cellular population in that compartment [77] and are not the primary phagocytic cells after nerve injury. Instead, the vast majority of

macrophages involved in the degenerative process are of hematogenous origin [78-81]. These cells, however, are relatively slow to infiltrate the damaged nerve. Previous studies have found that infiltration of hematogenous macrophages is not significant until 2-4 days postinjury [49, 82-84], after which time numbers continue to increase until a peak presence 2 weeks after injury [60, 83, 84]. Macrophages continue to phagocytose myelin until the debris has been cleared, a process which typically takes several months [85].

Macrophages have also been implicated in the increased production of several different cytokines following nerve injury. These include IL-1, IL-12 and IL-18 which all promote interferon-γ (IFNγ) production [86, 87], and IFNγ and TNF-α which are potent proinflammatory cytokines [62, 88-90].

Permeability Changes

In addition to the changes described above, several other notable changes have been observed and reported in the literature. One such change is the breakdown of the perineurium, allowing the diffusion of molecules or tracers into the endoneurium which would not normally be able to penetrate [27, 91]. This occurs even when the nerve is not transected. Blood vessel luminal perimeters also significantly increase following crush injury for at least 6 weeks [92]. Additionally, endoneurial vessel permeability increases following injury [93, 94], likely due to active trafficking of phagocytic cells. Interestingly, it has also been observed that endoneurial vessel permeability increases in the unoperated contralateral nerve following unilateral nerve transection [94].

A Note on Morphometric Parameters

Because the process of Wallerian degeneration and regeneration is difficult to quantify, it is helpful to employ the use of morphometric parameters. A number of parameters may be measured to aid researchers in understanding the degree to which changes in the nerve are occurring. These parameters include the total fascicular area, total myelinated fiber count, myelinated fiber density, fiber packing (the percent of the fascicular area occupied by fibers), g-ratio (the ratio of the axon diameter to the fiber diameter which includes both the axon and the myelin), and fiber diameter. Quantification of these parameters allows researchers to provide an unbiased comparison between injured or implanted and naïve nerves. Therefore, many reports, particularly in recent years, have made an effort to incorporate such quantification in their analysis.

Peripheral Nerve Electrode Applications

Microelectrode arrays implanted into the PNS offer the potential to record from and stimulate nervous tissue for the control of neuroprosthetic devices or for functional electrical stimulation. These arrays vary in design and include devices such as multilead cuff electrodes, sieve or regenerating electrodes, multilead single shank electrodes, and multishank electrodes (Figure 1-4:A-D). Such devices have found clinical use in respiratory pacing [95-98], sacral root stimulators for the treatment of bladder incontinence [99-101], and peroneal nerve stimulators for the treatment of foot drop [102-104]. In addition to these current clinical applications, PNS electrodes have the potential for use in neuroprosthetic control. According to Owings and Kozak, in the United States an estimated 185,000 amputations are performed each year [105]. This has

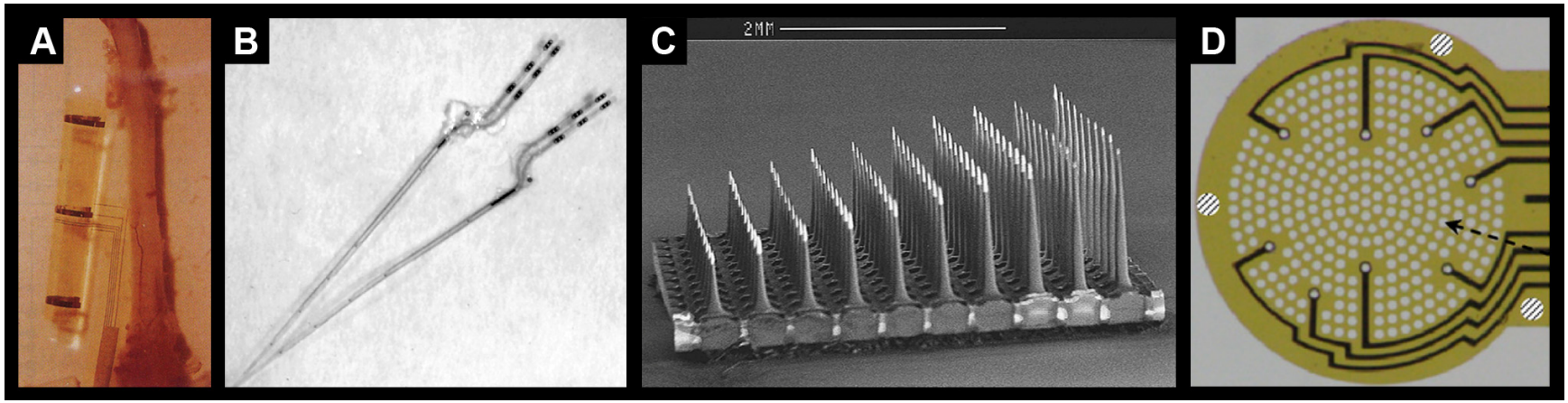

Figure 1-4: Examples of the different types of peripheral nerve electrodes. **A)** Example of a cuff electrode which wraps around the nerve and does not cause a penetrating injury. They are typically composed of silicone rubber. Several adaptations of cuff electrodes exist including cuffs that spiral around the nerve rather than encapsulate it (helical electrodes) and those that attempt to increase electrical selectivity by flattening or reshaping the nerve (flat interface nerve electrodes or FINEs). Adapted from Rodriguez et al. [41]. **B)** Example of longitudinal intrafascicular electrodes (LIFEs) which are implanted into single fascicles. Adapted from Lago et al. [39]. **C)** Example of a Utah Slant Electrode Array (USEA). These arrays typically contain a 10x10 arrangement of tines with rows ranging in length from 0.6-1.5 mm and are modifications of the Utah Electrode Array (UEA) which is used more frequently in cortical applications. Adapted from Branner et al. [106]. **D)** Example of a sieve or regenerative electrode. These electrodes are placed in an encapsulating tube, typically made of silicone, which is placed between the two ends of a transected nerve. The principle is that regenerating nerve fibers will then grow through the sieve or via holes placed in the electrode. Adapted from Kim et al. [107].

resulted in a current population of amputees estimated to be around 1.6 million and which is expected to double by 2050 [108]. Of the current amputee population, 664,000 represent major limb amputations (i.e., other than toes or fingers) [108]. One recent source of such major limb amputations has been the wars in Iraq and Afghanistan where, from a period of 2001-2005, there were approximately 400 military personnel who underwent major limb amputation [109, 110]. Such individuals as these could obviously benefit from the development of neuroprosthetic devices which could restore lost limb function.

While cuff electrodes have typically been used for clinical PNS stimulation, these applications require only nonspecific stimulation of the implanted nerve to achieve the desired results. This all or nothing stimulation does not provide the selectivity necessary for fine control of a neuroprosthetic device. Further, current clinical cuff electrode uses are limited to small nerves compared with those that would likely be used in neuroprosthetic applications. The control of neuroprosthetic devices would likely require implantation around a large, multifascicular mixed nerve such as the median, ulnar, or radial nerves in the upper arm or the sciatic nerve in the leg. Therefore, cuff electrodes might not be the ideal choice for some forms of neuroprosthetic control due to their lack of specificity. This issue may be overcome by using penetrating electrode arrays [106].

Histological Response to PNS Electrode

The definition of biocompatibility is "the ability of a material to perform with an appropriate host response in a specific application" [111]. Therefore, in order to evaluate the biocompatibility of potential peripheral nerve electrodes, not only is an understanding of the device's electrophysiological capabilities and limitations essential, but also an

understanding of the inflammatory reaction accompanying the chronic implantation of that device must be obtained. Additionally, in the case of penetrating arrays, knowledge of the foreign body reaction to an encapsulating cuff which may be used to hold the electrode in place is necessary. While the electrophysiological properties of peripheral nerve electrodes will not be reviewed here, a review of the foreign body response to such devices is discussed below.

Cuff Electrodes

Cuff style electrodes have been used in peripheral neuroprosthetic applications since the late 1940s when Whittenberg et al. stimulated the phrenic nerve to assist in diaphragm pacing [112]. Since cuff electrodes have been under investigation for a longer period of time than penetrating electrodes, the tissue response to cuff electrodes has been relatively well studied, although the number of reports describing histology is still limited compared to the volume of literature describing central nervous system (CNS) implants. An outline of the specific findings of individual studies is included in Table 1-1. In general, cuff electrodes have most commonly been associated with fibrous connective tissue encapsulation containing inflammatory cells, predominantly at the biotic-abiotic interface. Many early papers containing quantitative analysis also observed morphometric changes in the implanted nerves including decreases in fiber densities and shifts in fiber diameter distributions toward smaller fibers, although these changes have not been observed in more recent reports. Of note in these studies is that the majority use silicone as the cuff material, and only one paper uses a device that is not a solid cuff. Therefore, the potential effect of material composition and design on the inflammatory response has not been well studied and needs to be further investigated.

Table 1-1: The histological response to nerve cuff electrodes

Author Year [Ref.]	Species	Cuff Type	Qualitative Observations	Quantitative Observations
Waters 1975 [113]	Human	Solid silicone	Fibrous connective tissue surrounding implanted cuff	Implanted nerves had a lower fiber density and shifted fiber diameter distributions compared to control nerves, although changes were stated as nonsignificant
Kim 1976 [95]	Human	Solid silicone	Fibrous connective tissue surrounding implanted cuff Epineurial macrophages were observed beneath the cuffs	None taken
McNeal 1977 [102]	Human	Solid silicone	Occasional excessive inflammatory reaction including endoneurial and epineurial fibrosis Fibrotic tissue surrounding all evaluated electrodes Myelinated nerves and perineurium appeared normal	None taken
Picaza 1977 [114]	Human	Solid silicone	Inflammatory reaction and fibrosis were observed around implanted cuffs Note – only cuffs that were removed because of pain or discomfort were analyzed	None taken
Stein 1977 [115]	Cat	Solid silicone	Nerves implanted with cuffs appeared to have a decreased axonal density No gross signs of inflammation were noted, although occasional polymorphonuclear leukocytes were observed using EM	Fiber diameter distributions suggest a loss of large diameter fibers compared with controls, although a statistical analysis was not performed

Table 1-1: cont

Author Year [Ref.]	Species	Cuff Type	Qualitative Observations	Quantitative Observations
Rosenkranz 1986 [116]	Rat	Solid silicone	Increased endoneurial connective tissue was observed in implanted nerves Alterations in nerve structure were observed in implanted nerves, but the nature of these alterations is not addressed	None taken
Krarup 1988 [117]	Cat	Solid silicone	Inferred from conduction velocities that implanted nerves had a slight loss of large fibers	30% lower fiber density in implanted nerves
Naples 1988 [118]	Cat	Solid silicone	All cuffs were covered in fibrous connective tissue consisting of polymorphonuclear leukocytes, and occasional monocytes Axon diameters and myelin thickness appeared normal There appeared to be a slight increase in endoneurial connective tissue	None taken
Agnew 1989 [119]	Cat	Helical (3-7 turns) silicone	All nerve cuffs were encapsulated in connective tissue containing collagen and mononuclear cells Occasionally observed degeneration of myelinated fibers	None taken
Jellema 1995 [120]	Rat	Solid polyether rubber	Deterioration of fibers was not observed up to 30hrs after implantation	Shifts in fiber diameter distributions toward small diameter fibers

Table 1-1: cont

Author Year [Ref.]	Species	Cuff Type	Qualitative Observations	Quantitative Observations
Walter 1995 [121]	Cat	Solid Teflon	Connective tissue was observed around all cuffs Cross-sections from implanted nerves appeared normal	No differences were detected in fiber diameter distributions from implanted nerves
Loeb 1996 [122]	Cat	Solid silicone	Connective tissue was observed encapsulating the implanted cuffs	None taken
Larsen 1998 [123]	Rabbit	Solid silicone	Epineurial and perineurial fibrosis was observed underneath all cuffs Axonal degeneration was evident beneath and distal to the cuff	Significant loss of myelinated fibers beneath and distal to the cuff at 2 weeks but not 16 months Mean axons areas did not change The largest 20% of fibers never regained their original size
Agnew 1999 [124]	Cat	Helical silicone	Nerve fibers appeared normal	G-ratio plots are presented and do not appear different than controls, but no statistical test is reported
Rodriguez 2000 [41]	Rat	Solid polyimide	All cuffs covered in fibrous tissue	No differences detected between implanted and contralateral nerves for cross-sectional area, fiber count, fiber density, mean g-ratio, mean fiber diameter, or fiber diameter distributions

Table 1-1: cont

Author Year [Ref.]	Species	Cuff Type	Qualitative Observations	Quantitative Observations
Grill 2000 [125]	Cat	Solid silicone	All cuffs were covered in fibrous tissue which included fibroblasts, macrophages, and polymorphonuclear leukocytes Changes at or distal to the cuff, including perineurial thickening, reduced fiber density, and thinly myelinated fibers, were observed in some animals	None taken
Romero 2001 [43]	Cat	Solid silicone	All cuffs were covered in fibrous tissue Fibrous tissue was also observed in the epineurium, near the electrode surface In some animals this layer contained macrophages No evidence of damage to nerve fibers was observed	Fascicular areas, fibers counts, and fiber diameter and myelin thickness distributions did not differ between implanted nerves and controls
Tyler 2003 [126]	Rat	FINE – unspecified material	Three sizes of FINEs were implanted, flattening the nerve to different degrees The largest FINE elicited no observable changes in axon density or myelin thickness, while the other two designs showed marked decreases in both parameters	The largest FINEs showed no increase in BNB permeability, while the other two designs showed significant increases in BNB dysfunction
Vince 2005 [127]	Rat	Solid silicone	All cuffs were covered with fibrous tissue Epineurial thickening with an inflammatory component was present at the nerve/cuff interface (used IHC)	CD68+ cells were significantly increased after cuff implantation at 7 days, but returned to control levels by 30 days

Table 1-1: cont

Author Year [Ref.]	Species	Cuff Type	Qualitative Observations	Quantitative Observations
Vince 2005 [128]	Rat	Solid silicone	All cuffs were covered with fibrous tissue Epineurial thickening with an inflammatory component was present at the nerve/cuff interface (used IHC)	TNF-α and TGF-β were significantly increased in nerve implanted with cuffs
Leventhal 2006 [42]	Cat	FINE – solid silicone	In general, no observable differences in myelin thickness, fiber diameters, or fiber densities were found	No differences were detected in fiber numbers of densities
Thil 2007 [129]	Rat	Solid silicone	Epineurial thickening was present under all implanted cuffs and consisted of macrophages, mast cells, and polymorphonuclear cells Evidence of axonal degeneration was sometimes noted in the peripheral areas of the fascicles	Epineurial area was significantly increased in implanted nerves The number and area of blood vessels was not increased in the endoneurium, but were significantly increase in the epineurium at 2 and 7 days, but not at 30 days

LIFEs

Penetrating electrodes offer increased selectivity over cuff electrodes, but generally lead to increased morphologic changes in the implanted nerve. One such penetrating array is the LIFE, which is implanted in a longitudinal orientation within a fascicle of a nerve. While these electrodes offer higher specificity than cuff electrodes due to their close approximation to nerve fibers, the fact that they run longitudinally means that they are still interacting with a limited number of fibers within the nerve. The histological findings of nerves implanted with LIFEs are listed in Table 1-2. In general, LIFEs are surrounded by a layer of endoneurial connective tissue that has sometimes been found to contain macrophages. A decrease in axonal density and axon size is frequently observed in the area immediately surrounding the electrode, although whole nerve changes are not often observed.

Sieve Electrodes

Sieve electrodes, also called regenerating electrodes, are highly selective and highly invasive and have been investigated since the late 1960s [130]. They are implanted into a nerve by transecting the nerve, placing the electrode between the transected ends, and suturing the ends of the nerve into a regeneration tube, typically composed of silicone. Regenerating fibers then grow through via holes which can have electrodes built into them. The histological responses to this type of electrode are listed in Table 1-2. It should be considered when evaluating this table that the design of these devices, including the number, size, and spacing of via holes, rarely remains constant between reports. Generally, the silicone tube used to guide regeneration of fibers through the electrode is covered with connective tissue. As expected with transected nerves

Table 1-2: The histological response to penetrating peripheral nerve electrodes

Author Year [Ref.]	Species	Electrode Type	Qualitative Observations	Quantitative Observations
Bowman 1985 [131]	Rabbit	Interfascicular coiled wire	Generally, no histological abnormalities were detected proximal or distal to the implant At the implant site, slight connective tissue infiltration and focal demyelination in the area of the electrode were observed	None taken
Malagodi 1989 [132]	Cat	LIFE	No observable changes in nerve organization after acute implantation	None taken
Lefurge 1991 [133]	Cat	LIFE	A connective tissue layer around the electrode was observed which contained multinucleate giant cells but no evidence of actively phagocytic cells The endoneurium around the electrode showed increased connective tissue and a decrease in axon density, size, and myelin thickness	Mean myelinated axon diameter measurements were statistically lower at the implant site than controls, but not at proximal and distal sites
Tyler 1997 [134]	Cat	Interfascicular penetrating silicone cuff	Myelination and axon density appear normal around the implant after acute time periods	None taken

Table 1-2: cont

Author Year [Ref.]	Species	Electrode Type	Qualitative Observations	Quantitative Observations
Malmstrom 1998 [135]	Cat	LIFE	Implanted electrodes were encapsulated by connective tissue Axon density appeared to be reduced in the region surrounding the electrodes	Electrodes implanted with associated cuffs demonstrated a significant shift in axon diameter distributions toward smaller fibers at and distal to the implant, but not proximal to the implant Electrodes implanted without an associated cuff showed no changes in axon diameter distributions
Lawrence 2002 [136]	Rabbit	LIFE	Electrode were encapsulated in connective tissue whose cellular components were not evaluated	No differences were observed in fiber count or fiber diameter of myelin thickness distributions between implanted and control nerve (p values for significance set at 0.01, actually p-values are not given)
Lago 2007 [39]	Rat	LIFE	Connective tissue encapsulated all implanted electrodes Nerves adjascent to implanted electrodes appeared to be of small caliper compared to the rest of the nerve The presence of macrophages was observed near the implants (confirmed by IHC)	Fiber counts were not different in implanted nerves compared with control nerves Nerve area was significantly smaller distal to the implant compared with control nerves

Table 1-2: cont

Author Year [Ref.]	Species	Electrode Type	Qualitative Observations	Quantitative Observations
Zheng 2008 [137]	Rabbit	LIFE	Electrodes were surrounded by connective tissue consisting of fibroblasts, but no leukocytes were observed Axon density around the electrodes appeared reduced with smaller axons present Phagocytic cells were observed under TEM in nearby axons	None taken
Edell 1982 [138]	Rabbit	Sieve	Regenerative cuffs were encased in connective tissue Increased connective tissue within the nerve was observed both proximal and distal to the implant	Mean axon diameter in sections proximal to the implant were slightly less than in control nerves, while axon density was higher (significance level not given) Fiber counts in proximal sections were not different from controls Mean axon diameter in sections distal to the implant was greatly reduced compared with control nerves, while axon density and fiber number were much higher (significance level not given)

Table 1-2: cont

Author Year [Ref.]	Species	Electrode Type	Qualitative Observations	Quantitative Observations
Kovacs 1994 [139]	Rat	Sieve	Regenerative cuffs and silicon electrodes were covered with fibrous connective tissue Total nerve diameter proximal to the implant increased as the implant was approached, and then greatly decreased after the implant Evidence of regenerating axons distal to the implant is reported, although the number of these fibers in comparison to control nerves is not mentioned	None taken
Navarro 1998 [140]	Rat	Sieve	Regenerative cuffs were covered by fibrous tissue Axons proximal, at, and distal to the electrode did not exhibit signs of degeneration Axon size and myelin thickness at the level of the implant appeared to increase over time	The mean number of myelinated fibers distal to the implant increased over time, but no comparison is made to control nerves
Klinge 2001 [141]	Rat	Sieve	Evidence of regenerative fibers through and distal to the electrode was confirmed by IHC, although their relative number compared with controls is not mentioned Macrophages were found through IHC to be chronically present at the electrode interface	None taken

Table 1-2: cont

Author Year [Ref.]	Species	Electrode Type	Qualitative Observations	Quantitative Observations
Ceballos 2002 [35]	Rat	Sieve	Regenerative cuffs were covered by fibrous tissue Occasional macrophages were observed within the endoneurial space Axons distal to the electrode appeared to have thinner myelination than axons from control nerves	A decease in nerve area at the implant was observed at 2, 7, and 12 months, while a decrease was observed only at 12 months distal to the implant A decrease in fiber count was observed only at 2 months at the level of the implant and never distal to the implant Perineurial thickness was significantly increased in all implanted nerves Mean axon diameter and myelin thickness values were significantly reduced both at and distal to the electrode at all time points Fiber diameter distributions exhibited a significant shift towards smaller fibers compared with controls
Lago 2005 [34]	Rat	Sieve	Regenerative cuffs were covered by fibrous tissue	Nerve area was significantly decreased distal to the electrode at 2, 6, and 12 months, while fiber counts were reduced only at 2 and 12 months Mean axon diameter and myelin thickness distal to the implant were significantly smaller than controls at all time points

Table 1-2: cont

Author Year [Ref.]	Species	Electrode Type	Qualitative Observations	Quantitative Observations
Ramachandran 2006 [142]	Rat	Sieve	Regenerative cuffs were covered by fibrous tissue No evidence of activated macrophages at the electrode were observed Fiber distal to the implant appeared to be of a smaller caliber and had thinner myelination than normal nerve fibers	Fiber counts distal to the implant are given, but not statistically compared to control nerves
Lago 2007 [143]	Rat	Sieve	Regenerative cuffs were covered by fibrous tissue Fibers distal to the implant appeared to be small in diameter and have thin myelin sheaths compared with control nerves	Sections distal to the electrode showed a significant decrease in nerve area at 2 and 6 months Fiber count results varied with some distal groups showing significant changes, both increases and decreases compared with controls, and others showing no changes
Castro 2008 [144]	Rat	Sieve	None described	Fibers counts proximal to the electrode showed no changes in fiber counts while distal sections showed a significant reduction Mean axons diameters were significantly reduced both proximal and distal to the implant, while g-ratios were significantly lower Fiber packing was also significantly reduced in the implanted nerve

Table 1-2: cont

Author Year [Ref.]	Species	Electrode Type	Qualitative Observations	Quantitative Observations
Panetsos 2008 [145]	Cat	Sieve	No peripheral histology was performed The number of calcium-binding proteins in subcortical and cortical sensory regions appeared down regulated after peripheral electrode implantation The normal spatial arrangement of neural clusters in the dorsal column nuclei was severely disorganized after electrode implantation	None taken
Kim 2009 [107]	Rat	Sieve	None described	Based on the numbers given, it appears that there were significantly fewer fibers in distal sections compared with proximal sections, but comparisons to control and significance values are not given
Branner 2000 [146]	Cat	UEA	Compression of axons in the immediate vicinity of electrode tips was observed after 5 hours, but all other sections of the nerve appeared normal	None taken
Branner 2004 [147]	Cat	USEA	Four different containment systems were used, all of which exhibited at least some tissue ingrowth There were some signs of neural degeneration in implanted nerves, but also viable neurons near electrode tips	The density of myelinated fibers did not differ between implanted nerves and control nerves Fiber diameter distributions are presented but a statistical comparison between the distributions was not conducted

Table 1-2: cont

Author Year [Ref.]	Species	Electrode Type	Qualitative Observations	Quantitative Observations
Garde 2009 [148]	Rat	18-pin axial array	Electrodes and containment cuffs were encapsulated with fibrous tissue Macrophages were found at the electrode-tissue interface (IHC)	None taken

regenerating into a distal stump, fiber counts, axon diameters, and myelin thickness are all typically reduced at and distal to the implanted electrodes. Total nerve area is also typically reduced by proximal and distal to the implant. Macrophages have been observed at the device interface as well as away from the device in the endoneurium, but markers to identify these cells are seldom used.

Axially Penetrating Electrodes

Axially penetrating arrays offer the potential for high selectivity without requiring transection of the nerve. However, while recent studies involving histology with multishank penetrating arrays have focused on implantation in cortical targets [149-154], similar studies in the peripheral nervous system are limited. In fact, only 1 study has been conducted which provides any quantitative description of morphometric parameters in the nerve following electrode implantation (Table 1-2). While it is clear that the implantation of these arrays and their associated containment systems are encapsulated in connective tissue, as with all other electrodes described here, it is not clear from these limited studies the extent of the inflammatory reaction caused by the chronic implantation of these devices. In order to access and improve the potential clinical efficacy of these devices, studies describing their histological impact need to be conducted. Such studies could lead to a better understanding of the foreign body response to such implants and help motivate the design of the next generation of electrodes.

CHAPTER 2

THE FOREIGN BODY RESPONSE TO PENETRATING ELECTRODE ARRAYS IN THE CAT SCIATIC NERVE

Introduction

Microelectrode arrays offer the potential to record from and stimulate nervous tissue, lending themselves to applications in both basic research and neuroprosthetic development. Such devices have found clinical use as cochlear implants to aid the deaf [155], sacral nerve stimulators for the treatment of bladder incontinence [100, 101], peroneal nerve electrodes for the treatment of foot drop [103, 104], and deep brain stimulators for the treatment of Parkinsonian tremors [156, 157]. More advanced prosthetic devices such as robotic arms for amputees or nerve stimulation for patients with spinal cord injury are still in investigational stages of development.

Although cuff style electrodes have been the most widely used and best studied type of microelectrode for nerve stimulation [158], they may not be ideal for some forms of neuroprosthetic control due to their lack of specificity. This issue may be overcome by the use of penetrating electrode arrays that place their active surface near the desired site of stimulation [106]. Additionally, available evidence indicates that the chronic use of cuff, sieve, or intrafascicular electrodes is accompanied by alterations in nerve structure, including changes in fiber count [34, 107, 144], fiber density [126], fiber diameter and g-

ratio (ratio of axon diameter to the outer diameter of the myelinated fiber) distributions [34, 35, 120, 135, 138], connective tissue deposition [43, 102, 119, 125, 127, 128, 133, 135-140, 143], and the infiltration of macrophages into the endoneurial space [39, 128, 137, 141]. These changes in nerve structure, if severe enough, can negatively affect nerve function [34].

Although the foreign body response has been studied for cuff, sieve, and intrafascicular electrodes, few studies have examined the tissue response to axially penetrating arrays in peripheral nerves. The few previous studies using penetrating arrays have shown compression of the nerve under an array tip 5 hours after implantation [146], whereas longer-term studies showed a buildup of connective tissue beneath the array. This later observation was accompanied by an apparent shift in fiber diameter distribution toward smaller diameter fibers [147], although the number of animals used for quantification of morphometric parameters for each condition (n=2) made any statistical comparison in this study impossible. Additionally, only one group has investigated the inflammatory reaction surrounding the electrode shanks of a penetrating array using cell-specific markers [148]. However, this particular study investigated regrowth of axons through an array after transection rather than investigating the response around the array in previously naïve tissue. Additionally, our lab has previously investigated the response to chronically implanted arrays in the nervous tissue; however, these studies were conducted using single-shank arrays in the CNS rather than multishank arrays in the PNS [159]. Therefore, we know of no previous work pertaining to axially penetrating arrays implanted in naïve tissue in the PNS that have investigated the foreign body response to these devices using cell-specific markers or that have used a sufficient

number of animals to statistically compare changes in morphometric parameters in implanted nerves.

To fill this gap in the literature, the foreign body response to multielectrode penetrating arrays implanted into the sciatic nerve was studied here. Nerves were assessed at the gross level, and by using high magnification images from thin sections both distal and proximal to the implant. We examined the degree of epineurial cellularity, as well as monocyte presence and activity in both the epineurial and endoneurial spaces. In addition, quantitative morphological parameters for myelinated fibers were examined, including fascicle areas, fiber counts, fiber densities, fiber packing (the percent of fascicle area occupied by fibers), and fiber diameter and g-ratio distributions. Additionally, selected specimens were examined at or just proximal to the implant site using immunohistochemical techniques.

Methods

Animals

All studies were conducted with the approval of the Institutional Animal Care and Use Committee (IACUC) at the University of Utah. Eleven purpose-bred cats with a mean weight of 2.97 ±0.14kg were implanted with USEAs, with indwelling times ranging from 13 to 350 days (mean of 109 days). Animals were kept in a common housing area and were allowed to freely roam after recovery from surgical implantation. All animals underwent periodic anesthetized and awake electrophysiological characterization sessions. During anesthetized sessions, neuronal unit activity was recorded during manual leg manipulations, either electrical stimulus threshold parameters or electrical stimulus input/output characterization was collected, and the observed,

actual, and equivalent shunting impedance was collected for all electrodes. During awake electrophysiological characterization sessions, neuronal unit activity for all electrodes was recorded while the animal was stationary and moving. Occasionally, the impedance was collected for all electrodes during an awake session. The results of these experiments are outside of the scope of this paper and will be reported in a separate manuscript.

Electrode Insertion

Prior to surgery, animals were anesthetized with an intravenous Telazol injection (10 mg/kg) that was maintained by isoflurane inhalation (1%-2.5%). USEAs (Figure 2-1:A) were implanted into the sciatic nerve, approximately 2 cm proximal to the bifurcation of the tibial and peroneal nerves, as previously described [147]. Briefly, the surgical site was shaved and treated with betadyne, and an incision was made from the hip to the knee. The biceps femoris and vastus lateralis muscles were separated to expose the sciatic nerve. The array was positioned on the nerve and inserted using a pneumatically actuated impulse inserter (Cyberkinetics, Salt Lake City, UT). The array was encapsulated with silicone (kwik-cast, WPI, Sarasota, FL) or wrapped with a gold mesh (Alfa Aesar, Ward Hill, MA) and then covered with silicone. Wires exited subcutaneously from the array to the connector, which was secured to the iliac crest. Contralateral nerves served as controls.

Euthanasia and Tissue Preparation

Animals were terminally anesthetized using a 10:1 ketamine/xylazine cocktail administered at 0.2 ml/kg intravenously at the following time points: 13, 15, 36, 40, 43,

95, 104, 154, 161, 182, and 350 days. Following anesthesia, the animals were transcardially perfused with pH 7.4 phosphate buffered saline (PBS) followed by 4% paraformaldehyde in PBS. The sciatic nerve and its two main branches, the tibial and common peroneal nerves, were exposed from the latero-posterior thigh by blunt dissection of the biceps femoris and photographed *in situ*. The main sciatic trunk from each leg was dissected free and postfixed in 4% paraformaldehyde in PBS overnight and then stored in PBS with 0.01% sodium azide at 4°C. Implanted electrodes and the associated silicone cuffs were removed from the nerve following the postfixation period.

Following removal of the encapsulation cuff and array, nerve cross-sectional areas were calculated. The major and minor axes of the nerves were measured, using digital calipers, at the bifurcation and at 1 cm intervals proximal to the bifurcation over a span of 4 cm. Cross-sectional areas were calculated assuming an elliptical geometry. The measurements were repeated by two independent investigators and grouped together.

Following area measurements, nerves were cut in cross-section approximately 1 cm proximal and distal to the implantation site, and at 3 cm proximal to the bifurcation on the contralateral nerve, to produce nerve segments approximately 2 mm in length (Figure 2-1:B). The nerve segments were then further postfixed in 4% paraformaldehyde / 2% glutaraldehyde in PBS for 24 hours followed by equilibration in 2% osmium tetroxide in 0.1 M sodium cacodylate buffer for 24 hours. Sections were dehydrated through a graded series of ethanols, cleared with propylene oxide, and embedded in Embed 812 (Electron Microscopy Sciences, Hatfield, PA). Sections were cut at 0.7 μm using an Ultracut EMUC6 (Leica, Bannockburn, IL), placed on Superfrost Plus glass slides, and stained with thionin and acridine orange (Sigma-Aldrich, St. Louis, MO).

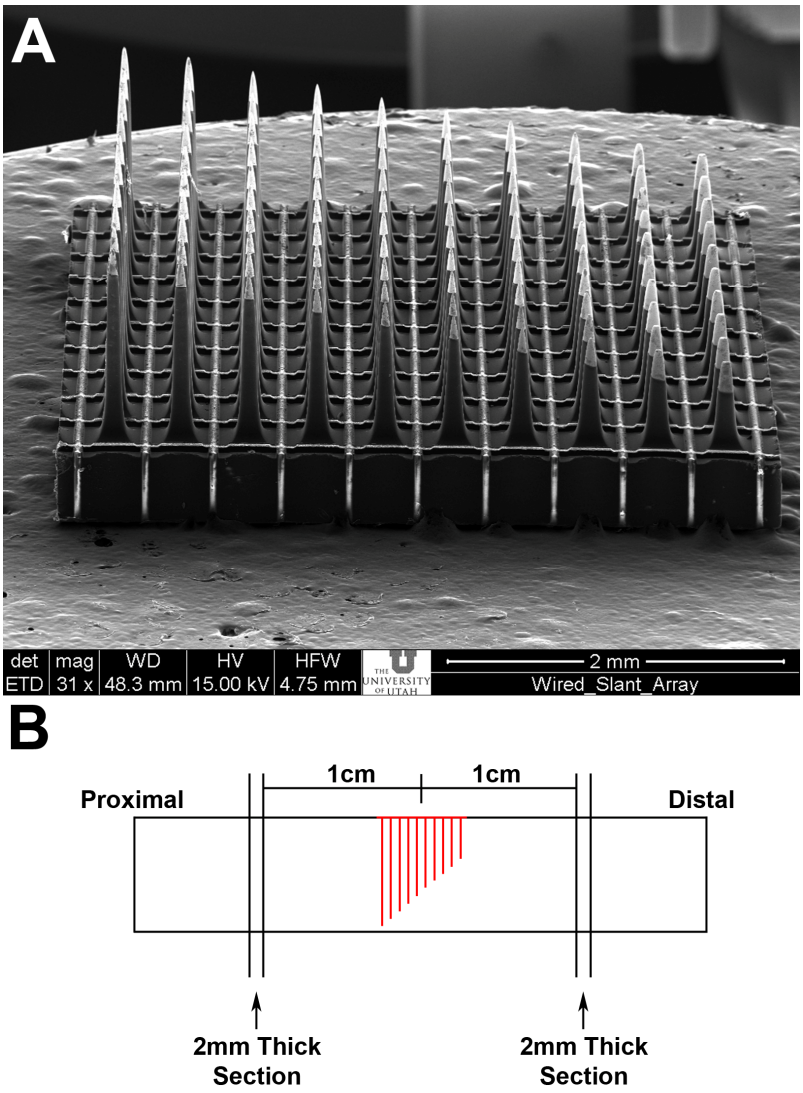

Figure 2-1: Tissue implantation and processing. **A)** SEM image of a USEA. Arrays consisted of a 10x10 arrangement of tines, with rows ranging in length from 0.6-1.5 mm. Each tine is 80 µm wide at the base and tapers to a point. Tines are spaced at 400 µm centers and project out of a 0.2 mm thick silicon substrate. **B)** Schematic (not to scale) showing positioning of the array in the nerve and location of nerve segments processed for thin sectioning. Nerve segments used for thin sectioning were approximately 2 mm in thickness and located 1 cm proximal and distal from the center of the implant site.

Sections were dried and coverslipped using Cytoseal XYL (Richard-Allan Scientific, Kalamazoo, MI).

For immunohistochemistry, nerve sections at the implant site or immediately proximal to the implant were equilibrated in a 30% sucrose solution, embedded in Tissue Freezing Medium (Triangle Biomedical Sciences, Durham, NC) and sectioned using a Leica CM3050 S cryostat at 40-50 μm. Free-floating sections were placed in a blocking solution consisting of 4% (v/v) goat serum (Invitrogen, Carlsbad, CA), 0.05% (v/v) Triton-X 100, and 0.01% (w/v) sodium azide overnight at 4°C. Sections were then treated with primary antibodies (Table 2-1) in blocking solution for 48 hrs at 4°C and followed by 3 room temperature rinses in PBS (2 hour/rinse). The appropriate secondary antibodies in blocking solution were added for 48 hrs at 4°C and followed by 3 additional room temperature rinses in PBS. All sections were counterstained with 10 μM DAPI to visualize cell nuclei. Sections were then mounted on slides and coverslipped using Fluoromount-G (Southern Biotech, Birmingham, AL).

Quantitative Analysis

Images were obtained using ImagePro Plus 4.0 (MediaCybernetics, Bethesda, MD) and a color CCD camera (Photometrics, Tucson, AZ) attached to a Nikon E600 microscope. For cryosections, sections were imaged at 100x final magnification. For thin sections, whole nerve images were obtained at 200x final magnification, while fascicle images were obtained at 1000x final magnification using a 100x oil objective.

For both whole nerve and fascicle imaging, serial overlapping images were taken over the entire area of interest. Using the photomerge command in Adobe Photoshop CS, serial images were reconstructed to form a mosaic image from which morphometric

Table 2-1: List of primary and secondary antibodies used.

Antibody	Antigen	Cell Type(s)	Isotype	Conc. (µg/ml)	Vendor
NF-200	Neuronal 200kD intermediate filament	Neurons	Rabbit IgG	8.3	Sigma-Aldrich
S-100β	β-chain of S-100 dimer protein	Glial/Schwann Cells	Mouse IgG_1	14.6	Sigma-Aldrich
β-III Tubulin	Isotype 3 of β-tubulin	Neurons	Mouse IgG_{2b}	7.6	Sigma-Aldrich
MAC387	L1 or Calprotectin protein	Monocytes/ Macrophages	Mouse IgG_1	0.5	Millipore

parameters were derived. The reconstructed images were then processed through a series of contrast enhancement steps in Photoshop to further differentiate myelin from background. Fascicle areas were calculated by manually tracing the inner edge of the perineurium and total myelinated fiber counts were performed manually. All other morphometric measurements were automatically obtained using ImagePro Plus.

Statistics

Nerve cross-sectional areas, fiber counts, fascicle areas, fiber densities, fiber packing, and mean g-ratios from implanted locations were grouped as a whole and compared with contralateral nerves, and to each other, using a one-way ANOVA with a Tukey's posthoc test. Additionally, data from sections distal and proximal to the implant were grouped based on animal implant duration into short (13 and 15 days animals), medium (36, 40, and 43 days animals), long (95 and 104 day animals), and chronic (154, 161, 183, and 350 day animals) time points which were compared to each other using a one-way ANOVA with a Tukey's posthoc test to reveal any changes in morphometric parameters over time. Because fiber diameters exhibited a nonnormal distribution, mean

bin data from proximal and distal sections of implanted nerves were compared with the mean bin data of contralateral nerves, as well as to each other, using a Wilcoxon signed-rank test by comparing and ranking all bins less than 10 μm (to compare the amount of small diameter fibers) and greater than or equal to 10 μm (to compare the amount of large diameter fibers). P-values below 0.05 were considered significant. All data are represented as average ±SEM.

Results

Macroscopic Analysis

During dissection of the contralateral nerves, the sciatic nerve and its derivative tibial and peroneal branches had a white appearance and were surrounded by a clear epineurial layer (Figure 2-2:A). In general, the main trunk of the sciatic nerve was elliptical in shape. Implanted nerves were covered with an excess of connective tissue which was primarily present around and within the silicon cuff and around the electrode wires (Figure 2-2:B). In shorter-term animals (13 and 15 days), the connective tissue exhibited a high degree of discolorization compared to contralateral nerves after perfusion (Figure 2-2:C). At all time points, blood products could be identified at the implant site, although no discolorization of the nerve was visible proximal or distal to the implant site after 15 days. Necrosis of tissue beneath the array was present at longer time points and increased as indwelling time increased (Figure 2-2:D-F).

Nerve areas from the implanted and contralateral nerves were calculated (Figure 2-3). Our results indicate that implanted nerves had significantly larger cross-sectional areas than contralateral nerves.

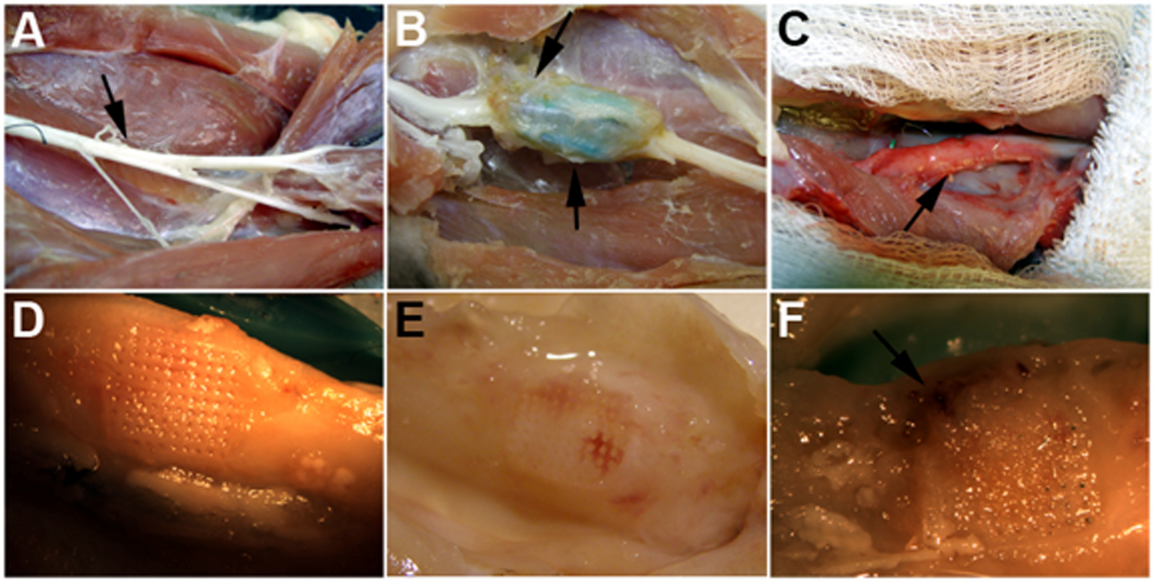

Figure 2-2: Gross appearance of the nerve during or following dissection. **A)** Contralateral nerve shows no discolorization of the nerve or buildup of connective tissue (arrow). **B)** Device after 43 days of implantation. Connective tissue buildup has occurred around the silicone and wires (arrows). **C)** Nerve 15 days after implant. Even after perfusion, the connective tissue surrounding the nerve shows a high degree of discolorization compared to contralateral nerves (arrow). **D)** At 36 days, the tissue beneath the array appears firm and exhibits minimal discolorization. **E)** After 104 days, the tissue beneath the array exhibits evidence of blood products, particularly around the edges of the footprint. **F)** By 350 days post implantation, the tissue under the array has developed into periprosthetic granulation tissue with continued evidence of blood products around the footprint (arrow).

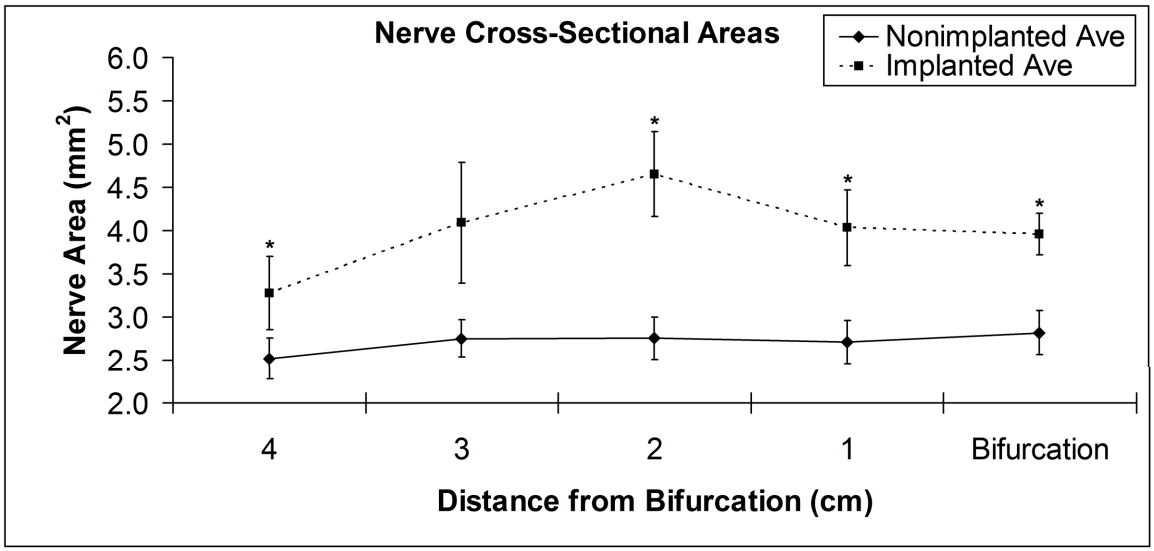

Figure 2-3: Nerve cross-sectional areas calculated assuming an elliptical geometry. Nerves were measured along the main sciatic trunk starting at the bifurcation and proceeding proximally in 1 cm intervals. Implanted nerves showed a significant increase in size compared with contralateral nerves at almost all points measured. Implanted nerves also showed increased variability compared with contralateral nerves (SEM: 0.24-0.70mm for implanted nerves verse 0.21-0.25 mm for contralateral nerves). Average ±SEM *P≤0.05 compared with contralateral controls.

Microscopic Analysis

All fascicles imaged using light-field microscopy were examined at a final magnification of 1000x, which is sufficient to examine individual myelinated axons and surrounding cellularity throughout the entire nerve. Contralateral nerves showed no evidence of hypercellularity in the epineurial space or of infiltrating macrophages in the endoneurial space, and showed little axonal degeneration. To the eye, fiber distribution and myelin thickness appeared uniformly distributed in all contralateral nerves.

Implanted nerves showed varying degrees of damage with no definite trend as a function of indwelling time. For proximal sections, animals which had been implanted for 43 days or less showed some evidence of a degenerative process, whereas animals at longer indwelling times showed little evidence of ongoing damage (Figure 2-4:A). In

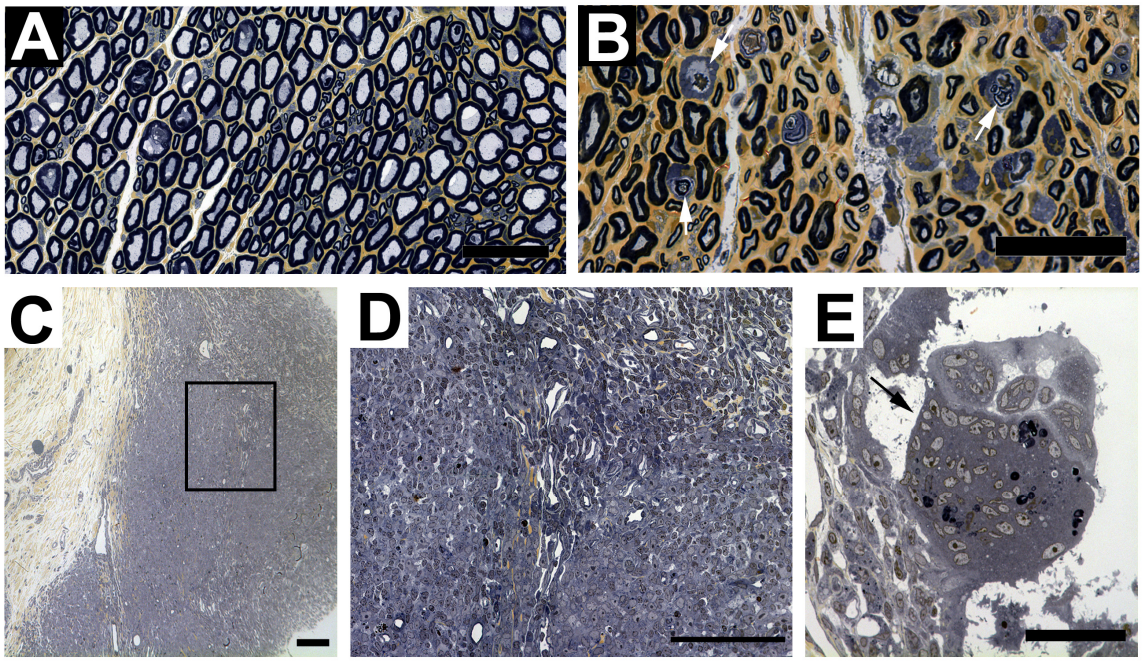

Figure 2-4: Microscopic appearance of implanted nerves. **A)** Endoneurial space proximal to the implant 104 days after implantation. Macrophages are not typically present in the proximal space after the initial degradation of axons. **B)** Endoneurial space distal to the implant 104 days after implantation. Numerous foamy macrophages can be seen actively degrading axons and their associated myelin sheaths (arrows). There appears to be preferential degradation of large diameter fibers. **C)** Epineurial space showing hypercellularity in tissue adjacent to a silicone cuff. **D)** Higher magnification view from C. Several different cells types are present, although individual cell boundaries are often not distinguishable. Cells are occasionally visible in the vasculature, even after perfusion. **E)** Foreign body giant cells are present in the hypercellular zone encapsulating presumptive myelin debris (arrow). Scale bars: A,B,E=50 μm, C,D=100 μm

general, distal sections of implanted nerves displayed infiltration by presumptive macrophages in the endoneurial space, particularly in smaller fascicles. These macrophages appeared to be involved in active phagocytosis of myelin and axons at all time points (Figure 2-4:B). Nerves typically showed signs of Wallerian degeneration characterized by axon degradation, myelin breakdown, and the presence of myelin-laden phagocytic cells. Regeneration was also evident at longer indwelling times (>15 days) as

evidenced by an apparent shift in fiber distributions toward small diameter fibers and thinner myelination of fibers. Fiber density in distal sections almost always appeared to be decreased compared with contralateral sections.

Nerve sections that were taken proximal to the implant, but still under the encapsulation cuff, showed an inflammatory reaction around the periphery of the nerve. This reaction included connective tissue deposition, presumptive macrophages, and foreign body giant cells (Figure 2-4:C-E, Figure 2-5:A).

To further analyze this reaction, tissue from animals implanted for 36, 40, 95, and 161 days was examined using immunohistochemical techniques. To verify the presence of macrophages in the periphery of nerves maintained within the encapsulation cuff, a nerve section from the 36-day animal was taken just proximal to the implant site. Using cell-specific markers for macrophages, we found a pronounced inflammatory reaction at the periphery of the nerve which correlated to the reaction seen in thin sections (Figure 2-5:A-B). We also examined the presence of macrophages at the implant site by cutting cross-sections (95-day animal) and longitudinal sections (40- and 161-day animals). In cross-sections, we again found a pronounced inflammatory reaction that extended from the base of the array down the electrodes to the tips (Figure 2-5:C). Additionally, we found evidence of axonal disruption including aberrant sprouting near the electrode tines (Figure 2-5:D). Longitudinal sections revealed a pronounced inflammatory reaction near the base of the array (Figure 2-6:A) that followed the electrodes down to the tips. However, the macrophage concentration around tips located in the endoneurial space appeared to be reduced compared with tips in the epineurial space (Figure 2-6:B). There was also positive staining for macrophages in the endoneurial space away from the

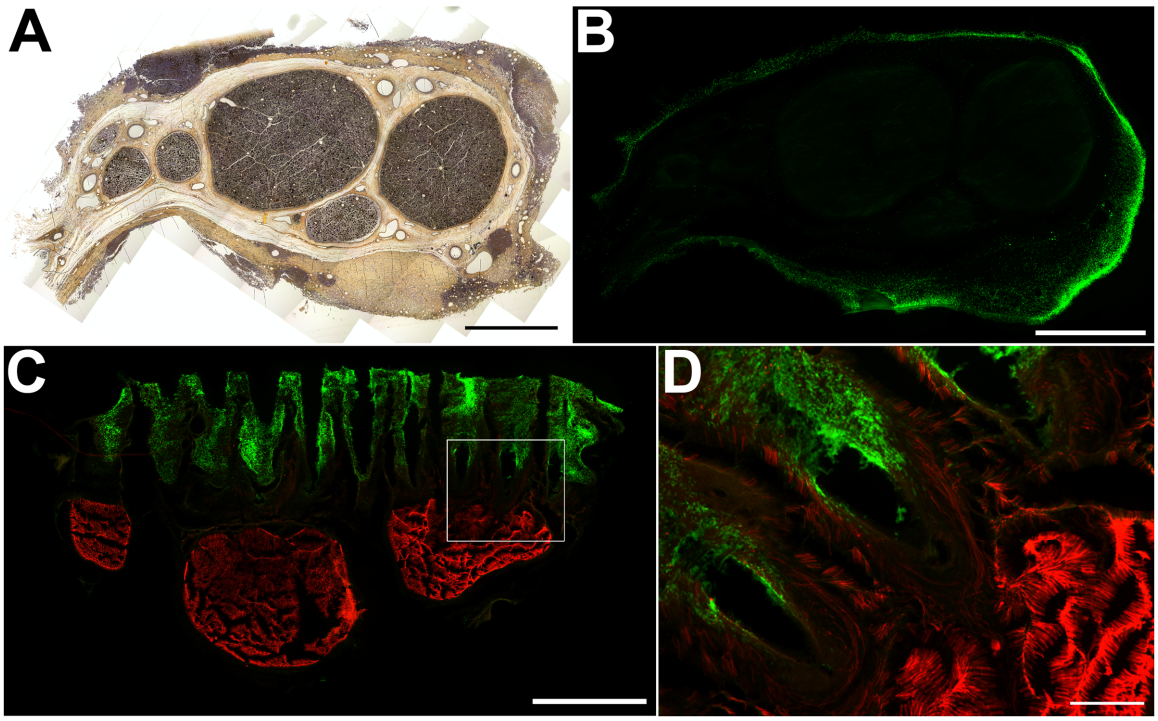

Figure 2-5: Inflammation evaluated in nerve cross-sections. **A)** Cross-section of nerve beneath silicone which had been implanted for 36 days. The epineurial area adjacent to the silicone (outer edge of the nerve) shows a large degree of hypercellularity which includes numerous foreign body giant cells (Figure 4). **B)** Same nerve as in A, stained with MAC387 which confirms that a large number of cells adjacent to the silicone are phagocytic cells. **C)** Cross-section of nerve, implanted for 95 days, at the implant site, stained with MAC387(g) and β-III Tubulin(r). The hypercellular tissue underneath the base of the array and around the electrode tines is heavily populated with MAC387 positive macrophages. It is also evident that the electrode tines have disrupted the fascicular organization of this nerve. **D)** Higher magnification view from C showing macrophages around the electrode tines and sprouting of neuronal processes around the tines, outside of the normal fascicular structure. Scale bars: A-C=1 mm, D=100 μm

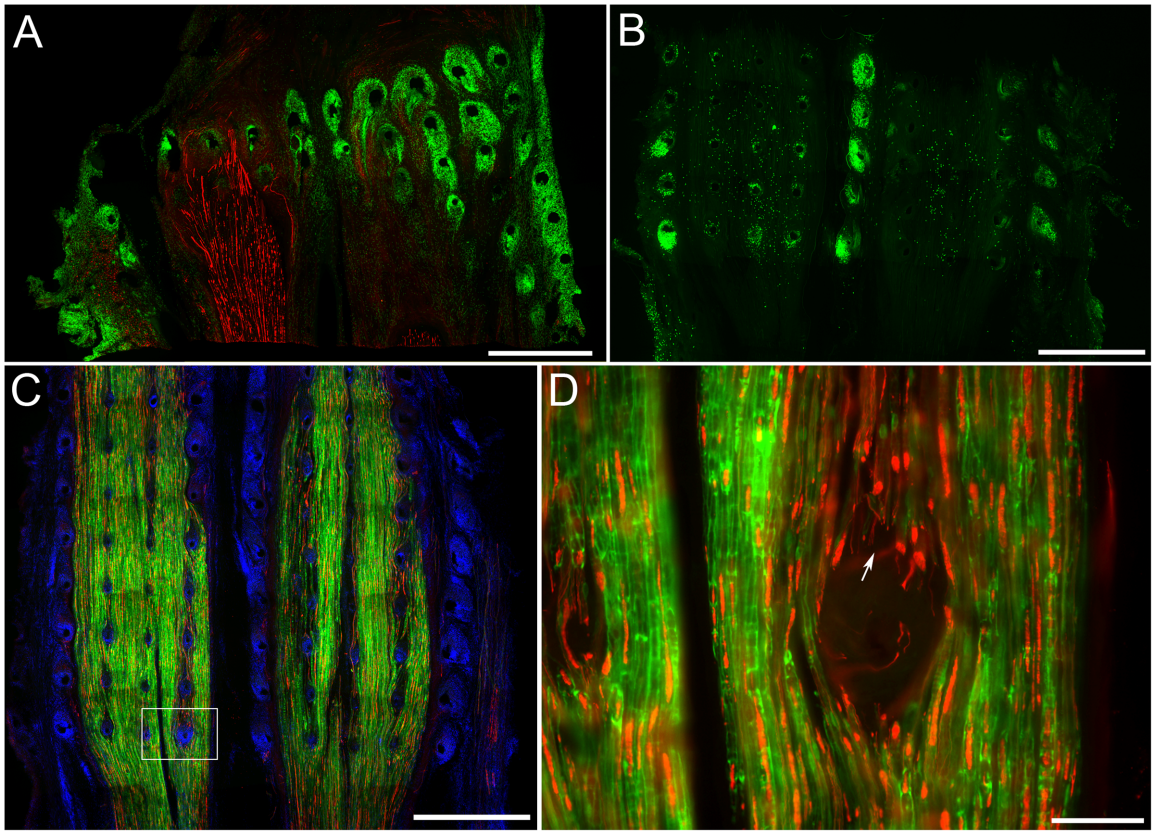

Figure 2-6: Immunohistochemical characterization in longitudinal sections. **A)** Section taken at the implant site from the 40-day animal, stained for MAC387(g) and NF200(r). This section was taken near the surface of the nerve, at the base of the array. Numerous MAC387 positive cells surround each tine and fill the epineurial space. Axons are also disrupted around tines. **B)** MAC387(g) positive cells from the 161-day animal continue down the electrode tines into the endoneurial space, although they are not as concentrated as in the epineurial space. Cells positive for MAC387 are also found in the endoneurial space away from the electrodes. **C)** Adjacent section to that shown in B stained for S-100β(g), NF200(r), and DAPI(b). Axons and their associated myelin sheaths are diverted around the electrodes, greatly increasing the width of the fascicles under the implant. **D)** Inset from C. Severed or dead-end regenerating axons are seen adjacent to an electrode tine. Scale bars: A-C=1 mm, D=200 μm

electrode tips (Figure 2-6:B). Longitudinal sections also showed disruption of axons and their associated myelin due to the presence of electrode tines. Several axons appear to have been severed, whereas many have diverted around the electrode, substantially increasing the width of the fascicles in the area (Figures 2-6:C-D). Nerve fibers just outside the reactive zone appeared normal.

Quantitative assessment of nerves was performed by measuring morphometric parameters including fiber counts, fascicle areas, fiber density and packing, mean g-ratio values, and fiber diameter and g-ratio distributions. Fiber densities showed a trend toward smaller densities proximal and distal to the implant compared with contralateral nerves. This trend was due to an increase in fascicular area rather than a decrease in fiber numbers (Table 2-2). Proximal and distal sections also showed a statistically significant decrease in fiber packing compared with contralateral nerves. No statistically significant differences in fascicle areas, fiber counts, fiber densities, or fiber packing existed between proximal and distal sections in implanted nerves.

Additionally, sections distal and proximal to the implant were compared over time to see if changes in indwelling period produced any significant changes in morphometric

Table 2-2: Average ±SEM of measured morphometric parameters. *P≤0.01 compared with contralateral nerve.

Location	Total Fascicle Area (mm^2)	Total Fiber Count	Fiber Density (fibers/mm^2)	Fiber Packing	Mean g-ratio
Contralateral	2.75 ±0.15	19551 ±567	7241 ±291	65.7% ±3.5%	0.55 ±0.01
Implant Proximal	3.24 ±0.27	18300 ±828	6078 ±631	49.2% ±5.7%*	0.56 ±0.01
Implant Distal	3.26 ±0.25	19099 ±1011	6076 ±453	46.2% ±4.3%*	0.56 ±0.01

data. No differences in any of the aforementioned parameters were detected as a function of time for either distal or proximal sections.

Average fiber diameter distributions for contralateral nerves showed a trimodal distribution with peaks around 4-6, 10-11, and 13-14 μm. Mean bin data from small (<10 μm) and large (≥10 μm) fiber groups were statistically compared across locations using a signed-rank test. Distributions from proximal and distal sections showed statistically significant differences from contralateral nerves with increases in the amount of small fibers ($p<0.05$) and decreases in the amount of large fibers ($p\leq0.001$). Additionally, distributions for distal sections showed a statistically significant decrease in the number of large fibers compared with proximal sections (Figure 2-7:A).

Mean g-ratio values for all locations tested were about 0.56 and were not statistically different from each other (Table 2-2). G-ratio distributions from all locations demonstrated a normal distribution (Figure 2-7:B).

Discussion

This study shows that the chronic presence of USEAs in cat sciatic nerve is accompanied by a persistent inflammatory response that is signaled by the enhanced deposition of connective tissue, swelling of the implanted nerve, the infiltration of macrophages into the epineurial and endoneurial spaces around the electrode, and significant changes in some morphometric parameters. However, the number of presumptively viable fibers around the implant site did not differ from that of contralateral controls.

During gross dissection of the nerve, we observed connective tissue buildup around the silicone and wires. This was not unexpected as others using encapsulation

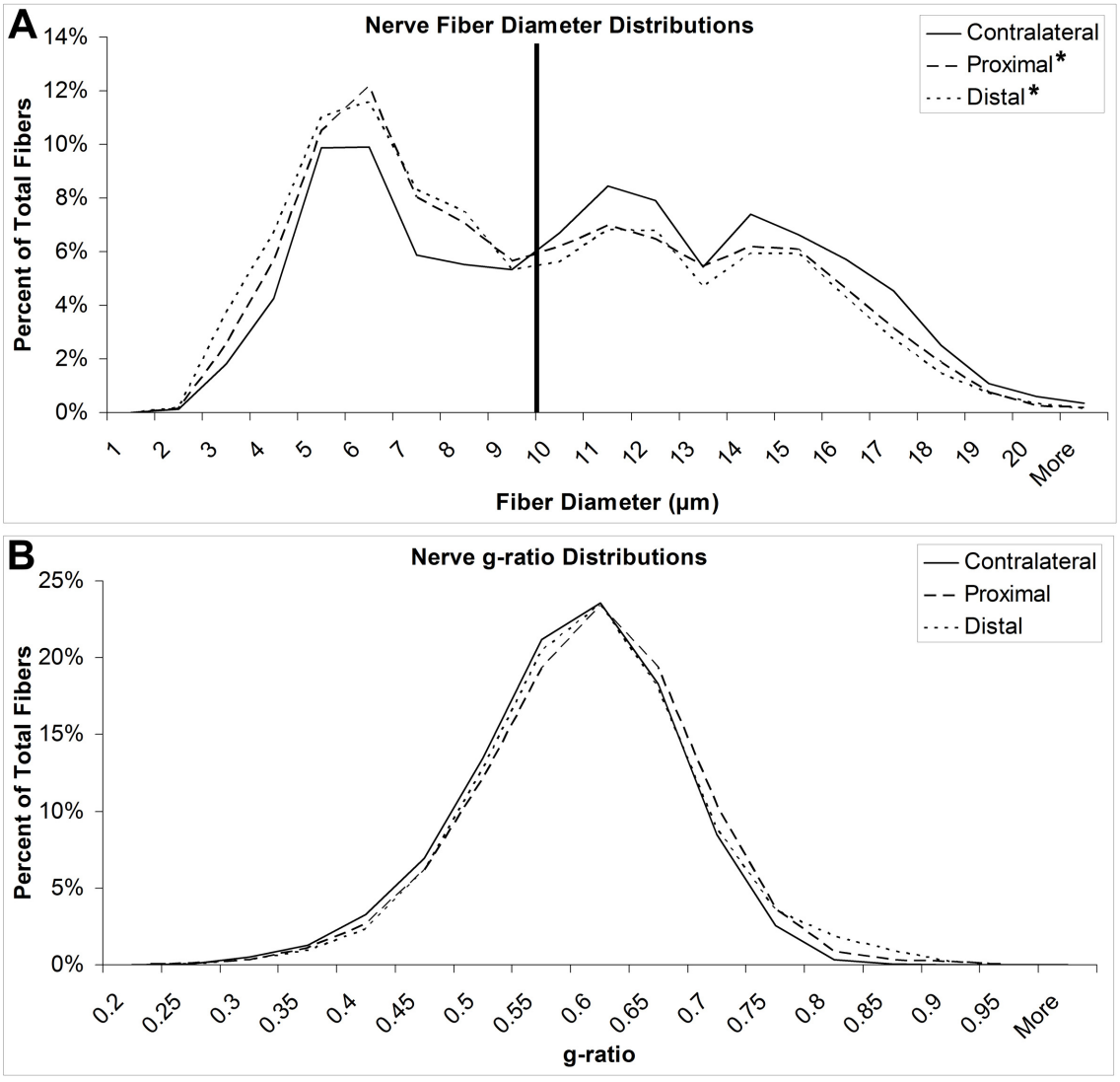

Figure 2-7: Fiber diameter and g-ratio distributions. **A)** Mean fiber diameter distributions for contralateral, proximal, and distal sections. The vertical line represents the point at which bins were separated for statistical analysis. All bins below 10 µm were ranked and compared while all bins greater than 10 µm were likewise evaluated. Distributions from proximal and distal sections show a significant increase in the amount of small diameter fibers and a decrease in the amount of large diameter fibers compared with contralateral sections. **B)** Mean g-ratio distributions for contralateral, proximal, and distal sections. All sections show normal distributions which are not significantly different from each other.

cuffs have seen similar reactions [35, 41, 125, 138]. Although this excessive tissue could include reactive macrophages, some connective tissue around the implanted device might be desirable to provide stability to the implanted electrode. During dissection we also noted blood products at the implant site. The blood products were present after transcardial perfusion and suggest the presence of leaky blood vessels under the array or newly formed blood vessels that have failed to make a terminal connection, thus preventing blood evacuation from their ends. Previous acute studies using UEAs showed evidence of bleeding after electrode removal, confirming that these electrodes do disrupt blood vessels in the nerve [146]. Even without direct disruption of these vessels, Bouldin et al. have shown that the blood-nerve-barrier (BNB) is disrupted after crush injury for up to 2 weeks, whereas after transection injury the permeability of the blood vessels distal to the injury has not been restored to control values by 18 weeks [160]. BNB integrity has also been shown to be compromised in the presence of flat interface nerve electrodes four weeks after implantation [126]. Additionally, it has been shown that macrophage recruitment to an injury site increases vascular permeability [161]. Given the likelihood that the insertion of these electrodes induces a variety of injury mechanisms including crush and cut, and the fact that these electrodes cause a persistent inflammatory reaction as evidenced by our immunohistochemical analysis, it is plausible that the permeability of the BNB remains compromised throughout the duration of the indwelling period.

We also found a statistically significant increase in the size of implanted nerves compared with contralateral nerves. Swelling could be due to the infiltration of cells into the injured area, vasodilation, and/or connective tissue deposition. Sections taken within the bounds of the silicone cuff suggest that infiltrating cells and connective tissue

deposition are indeed present in these nerves (Figures 2-4:C-E, 2-5:A). Although blood vessel area was not calculated in this study, others have shown an increase in endoneurial luminal perimeters in rats after crush injury that persists up to 9 weeks [92], as well as vasodilation in the epineurium following cuff implantation [128], suggesting that vasodilation is also a plausible explanation for our observations.

In the standard time course of Wallerian degeneration after crush or cut injury, peripheral macrophages are recruited into the injured endoneurial space by 2-3 days, peak by 14-21 days, and are mostly resolved after several months [49, 58, 85]. In all animals we studied, we saw evidence of phagocytic cells present in the endoneurial space actively engaged in the phagocytosis of myelin and what appeared to be axonal structures. The fact that we observed presumptive macrophages distal to the implant up to 6 months after implantation suggests that the presence of a foreign body in the nerve prevents resolution of the earlier injury response, and that an inflammatory reaction persists throughout the indwelling period. This persistent inflammatory phenotype has been observed in other parts of the nervous systems with other implanted devices, such as hydrocephalic shunts [162], DBS electrodes [163-165], and microelectrodes [150, 159, 166-168]. Additionally, previous studies with acute crush or transection injuries have shown evidence that Wallerian degeneration of axons occurs retrogradely for only several millimeters proximal to the injury [169]. In this study we found evidence of acute retrograde degeneration of axons extending at least 1 cm proximal to the implantation site, as well as changes in fiber diameter distributions in proximal sections toward smaller diameter fibers, suggesting that the presence of a penetrating array in the peripheral nerve exacerbates the degenerative response of axons to the initial injury.

In addition to the presence of macrophages in the endoneurial space, we observed a pronounced inflammatory reaction in the epineurial space adjacent to the silicone and around the electrode. The macrophage response inside a cuff has been observed by others [43, 125, 127, 128] and could lead to an exacerbated response to the implanted electrode due to the secretion of proinflammatory cytokines from these cells. Although the presence of a silicone cuff could lead to an increase in the number of phagocytic cells around the electrode itself, it is likely that without a cuff a foreign body reaction around the electrode would still exist, given that numerous studies using penetrating electrodes in the brain have found activated macrophages cells at or near the implant surface [149, 150, 159, 166, 170-173]. Electrodes outside of the nervous system are also accompanied by a macrophage response [174, 175]. Our immunohistological sections corroborate these findings and show the presence of numerous macrophages near the base of the array (Figure 6A). However, the exact contribution of the cuff to the macrophage response, as well as to the changes in morphometric parameters, is impossible to elucidate from this study. Therefore, additional studies should be undertaken to parse out the individual contributions of the implanted devices on these responses.

We have reported here that distal sections from implanted nerves showed a trend towards decreased fiber densities compared with contralateral sections. We found in other studies that a 14% decrease in fiber density is standard between sections located 1 cm and 3 cm proximal to the bifurcation (data not provided). Therefore, although a decreasing trend in density between distal implanted sections and contralateral sections was suggested by the data, the differences are within the realm of what we would consider standard given the location of the sections being compared.

Previous studies on nonimplanted sciatic nerves in cats have shown that the fiber diameter distribution is bimodal with peaks around 6 and 12 μm [176] and that the g-ratio distribution is normally distributed with a peak centered at 0.6 [177]. Generally, our results from the contralateral nerves concur with these previous findings. Fiber diameter distributions from implanted nerves were significantly different from contralateral nerves with a shift in distribution from larger to smaller diameter fibers, although the location of the peaks remained the same. This is likely due to both the increased susceptibility of larger fibers to degeneration [178] and the fact that regenerating fibers tend to be small in diameter. The shift is similar to what others have observed in peripheral nerves following crush, cut, ischemic injury, or the implant of an electrode [115, 120, 123, 138, 178-182]. The shift in fiber diameter distribution was not accompanied by a shift in g-ratio distribution, which remained consistent across locations.

Because single animals were used at each time point, trends over time were difficult to interpret. While no differences over time were detected quantitatively, the number of animals available for analysis within each time group might not have provided sufficient power to be able to detect any subtle differences. Therefore, we focused on a holistic approach to our data comparison by grouping all time points together. Although this might have increased the variability in our data due to subtle changes which might occur over time, we were still able to detect differences in several morphometric parameters between implanted and contralateral nerves. However, it should be noted that there has been a long-standing debate concerning the effects of nerve injury on the contralateral nerve. Although some papers have stated that injury causes structural changes in contralateral nerves, such as a reduction in the number of myelinated fibers or

an increase in proinflammatory cytokines [169, 183], most current research assumes that contralateral nerves can be used as controls. This should be an area of future research as the current use of contralateral nerves as controls is commonplace. Nevertheless, we have shown that, regardless of changes that might have occurred to the contralateral nerves, the changes in implanted nerves are even more pronounced.

Conclusions

Although this study finds that the implantation and presence of penetrating arrays, along with their associated encapsulating cuffs, induces a foreign body reaction that is characterized by an increase in nerve cross-sectional area, a decrease in fiber packing, the persistent activation of inflammatory cells, and shifts in fiber diameter distributions, the reaction is not substantially different from what other have described with other types of electrode arrays that offer similar specificity. Further, implanted nerves continued to support large numbers of nerve fibers whose total number did not differ significantly from contralateral nerves. Although continuing efforts should be made to reduce the inflammatory footprint of these devices in order to produce more biocompatible implants, the ability of the nerve to support a large number of presumptively viable fibers adjacent to the implant site is promising for clinical applications.

CHAPTER 3

A MORPHOMETRIC COMPARISON OF CAT AND RAT SCIATIC NERVES

Introduction

The sciatic nerve has long been used as an experimental model in a variety of research areas. More specifically, the sciatic nerve is the peripheral nerve of choice when conducting animal studies with peripheral nerve electrodes. While the rat sciatic nerve has been used extensively in experiments with nerve cuff and regenerating electrodes [34, 35, 41, 120, 127, 128, 141, 144, 184], the cat sciatic nerve is commonly used in cuff studies [43, 115, 117, 121, 122, 125, 185] and is being more frequently used for experiments using penetrating peripheral nerve devices [42, 106, 147]. In order to understand the changes that might occur in the underlying nerve following the implantation of these peripheral nerve devices, it is necessary to have knowledge of the basic structure and composition of the nerve under normal conditions.

The composition of the rat sciatic nerve has been relatively well studied and morphometric parameters for myelinated fibers, such as fascicle area, fiber count, fiber density (number of myelinated fibers per fascicle area unit), fiber packing (the percent of the fascicular area occupied by myelinated fibers), mean fiber diameter, fiber diameter distributions, and mean g-ratio or g-ratio distributions, have been previously examined

(Table 3-1). However, when looking at these data it is important to recognize that they have been collected from multiple strains and from rats of varying ages, variables whose influence on morphometric parameters has not been examined. Additionally, many of these data were collected from the contralateral limb of animals undergoing some type of surgical procedure. As reviewed by Koltzenburg et al., such unilateral manipulation of peripheral nerves can cause changes in the contralateral nerve at the gene expression level that is accompanied by anatomical remodeling [186]. Additionally, it has been shown by others that unilateral manipulation can cause changes in morphometric parameters in the contralateral nerve [169, 187]. There is also reason to question the validity of using contralateral nerves as implant controls as others have reported that, even in naïve animals, differences may naturally exist between the left and right leg nerves [188]. Therefore, the contralateral nerve may not be an appropriate representation of normal data, and even if it is, naturally existing side differences need to be further identified before such data can be broadly applied.

Unlike the rat sciatic nerve, few studies have reported morphometric parameters for the cat sciatic nerve (Table 3-2). While some data, including fascicle areas, fiber counts, fiber densities, mean g-ratio, and fiber diameter distributions, do exist in the literature, these studies either used small numbers of animals or contralateral nerves and, where more than one group has reported data for a specific parameter, the data are often not in agreement with each other. To date, we know of no study that has used multiple animals and whole nerve sampling of naïve nerve to establish a control data set for the domestic cat sciatic nerve.

Table 3-1: Reported literature values of morphometric parameters from control rat sciatic nerves. Multiple values for a parameter are given if more than one control group existed in a study. SD=Sprague-Dawley.

Year [Ref.]	Author	Strain	Morphometric Parameter (Mean)
1976 [189]	Adhami	Wistar	G-ratio (0.651)
1985 [36]	Jenq	SD	Fiber Count (8198, 7853)
1986 [38]	Jenq	SD	Fiber Count (7186, 7938)
1986 [33]	Schmalbruch	Wistar	Fiber Count (7569)
1988 [190]	Le Beau	SD	Fiber Diameter (5.13μm)
1992 [191]	Koller	SD	Fiber Packing (54.2%) Fiber Diameter (6.78μm)
1993 [92]	Podhajsky	SD	Fascicular Area (0.484mm^2)
1994 [192]	De Angelis	SD	Fiber Density (21200, 13800 fibers/mm^2) G-ratio (0.69, 0.66) Fiber Diameter (7.54μm, 8.29μm)
1998 [193]	Di Benedetto	SD	Fascicular Area (0.511mm^2) G-ratio (0.538) Fiber Diameter (6.79μm)
2000 [41]	Rodriguez	SD	Fiber Count (8301, 8453) Fiber Density (13147, 13834 fibers/mm^2) G-ratio (0.648, 0.65)
2002 [35]	Ceballos	SD	Fiber Count (8356, 8453)
2003 [40]	Rafiuddin Ahmed	Wistar	Fiber Count (6338) G-ratio (0.659)
2005 [34]	Lago	SD	Fiber Count (8266)
2007 [39]	Lago	SD	Fiber Count (8076, 7954)
2007 [194]	Prodanov	Wistar	Fiber Count (7599, 8270) Fiber Diameter (6.61μm, 5.76μm)
2008 [181]	Mazzer	Wistar	Fiber Density (16426 fibers/mm^2) G-ratio (0.53)

Table 3-2: Reported literature values of morphometric parameters from control (either contralateral of from nonimplanted animal) cat sciatic nerves. Multiple values for a parameter are given if more than one control group existed in a study.

Year [Ref.]	Author	Morphometric Parameter (Mean)
1976 [32]	Bennett	Fascicular Area (2.65, 2.96mm^2)
1985 [5]	Friede	G-ratio (0.7)
2001 [43]	Romero	Fascicular Area (2.5mm^2) Fiber Count (16416)
2004 [147]	Branner	Fiber Density (7747 fibers/mm^2)
2006 [42]	Leventhal	Fascicular Area (2.9, 3.14mm^2) Fiber Count (20409) Fiber Density (5797 fibers/mm^2)

In order to more fully understand the morphometric composition of the naïve rat and cat sciatic nerves, and to investigate whether leg side differences naturally exist, we used quantitative approaches to examine several morphometric parameters for myelinated fibers, including fascicle areas, fiber counts, fiber densities, fiber packing, mean g-ratio and g-ratio distributions, and fiber diameter distributions, from sciatic nerves in both Fischer 344 rats and domestic cats.

Methods

Animals

All studies were conducted with the approval of the Institutional Animal Care and Use Committee (IACUC) at the University of Utah. Two groups of Fischer 344 rats were used in this experiment. Group 1 (young adults, n=7) was sacrificed at an average weight of 253 g ±6 g, (approximately 11 weeks of age) while group 2 (adults, n=8) was

sacrificed at an average weight of 357 g ±19 g (approximately 19 weeks of age). Seven cats with an average weight of 5045 g ±1508 g were also used.

Euthanasia and Tissue Preparation

Rats were terminally anesthetized using an intraperitoneal injection of ketamine (70 mg/kg) and xylazine (30 mg/kg). Cats were terminally anesthetized using a 10:1 ketamine/xylazine cocktail administered at 0.2 ml/kg intravenously. Following anesthesia, animals were transcardially perfused with pH 7.4 PBS followed by 4% paraformaldehyde in PBS. The sciatic nerve from each leg was dissected free and postfixed in 4% paraformaldehyde in PBS overnight and then stored in PBS with 0.01% sodium azide at 4 °C.

Postfixed nerves were hand cut in cross-section approximately 1 cm proximal to the bifurcation of the sciatic nerve into the tibial and common peroneal branches to produce nerve segments approximately 2 mm in length. In the cats, sections were also cut 3 cm proximal to the bifurcation. The nerve segments were then further postfixed in 4% paraformaldehyde / 2% glutaraldehyde in PBS for 24 hours followed by equilibration in a 2% osmium tetroxide in 0.1 M sodium cacodylate buffer for 24 hours. Sections were then dehydrated through a graded ethanol series, cleared with propylene oxide, and embedded in Embed 812 (Electron Microscopy Sciences, Hatfield, PA). Sections were cut at 0.6 μm using an Ultracut EMUC6 (Leica, Bannockburn, IL), placed on Superfrost Plus glass slides, and stained with thionin and acridine orange (Sigma-Aldrich, St. Louis, MO). Sections were coverslipped using Cytoseal XYL (Richard-Allan Scientific, Kalamazoo, MI).

Quantitative Analysis

Nerve thin sections were imaged using ImagePro Plus 4.0 (MediaCybernetics, Bethesda, MD) and a color CCD camera (Photometrics, Tucson, AZ) attached to a Nikon E600 microscope. Whole nerve images were obtained at 200x final magnification, while fascicle images were obtained at 1000x magnification. For both whole nerve and fascicle imaging, serial overlapping images were taken over the entire area of interest using a Labview driven motorized stage. These images were then reconstructed in Adobe Photoshop CS to form mosaic images from which morphometric parameters were derived. Fascicle areas were calculated by manually tracing the inner edge of the perineurium and total myelinated fiber counts were performed manually. All other morphometric measurements were automatically obtained using ImagePro Plus.

Statistics

Total myelinated fiber counts, fascicle areas, fiber densities, fiber packing, and mean g-ratio values were compared between animal groups using a one way ANOVA with a Dunnett T3 posthoc test. These parameters were also compared within the cat group using a one way ANOVA with a Tukey's posthoc test, and within the rat groups using a paired t-test. Fiber diameter distributions were compared using a Wilcoxon signed-rank test. P-values below 0.05 were considered significant. All data are represented as mean ±stdev.

Results

Macroscopic Observations

Representative images of rat nerve cross sections are shown in Figure 3-1 and of cat nerve cross sections are shown in Figure 3-2. Young adult rats typically were unifascicular in the left nerve, while the right varied with 1-2 large (>0.1 mm^2) fascicles. The number of large fascicles in the left and right nerves was not significantly different. Adult rats typically had two large fascicles in both the left and right nerves. Smaller fascicles were rarely seen in either rat group. Cat nerves generally had two large fascicles (>0.8 mm^2) and two small fascicles (<0.1 mm^2). The number of medium size fascicles (0.1 $mm^2 < x < 0.8$ mm^2) varied significantly depending on the distance from the bifurcation, with sections 1 cm away having an average of three and sections 3 cm having an average of two. No obvious differences were observed between left and right nerves in the cat group.

Morphometric Analysis

Mean values for morphometric data are reported in Table 3-3. Total fascicular areas were statistically larger in the cat group than the two rat groups, and larger in the adult rat group compared to the young adult group. Fascicular areas also significantly increased in the cat group as the nerve approached the bifurcation, with sections 1 cm from the bifurcation showing a 17% increase in area over sections 3 cm away. No differences existed in fascicular area between the left and right nerves of any group.

Myelinated fiber counts were significantly greater in the cat sciatic nerve compared to both rat groups, with no differences existing between the rat groups or

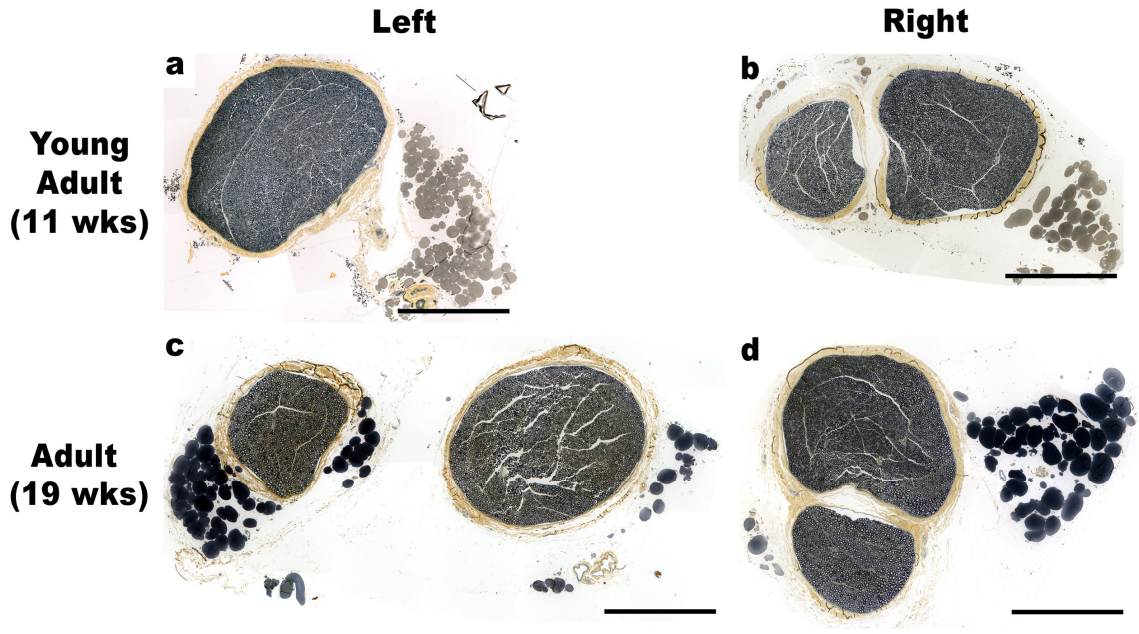

Figure 3-1: Representative nerve cross-sections from rat groups. **A,B:** Representative left and right nerve cross-sections, respectively, from the young adult rat group. The left nerve was typically unifascicular while the right nerve had between one and two fascicles. **C,D:** Left and right nerve cross-sections, respectively, from the adult rat group. Adult rats typically had two fascicles in both the left and right nerves. Scale bars = 500 µm

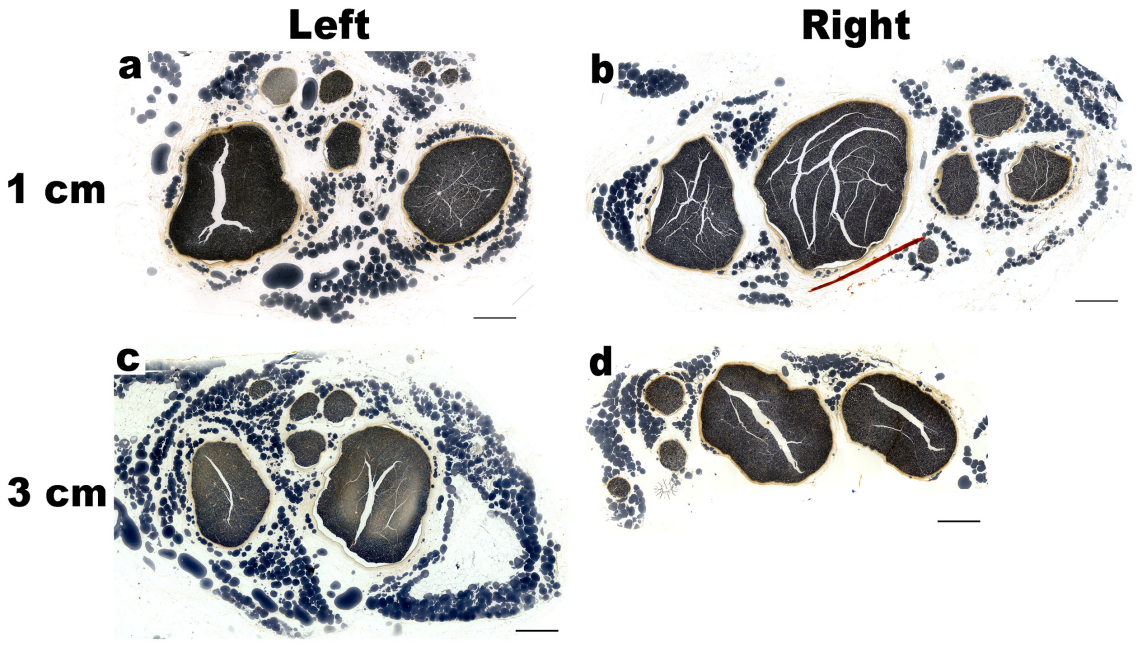

Figure 3-2: Representative nerve cross-sections from cat group. Cross-sections from the cat group representing the left (A,C), right (B,D), 1 cm (A,B) and 3 cm (C,D) locations. Cat nerves typically had two large fascicles (>0.8 mm^2), two small fascicles (<0.1 mm^2), and three medium fascicles at the 1 cm location or two medium fascicles at the 3 cm location. Scale bars = 500 µm

Table 3-3: Morphometric parameters from the sciatic nerve for each location and animal group tested. Data are reported as mean ±stdev. Location is the side (L=left, R=right) and distance proximal to the bifurcation of the sciatic nerve into the tibial and common peroneal branches.

Group	Location	Fascicular Area (mm^2)	Fiber Count	Fiber Density (Fibers/mm^2)	Fiber Packing	G-ratio
Young Adult Rats	L 1cm	0.44 ±0.08	7536 ±282	15745 ±1827	58.4 ±7.4%	0.60 ±0.04
Young Adult Rats	R 1cm	0.44 ±0.09	7950 ±1706	16719 ±2508	63.6 ±4.8%	0.62 ±0.02
Adult Rats	L 1cm	0.66 ±0.05	7613 ±292	11551 ±872	67.4 ±3.2%	0.64 ±0.02
Adult Rats	R 1cm	0.59 ±0.13	6782 ±1294	11671 ±1057	67.4 ±6.0%	0.62 ±0.02
Cats	L 1cm	3.42 ±0.30	18955 ±1183	5504 ±453	60.8 ±3.6%	0.52 ±0.01
Cats	L 3cm	2.89 ±0.24	20323 ±1518	6804 ±1058	60.0 ±9.2%	0.55 ±0.03
Cats	R 1cm	3.70 ±0.73	21142 ±2800	5779 ±546	68.0 ±5.3%	0.52 ±0.01
Cats	R 3cm	3.06 ±0.45	19978 ±1362	6666 ±1240	68.1 ±11.6%	0.55 ±0.03

between left and right nerves within any group. Additionally, counts were not different between locations within the cat group with respect to distance from the bifurcation.

Fiber densities exhibited the same significant differences as seen in fascicle area data with densities between the three groups and between the 1 cm and 3 cm locations within the cat group being different, while side differences did not exist.

Data for fiber packing, or the percent of the fascicle area occupied by myelinated fibers, were significantly greater in adult rats compared to young adults, while neither rat group differed from the cat group. Additionally, the right nerve in the cat had statistically higher values than the left nerve, while no difference existed with respect to the distance from the bifurcation or between left and right nerves in either rat group.

Mean g-ratios (the ratio of the axon diameter to the total fiber diameter) were significantly lower in the cat group than either rat group. Significant differences were also detected between the left and right nerves in both rat groups, although the side with the higher g-ratio values did not remain the same (right nerve in young adult, left nerve in adults). No differences were observed between left and right nerves or across locations in the cat group. G-ratio distributions for young adult rats, adult rats, and cats are shown in Figure 3-3. While no statistical difference was detected in mean g-ratio values between the two rat groups, it appears that the breadth of the distribution in the adult rat group is considerably narrower than in the young adult group.

Fiber diameter distributions for young adult rats, adult rats, and cats are shown in Figure 3-4. No leg side differences were detected in either rat group, although a significant difference is obvious between the two groups with the young adult group having significantly more small fibers (<8 μm) and fewer large fibers (≥ 8μm) than the

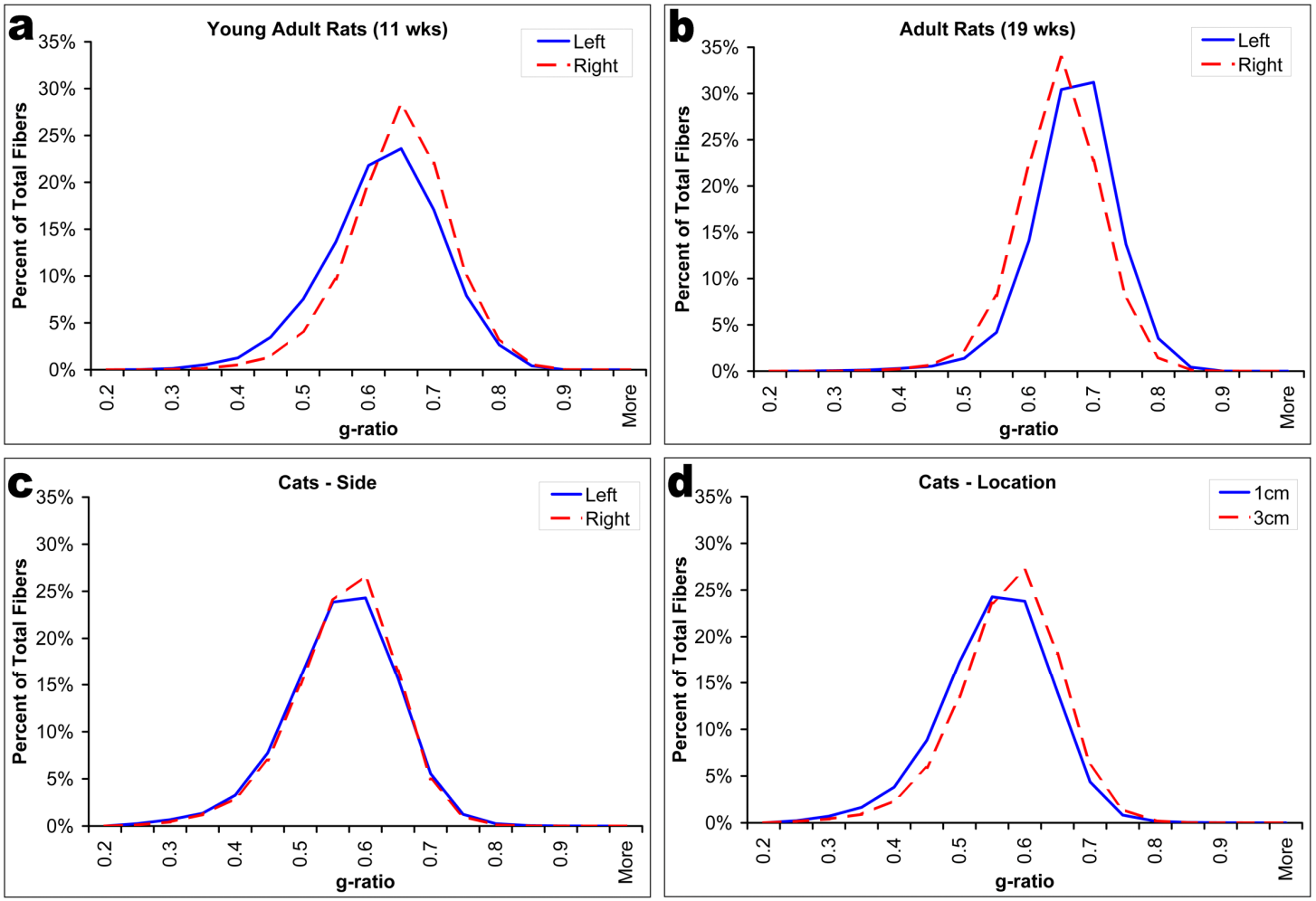

Figure 3-3: G-ratio distributions for each animal group. Significant differences in mean values between the left and right nerves were detected in both the young adult rat (A) and adult rat (B) groups. No differences were detected in the cat group with respect to either side (C) or location along the nerve (D).

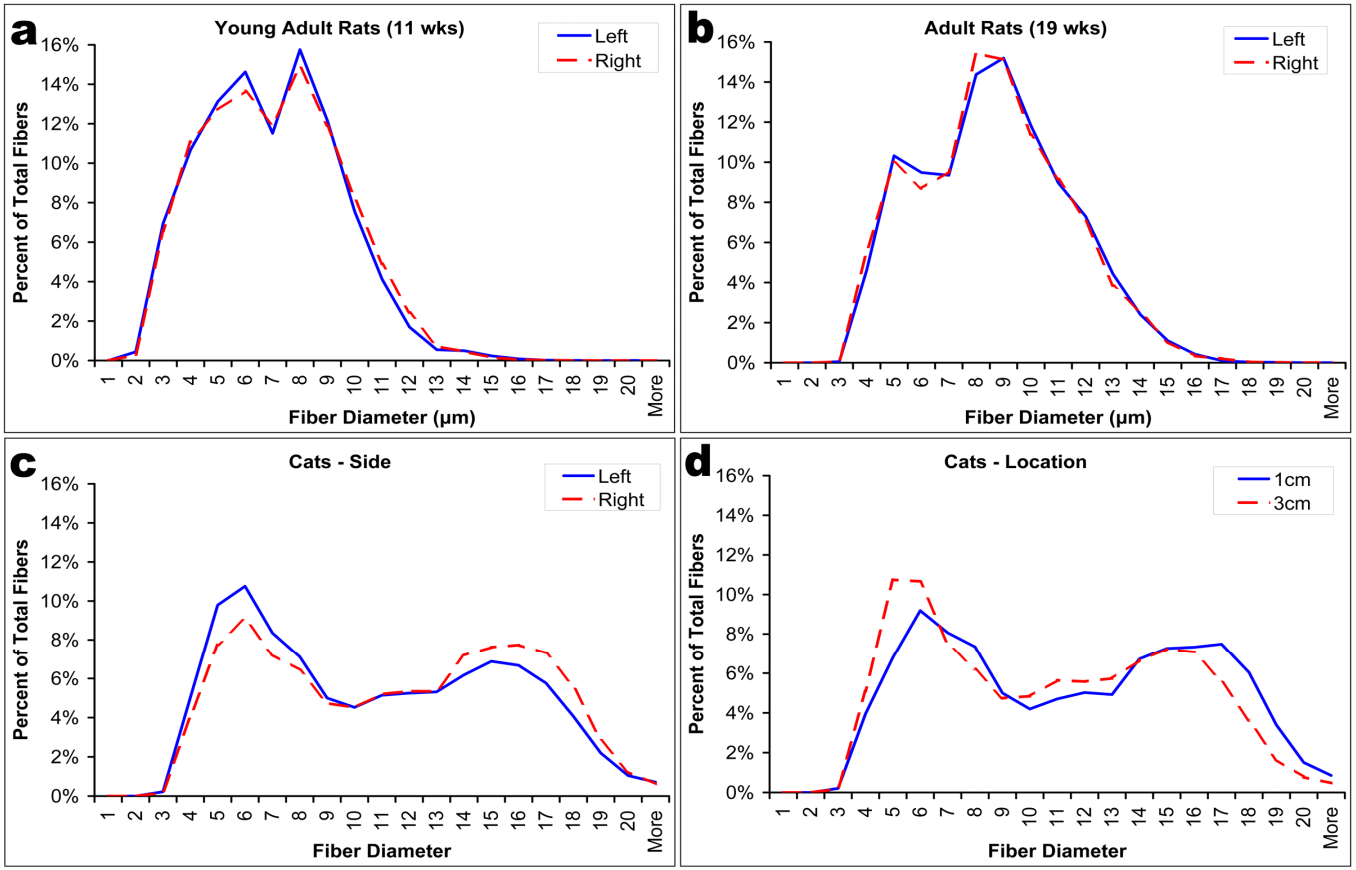

Figure 3-4: Fiber diameter distributions for each animal group. The vertical line represents the point in the distribution at which bins were separated for analysis. All bins to the left of the line (small fibers) were ranked and compared in a single analysis while all bins to the right (large fibers) were likewise evaluated. No side differences were detected in either the young adult rat group (A) or the adult rat group (B), although the two groups were significantly different from each other, with the young adult group having a larger proportion of small diameter fibers (<8 µm) and fewer large diameter fibers (≥8 µm). The cat group did show side differences with the left nerve showing a larger proportion of small diameter fibers (<10 µm) and fewer large diameter fibers (≥10 µm) than the right nerve (C). No significant differences were detected in the cat group with respect to distance from the bifurcation (D).

adult group. The cat group did exhibit significant differences between left and right nerves with the left nerves having significantly more small fibers (<10 μm) and fewer large fibers (≥10 μm) than right nerves. No differences in cat distributions were detected with respect to distance from the bifurcation.

Discussion

The results of this study establish morphometric parameters for sciatic nerves taken from both naïve rats and cats. Additionally, we have found that leg side differences do exist in certain parameters bringing the practice of using contralateral nerves as internal implant controls into question. Finally, we have established the importance of using age-matched controls and control samples from similar locations as experimental samples by reporting differences in parameters from animals of different ages and by examining nerves at different distances away from the sciatic bifurcation.

By examining fascicle organization, we have found that sciatic nerves in both rats and cats typically have two large fascicles, likely representing the tibial and peroneal branches of the nerve. In the cat, these larger fascicles are accompanied by varying numbers of smaller fascicles. An understanding of this organization is critical for the design of penetrating peripheral nerve electrodes. It has been previously observed that these types of electrodes are accompanied by a chronic inflammatory response including the recruitment of macrophages to the device interface [39, 141]. In order to reduce the number of inflammatory cells, an effort should be made to reduce the surface area of the implanted device [195]. Therefore, having an understanding of the fascicular organization of a nerve would provide the ability to manufacture devices that innervate

the zones of interest in the nerve while reducing the area of the biotic-abiotic interface outside of these zones.

The morphometric parameters we have reported here for Fischer 344 rats are in line with those previously reported for other rat strains (Tables 3-1 & 3-3). Of particular note are the changes in fascicle area, myelinated fiber density, and fiber packing between the two rat groups we tested. While 250 g rats are typically referred to in the literature as adult rats, it is clear that significant changes in the tested parameters continue to occur past this time point. Therefore, age-matched control animals should be used whenever morphometric data from an experimental nerve are being statistically evaluated. It is also interesting that while fascicle area increases with rat age, leading to a subsequent decrease in fiber density, fiber packing actually increases due to the increased size of the fibers. Further, fiber packing was the only parameter tested that was not significantly different between the cat group and either rat group. It is therefore possible that fiber packing plays a critical role in the conduction properties of nerve fibers and that other parameters, such as fascicle area, change in order to maintain fiber packing within a specific range. Alternatively, there may be a minimum amount of connective tissue space within the endoneurium (interaxonal space) required to maintain normal physiology of the nerve.

The only leg side differences that were observed in the rat groups were in g-ratio values. Interestingly, the side with the higher g-ratio values did not remain constant. It is unclear at this time what factors could be contributing to this change. However, the detection of differences, and the fact that they change over time, suggests that using contralateral nerves as internal controls for this parameter would be inappropriate.

Morphometric parameters for cats reported here are generally in the range of reported values (Tables 3-2 & 3-3). Notable exceptions are the fascicle area, which we found to be generally higher than previously reported values, and mean g-ratio values, which we found to be considerably lower than the previously reported values. To our knowledge, we are the first group to report fiber packing information for the cat sciatic nerve. Although values for the peroneal nerve have been previously published for fiber packing, they are considerably lower than the values we reported here [196].

We have also reported for the first time fiber diameter distributions from multiple animals for cat sciatic nerve. Our distributions share similar small diameter peaks to some of those using single animals previously reported, while larger diameter fibers show a broader distribution [43, 176]. Our distributions are also broader than those reported for tibial branches [179]. Average animal weights for cats used in this experiment were larger than those in the cited experiments, which suggests that the animals used here were of a more mature age or perhaps more sedentary. As our rat distributions showed a broadening of the larger fiber diameter distribution area with age, it is possible that a similar effect is being observed here.

Our results also indicate that the sciatic nerve in cat increases in fascicular area as the bifurcation into the tibial and peroneal branches is approached. Corresponding to this increase in area is a decrease in fiber density. Interestingly, fiber packing values do not change as the bifurcation is approached. It appears from distribution histograms (Figure 3-4:D) that this is due to a relative decrease in the number of smaller diameter fibers and a broadening of the distribution of larger diameter fibers as the bifurcation is approached;

however, these changes in the distribution are not significant. These data again suggest that there is a range of fiber packing values which are maintained within the nerve.

Leg side differences in the cat group were detected with fiber packing and fiber diameter distributions, with the right side having a larger proportion of large diameter fibers than the left side, and subsequently a higher fiber packing value. It is unclear at this time why the right side would have significantly larger fibers than the left. It is possible that this difference is due to handedness as others have found a right limb preference in female cats, but not in male cats [197]. However, as our study employed 4 female and 3 male cats, it seems unlikely that a significant difference in leg side preference across our study population would exist.

This study establishes baseline morphometric data for the sciatic nerve in domestic cat and Fischer 344 rats that can be used to help design and evaluate the response to peripheral nerve electrodes or other devices or techniques that manipulate the nerve. Additionally, while many researchers have used the contralateral nerve of experimental animals as internal controls, we have established here the fact that naturally occurring differences do exist in certain morphometric parameters. These differences are evident when evaluating different locations along the nerve, the side of the animal in which the nerve is located, and the age of the animal, emphasizing the importance of using age-matched control animals when analyzing these parameters.

CHAPTER 4

THE FOREIGN BODY RESPONSE TO NERVE CUFF IMPLANTATION IS ASSOCIATED WITH PERSISTENT INFLAMMATION AND CHANGES IN FIBER COMPOSITION OF THE ENCAPSULATED NERVE

Introduction

Microelectrode arrays implanted into the peripheral nervous system offer the potential to record from and stimulate nervous tissue for the control of neuroprosthetic devices. These arrays vary in design and include devices such as multilead cuff electrodes, sieve or regenerating electrodes, and other penetrating multilead or multishank electrodes. Such devices have found clinical use in respiratory pacing [95-97], sacral root stimulators for the treatment of bladder incontinence [99-101], and peroneal nerve stimulators for the treatment of foot drop [102-104].

Cuff style electrodes in particular have been used in such neuroprosthetic applications since the late 1940s when Whittenberg et al. stimulated the phrenic nerve to assist in diaphragm pacing [112]. Because of their simple design and current clinical use, the tissue reaction surrounding cuff electrodes in PNS applications has been relatively well studied. While the implantation of a cuff electrode does not cause a penetrating injury in the nerve, its chronic use has been shown to lead to alterations in nerve composition, including changes in fiber densities [113, 117, 125], fiber diameter and g-

ratio (ratio of axon diameter to total fiber diameter) distributions [113, 120, 123], connective tissue deposition [41, 43, 95, 102, 113, 119, 121, 123, 125, 127, 128], and the infiltration of macrophages into both the epineurial [95, 127, 128] and endoneurial [95, 128] spaces. Varying cuff designs have also been shown to increase blood-nerve-barrier permeability [126] and proinflammatory cytokine levels [127, 128] around the implant. In addition to their use in cuff electrodes, nerve cuffs are often used to help anchor penetrating PNS electrodes [34, 35, 135, 138, 140, 143, 144, 147, 148]. Changes in nerve composition have also been attributed to nerve cuffs used in these applications [35, 138]. The choice of material in the composition of the cuff, such as silicone, polyether, polyimide, or Teflon, does not seem to significantly alter these responses.

While the response to these nerve cuffs has been reported, these studies almost exclusively used solid nerve cuff devices. The use of solid cuffs could exacerbate the foreign body response by restricting connective tissue growth away from the nerve, causing compression of the nerve by tissue deposition [198], or by trapping proinflammatory cytokines within the cuff, preventing diffusion away from the nerve. An open mesh cuff design could potentially ameliorate these effects and reduce morphometric changes in the nerve. However, histological studies exploring the use of open mesh cuffs have not been conducted.

In this study, we sought to understand how open mesh cuffs might influence changes in the underlying nerve compared to commonly used solid silicone cuffs. Nerves were quantitatively assessed for morphometric parameters including total fascicular area, myelinated fiber count, density, and packing (percent of the fascicle area occupied by fibers), mean g-ratio values, and fiber diameter distributions. Additionally, retrieved

cuffs were immunohistochemically evaluated for activated macrophages at the material-tissue interface.

Methods

Cuff Implantation

All studies were conducted with the approval of the Institutional Animal Care and Use Committee at the University of Utah. Three groups of Fischer 344 rats (n=8 each group) were implanted with either solid silicon cuffs (kwik-cast, WPI, Sarasota, FL), size 52 mesh gold cuffs (Alfa Aesar, Ward Hill, MA), or size 52 mesh gold cuffs that had been coated with Parylene-C (~5.5 μm coating thickness). For implantation, animals were anesthetized by 4% isoflurane inhalation that was maintained by 2.5%-3% isoflurane inhalation. The left leg was shaved and treated with betadyne**,** an incision made from the hip to the knee, and the biceps femoris and vastus lateralis muscles were separated to expose the sciatic nerve. For gold mesh cuffs, meshes of approximately 5.5x6 mm were placed underneath the nerve and loosely wrapped around the nerve until the sides of the cuff were slightly overlapping. The sides of the nerve cuff were then tied together using surgeon knots and Ethicon Vicryl Plus 6-0 degradable sutures (esutures.com, Mokena, IL). Prior to implantation, the ends of the gold meshes were dipped in silicone to prevent any tissue damage from sharp ends. For silicone cuffs, the nerve was gently lifted from the underlying tissue and kwik-cast was applied around the nerve for a distance of approximately 6mm so that the nerve was encapsulated. The distal end of the nerve cuffs were generally located 1cm proximal to the bifurcation into the tibial and common peroneal branches. Following cuff implantation, the muscles were sutured using Ethicon Vicryl Plus 5-0 degradable sutures and the skin was closed using

Ethicon Ethilon 4-0 nylon sutures. A fourth group of age-matched animals (n=8) which did not undergo surgery were used as controls.

Euthanasia and Tissue Preparation

Following a 60-day implantation period, animals were terminally anesthetized using an intraperitoneal injection of ketamine (70 mg/kg) and xylazine (30 mg/kg). Following anesthesia, animals were transcardially perfused with pH 7.4 phosphate buffered saline (PBS) followed by 4% paraformaldehyde in PBS. The sciatic nerve from each leg was dissected free and postfixed in 4% paraformaldehyde in PBS overnight and then stored in PBS with 0.01% sodium azide at 4 °C.

Postfixed nerves were hand cut in cross-section immediately proximal and distal to the nerve cuffs to produce nerve segments approximately 2 mm in length. The cuffs were then carefully removed using microdissection scissors, and an additional 2 mm section was taken at the center of the cuff area. Nerve sections from the contralateral nerve were taken at approximately the same location as the cuff with respect to distance from the bifurcation. Sections from control animals were taken 1 cm proximal to the bifurcation. Nerve segments were further postfixed in 4% paraformaldehyde / 2% glutaraldehyde in PBS for 24 hours followed by equilibration in a 2% osmium tetroxide in 0.1 M sodium cacodylate buffer for 24 hours. Sections were then dehydrated through a graded ethanol series, cleared with propylene oxide, and embedded in Embed 812 (Electron Microscopy Sciences, Hatfield, PA). Sections were cut at 0.6 μm using an Ultracut EMUC6 (Leica, Bannockburn, IL), placed on Superfrost Plus glass slides, and stained with thionin and acridine orange (Sigma-Aldrich, St. Louis, MO). Sections were coverslipped using Cytoseal XYL (Richard-Allan Scientific, Kalamazoo, MI).

Explanted cuffs were immunohistochemically stained for CD68 to identify macrophages at the material-tissue interface. Briefly, cuffs were placed in wells and incubated in a blocking solution consisting of 4% (v/v) goat serum (Invitrogen, Carlsbad, CA), 0.05% (v/v) Triton-X 100, and 0.01% (w/v) sodium azide overnight at 4 °C. Sections were then treated with primary antibody against CD68 (0.5 μg/ml, AbD Serotec, Raleigh, NC) in blocking solution for 24 hours at 4 °C and followed by three room temperature rinses in PBS (2 hour/rinse). The appropriate secondary antibody (2 μg/ml, Invitrogen, Carlsbad, CA) in blocking solution was added for 24 hours at 4°C and followed by three additional room temperature rinses in PBS. Sections were then placed on slides and imaged using a FluoView 1000 confocal microscope (Olympus, Center Valley, PA).

Quantitative Analysis

Thin section images were obtained using ImagePro Plus 4.0 (MediaCybernetics, Bethesda, MD) and a color CCD camera (Photometrics, Tucson, AZ) attached to a Nikon E600 microscope. Whole nerve images were obtained at 200x final magnification, while fascicle images were obtained at 1000x final magnification. For both whole nerve and fascicle imaging, serial overlapping images were taken over the entire area of interest using a Labview driven motorized stage (Prior Scientific, Rockland, MA). These images were reconstructed in Adobe Photoshop CS to form mosaic images from which morphometric parameters were derived. Fascicle areas were calculated by manually tracing the inner edge of the perineurium and total myelinated fiber counts were performed manually. A custom Labview program was used to identify myelinated nerve fibers from which all other morphometric measurements were automatically obtained.

Statistics

Total fascicle areas, myelinated fiber counts, fiber densities, fiber packing, and mean g-ratio values were compared across groups at a given location (i.e., distal to the cuff), as well as across locations within each group, using a one way ANOVA with a Tukey's posthoc test. Contralateral nerves from implanted animals were compared to control nerves from nonimplanted animals using a Student's t-test. Fiber diameter distributions were compared using a Wilcoxon signed-rank test. P-values below 0.05 were considered significant. All data are represented as mean ±SEM.

Results

Macroscopic Analysis and Immunohistochemistry

Visual inspection of nerve cuffs following dissection of the nerve revealed the presence of fibrous connective tissue around all cuff materials and integrated into the mesh cuffs. Images from immunohistochemical staining of removed cuffs revealed CD68+ cells adjacent to all cuff materials. In the silicone cuff group, these CD68+ cells were contained at the interface between the cuff and the nerve, and at the outer surface of the cuff. In the mesh groups, these cells were ubiquitous within the connective tissue area surrounding and integrated into the nerve cuffs, although immunostaining in the gold with parylene mesh group appeared to be slightly mitigated compared with the gold mesh group (Figure 4-1).

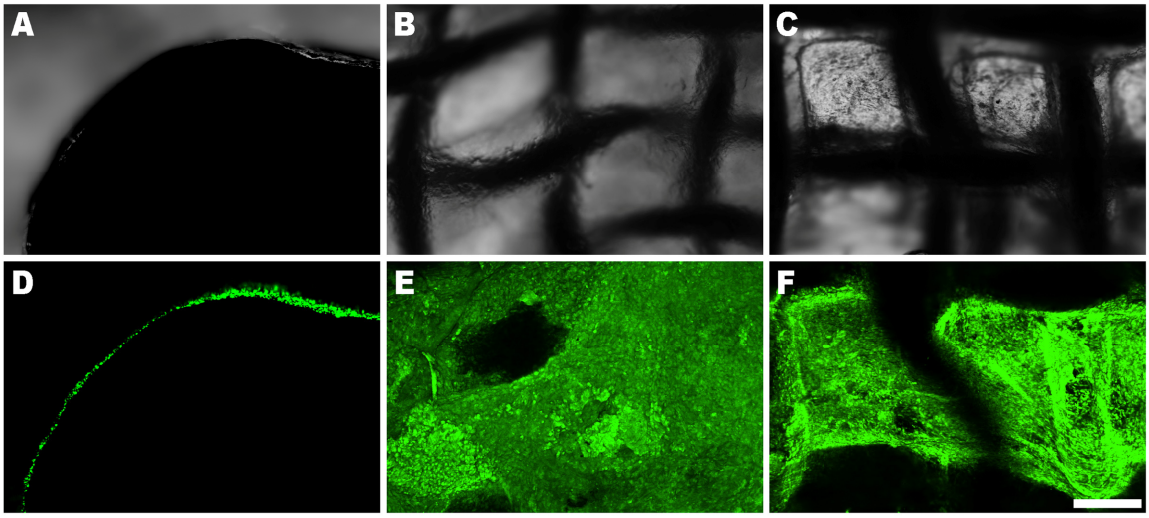

Figure 4-1: Inflammatory reaction to implanted cuffs. **A)** Transmitted light image from a cross-section of a silicone cuff after the nerve has been removed. **B,C)** Transmitted light images of a gold mesh and gold with parylene mesh cuff, respectively, after the cuff has been removed from the nerve and laid flat. **D-F)** Representative z-stack images from the same fields as shown in A-C stained with CD68 for activated macrophages. **D)** The silicone cuff has a thin layer of CD68+ cells lining the cuff-nerve interface. **E)** The gold mesh cuff demonstrates ubiquitous CD68+ staining. **F)** The gold with parylene mesh cuff also shows numerous CD68+ cells, although there appear to be some areas devoid of staining, unlike the gold mesh cuffs. Scale bar = 200 µm

Fascicle Areas, Fiber Counts, and Fiber Density

Nerve sections that were proximal to, distal to, and at the implant site, as well as from the contralateral nerve and control nerves, were evaluated for morphometric parameters including fascicle area, myelinated fiber count, fiber density, fiber packing, mean g-ratio, and g-ratio and fiber diameter distributions. No significant differences were detected for fascicle areas across experimental groups at a specific location, or within specific groups across locations (Figure 4-2). Additionally, no differences were detected between contralateral and control nerves.

Fiber counts also did not show differences across groups at a specific location; however, significant differences were detected across locations within each group. In the

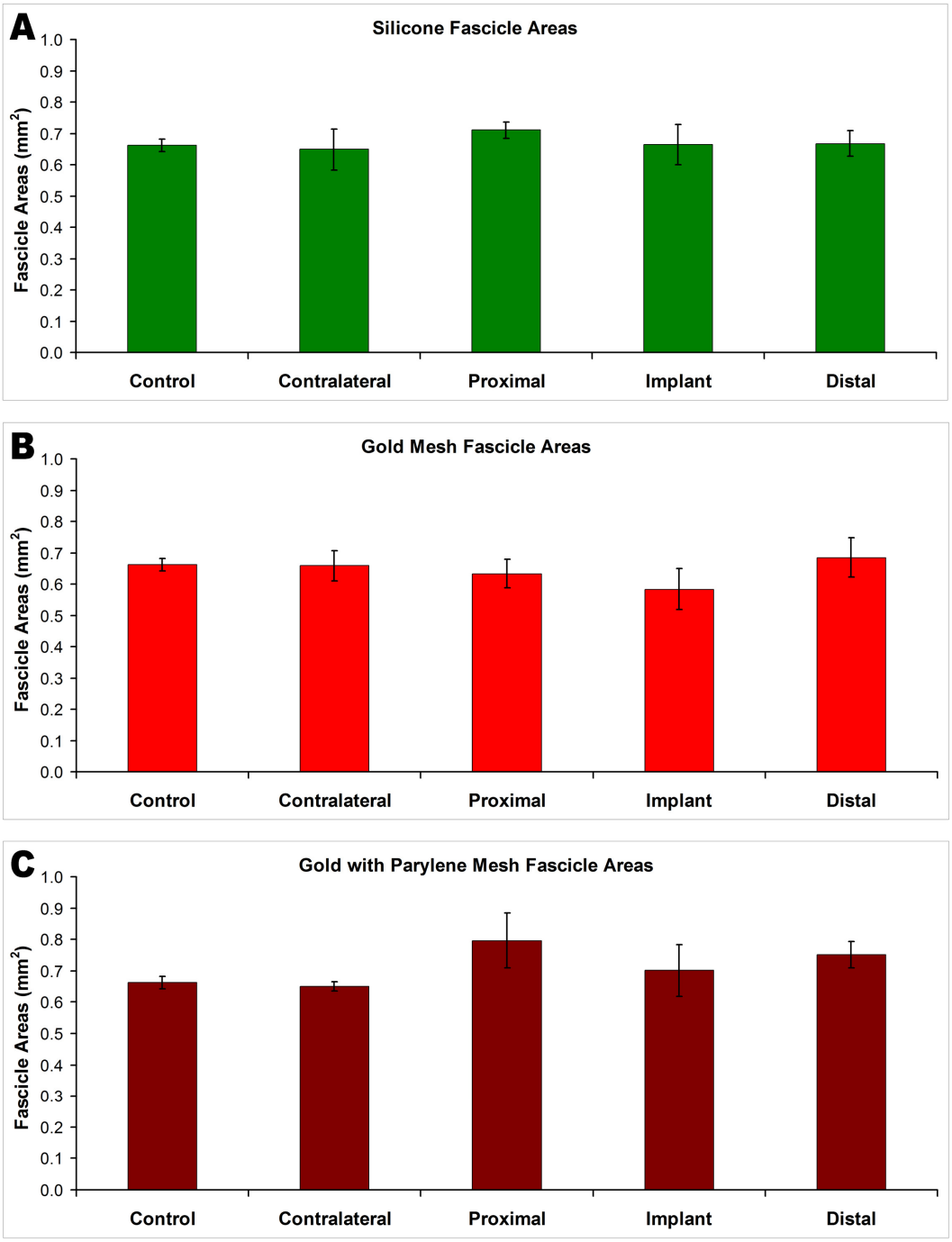

Figure 4-2: Fascicle areas for the silicone, gold mesh, and gold with parylene mesh groups, respectively. No significant differences were detected either across groups at a specific location, or within groups across locations. Additionally, no differences were detected between the contralateral nerves and control nerves.

silicone group, sections distal to the implant showed a reduction in fiber counts compared with proximal sections (Figure 4-3:A). In the gold mesh group, distal sections also showed a reduction in fiber number compared with both proximal and implant sections, as well as with control nerves. Additionally, contralateral nerves showed a significant increase in fiber number compared to control nerves (Figure 4-3:B). In the gold mesh coated with parylene group, sections at the implant site had a statistically smaller number of fibers than proximal sections (Figure 4-3:C). No differences in fiber density were detected in any comparison except in the silicone group where distal sections had a lower density compared with sections at the implant site (data not shown).

Fiber Packing and Mean G-ratio

Fiber packing comparisons revealed significant differences across groups at both distal and implant locations with the gold mesh group showing a decrease in fiber packing compared with the silicone group at the distal location and the gold with parylene group showing a decrease compared with the silicone group at the implant location. Differences were also detected within all three groups. In the silicone group, sections proximal to the implant showed a decrease in fiber packing compared with control nerves (Figure 4-4:A). The gold mesh group exhibited lower values for distal and implant sections compared with control nerves, while only distal sections were significantly lower than proximal sections (Figure 4-4:B). In the gold with parylene group, implant and distal sections also had significantly lower fiber packing values than control nerves and proximal sections (Figure 4-4:C). No differences existed between the contralateral nerves in any group and control nerves.

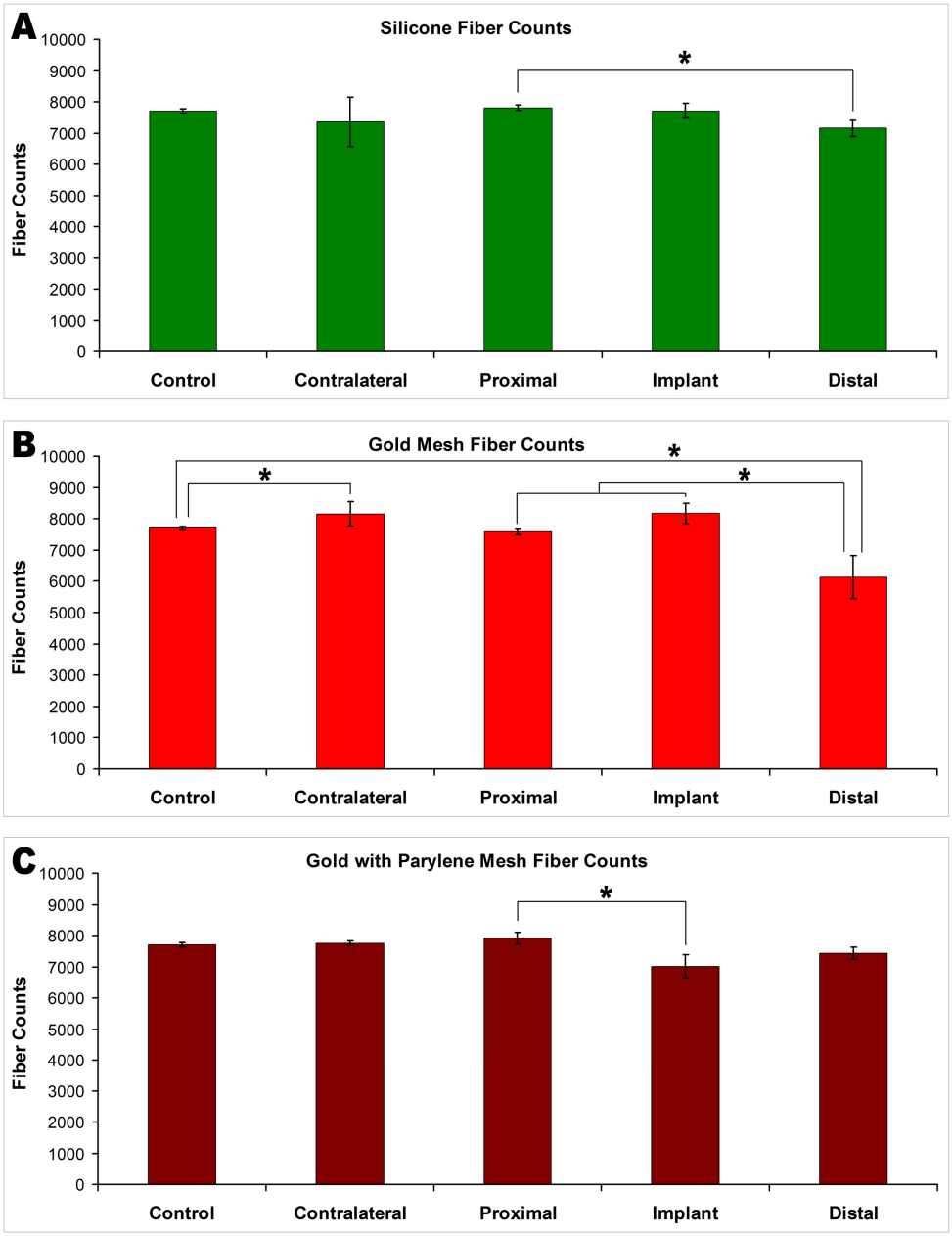

Figure 4-3: Fiber counts for the silicone, gold mesh, and gold with parylene mesh groups, respectively. **A)** Distal sections showed a statistical decrease in fiber counts compared with proximal sections. **B)** Distal counts were smaller compared with implant, proximal, and control sections. Additionally, sections from the contralateral nerve showed a statistical increase in the number of fibers compared with control sections. **C)** Implant sections showed a reduction in fiber count compared with proximal sections. *P<0.05

Figure 4-4: Fiber packing for the silicone, gold mesh, and gold with parylene mesh groups respectively. **A)** Proximal sections showed a reduction in fiber packing compared with control nerves. **B)** Implant and distal sections had lower fiber packing values than control nerves, while distal sections also had lower values compared with proximal sections. Additionally, distal sections from the gold mesh group had lower fiber packing values than distal sections from the silicone group. **C)** Implant and distal sections demonstrated reduced fiber packing compared with both proximal sections and control nerves. Additionally, implant sections from the gold with parylene mesh group had significantly lower fiber packing values than implant sections from the silicone group. No differences existed in any group between contralateral and control nerves. *$P<0.05$

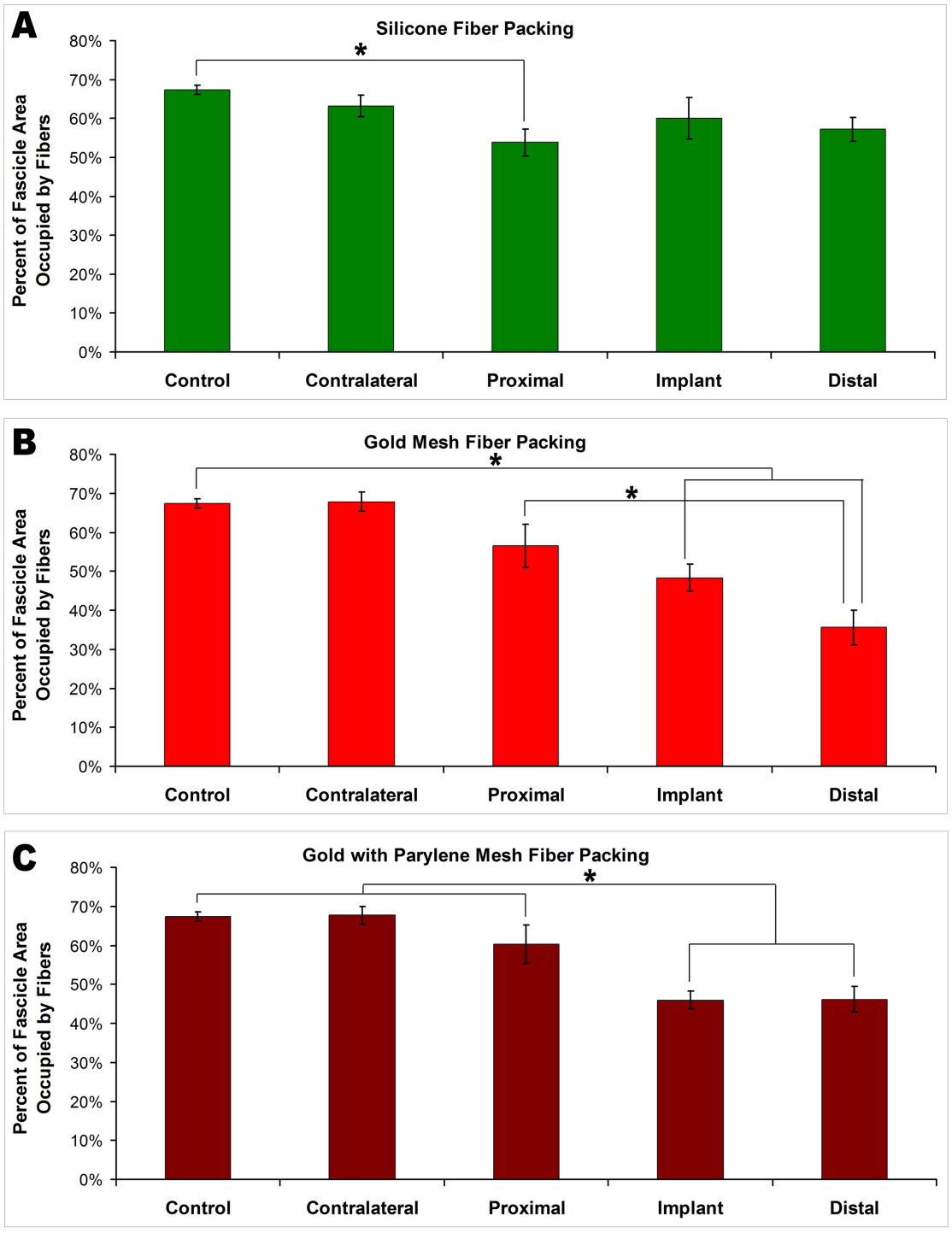
A
Silicone Fiber Packing
Percent of Fascicle Area Occupied by Fibers
80%
70%
60%
50%
40%
30%
20%
10%
0%
*
Control
Contralateral
Proximal
Implant
Distal
B
Gold Mesh Fiber Packing
Percent of Fascicle Area Occupied by Fibers
80%
70%
60%
50%
40%
30%
20%
10%
0%
*
*
Control
Contralateral
Proximal
Implant
Distal
C
Gold with Parylene Mesh Fiber Packing
Percent of Fascicle Area Occupied by Fibers
80%
70%
60%
50%
40%
30%
20%
10%
0%
*
Control
Contralateral
Proximal
Implant
Distal

Mean g-ratio values did not show any differences across groups at a given location. Sections within the silicone group did show differences, with the implant sections having a significantly higher value than both distal and proximal sections (Figure 4-5:A). The gold mesh group revealed the same significant differences between these same locations (Figure 4-5:B). No significant differences were detected in the gold with parylene group (Figure 4-5:C) or between the contralateral nerves of any group and control nerves.

G-ratio and Fiber Diameter Distributions

G-ratio distributions for implanted nerves in the gold and gold with parylene groups, as well as sections from the implant site in the silicone group, appeared to have broader distributions than control and contralateral sections, even when the mean g-ratios were not significantly different (data not shown).

Fiber diameter distributions for the different locations examined are reported in Figure 4-6. Mean bin data from small (<8 μm) and large (≥8 μm) diameter fiber groups were statistically compared across locations and at the same location across groups using a signed-rank test. In the silicone group, sections taken proximal and distal to the implant showed a significant increase in the percent of small fibers compared with control nerves. No changes were observed with large fibers. In the gold mesh group, sections from the implant site and distal to the implant both showed an increase in the percent of small fibers and a reduction in the percent of large fibers compared to both proximal sections and control nerves. Additionally, sections at the implant site had a lower percentage of large fibers than distal sections. Also, proximal sections showed an increase in the percent of small fibers compared to control nerves. Lastly, contralateral nerves exhibited

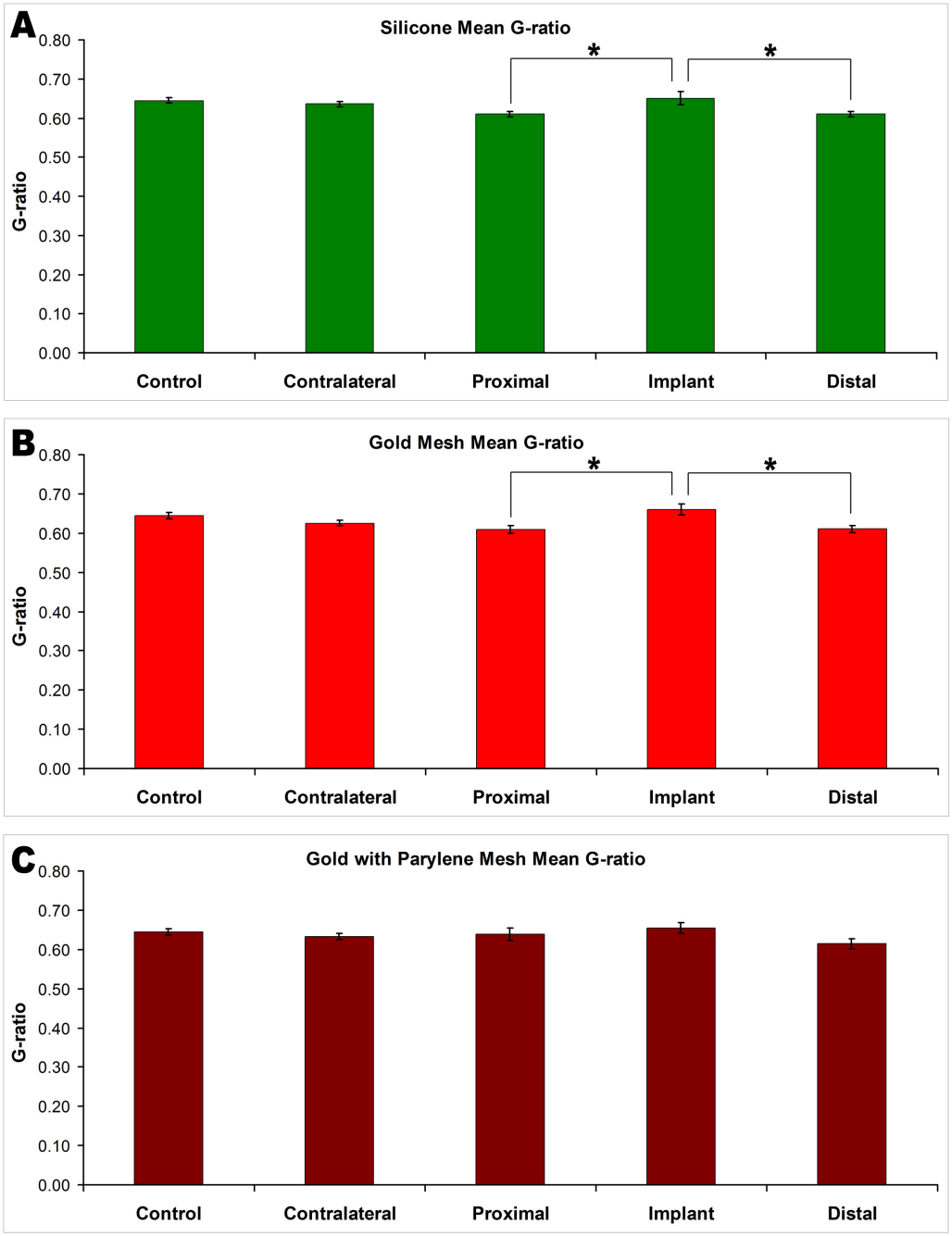

Figure 4-5: Mean g-ratio values for the silicone, gold mesh, and gold with parylene mesh groups respectively. **A)** Implant sections demonstrated higher g-ratio values (thinner myelination) than both proximal and distal sections. **B)** As with the silicone group, implant sections had higher g-ratio values than proximal and distal sections. **C)** No differences existed in mean g-ratio values between any locations. *P<0.05

Figure 4-6: Fiber diameter distributions for the silicone, gold mesh, and gold with parylene mesh groups, respectively. The vertical lines represent the points in the distributions at which bins were separated for statistical analysis. **A)** Distributions from sections proximal and distal to the implant showed a significant increase in the percent of small diameter fibers compared with control nerves. **B)** Distributions from proximal, implant, and distal sections showed an increase in the percent of small diameter fibers compared with control nerves, while implant and distal sections also showed an increase compared with proximal sections. Implant and distal sections also showed a decrease in the percent of large diameter fibers compared with both control nerves and proximal sections. Implant sections showed a reduction in large fibers compared with distal sections. Notably, the contralateral nerve showed a higher percentage of small fibers and a lower percentage of large fibers than control nerves (not shown). Distributions from the implant and distal sections also had a higher percentage of small fibers and a lower percentage of large fibers compared with the same locations in the silicone and gold with parylene groups. Proximal sections also had a larger percentage of small fibers than sections from the gold with parylene mesh group. **C)** Distributions from the implant and distal locations had a higher percentage of small fibers and a lower percentage of large fibers than control nerves, while implant sections also had an increased percentage of small fibers and a decreased percentage of large fibers compared with both proximal and distal sections. Additionally, distal sections demonstrated a higher percentage of small fibers than proximal sections. Distributions from the implant and distal sections also had a larger percentage of small fibers compared with the silicone group, while distal sections showed a decrease in the percentage of large fibers compared with the silicone group.

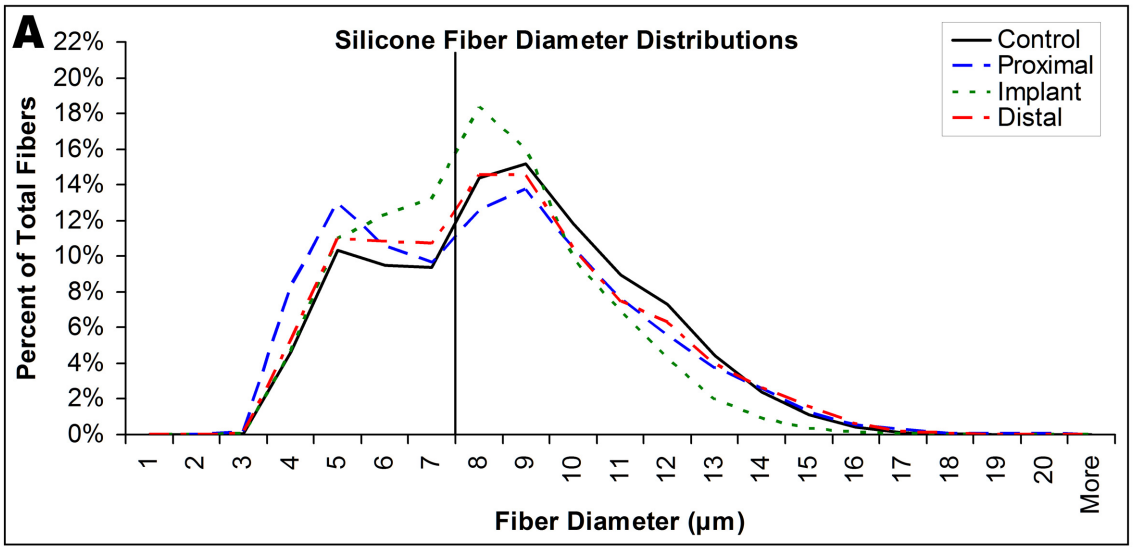
A
Silicone Fiber Diameter Distributions
Control
Proximal
Implant
Distal
Percent of Total Fibers
22%
20%
18%
16%
14%
12%
10%
8%
6%
4%
2%
0%
1 2 3 4 5 6 7 8 9 10 11 12 13 14 15 16 17 18 19 20 More
Fiber Diameter (µm)

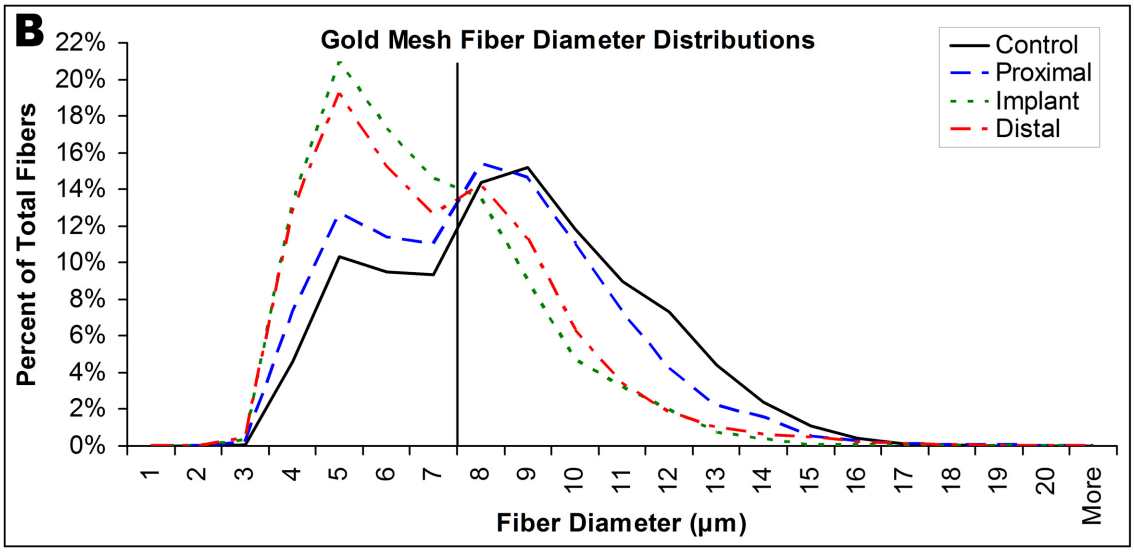
B
Gold Mesh Fiber Diameter Distributions
Control
Proximal
Implant
Distal
Percent of Total Fibers
22%
20%
18%
16%
14%
12%
10%
8%
6%
4%
2%
0%
1 2 3 4 5 6 7 8 9 10 11 12 13 14 15 16 17 18 19 20 More
Fiber Diameter (µm)

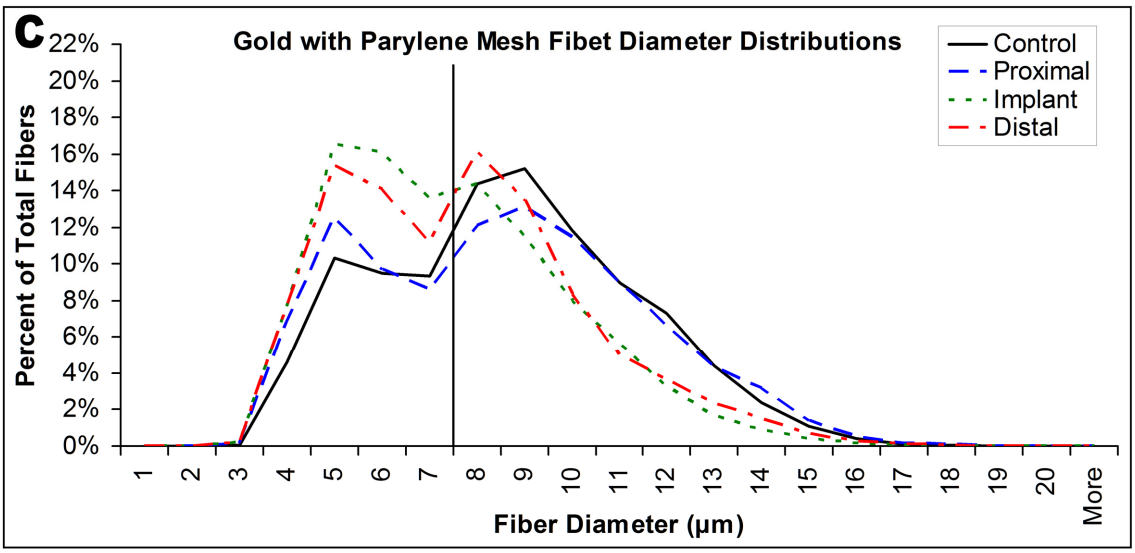
C
Gold with Parylene Mesh Fibet Diameter Distributions
Control
Proximal
Implant
Distal
Percent of Total Fibers
22%
20%
18%
16%
14%
12%
10%
8%
6%
4%
2%
0%
1 2 3 4 5 6 7 8 9 10 11 12 13 14 15 16 17 18 19 20 More
Fiber Diameter (µm)

were statistically compared across locations and at the same location across groups using a signed-rank test. In the silicone group, sections taken proximal and distal to the implant showed a significant increase in the percent of small fibers compared with control nerves. No changes were observed with large fibers. In the gold mesh group, sections from the implant site and distal to the implant both showed an increase in the percent of small fibers and a reduction in the percent of large fibers compared to both proximal sections and control nerves. Additionally, sections at the implant site had a lower percentage of large fibers than distal sections. Also, proximal sections showed an increase in the percent of small fibers compared to control nerves. Lastly, contralateral nerves exhibited a higher percentage of small diameter fibers and a lower percentage of large diameter fibers than control nerves. The gold with parylene group had similar results as the gold group with implant and distal sections having higher percentages of small fibers and lower percentages of large fibers compared to control nerves. Implant sections also had an increased percentage of small fibers and a decreased percentage of large fibers compared to both proximal and distal sections, while distal sections had a higher percent of small fibers than proximal sections. However, proximal and contralateral sections did not show differences from control sections.

Evaluating across groups at the same location, the gold mesh group had a higher percent of small fibers and a lower percent of large fibers than the silicone group at the implant and distal locations, with the same results compared with the gold with parylene group at the implant, distal, and contralateral locations. Proximal sections from the gold group also had a higher percentage of small fibers than did the gold with parylene group. The gold with parylene group also had a higher percentage of small fibers compared with

the silicone group at the distal and implant locations, while a decrease in the percent of large fibers compared with the silicone group was only observed at the distal location.

Discussion

This study suggests that the chronic presence of a nerve cuff in rat sciatic nerve, irrespective of the materials or designs we tested, elicits a foreign body reaction which includes the presence of activated macrophages, the deposition of connective tissue around, or incorporated into, the material, and significant changes in morphometric parameters, although such changes were more prevalent in the mesh groups compared with the silicone group.

During dissection of the nerve cuffs, we observed the presence of fibrous connective tissue surrounding the silicone cuffs and integrated into the mesh cuffs. Connective tissue deposition around solid silicone nerve cuffs has been described previously [43, 125, 128]. However, to our knowledge mesh materials have never been histologically evaluated as nerve cuffs although they have been extensively studied in hernia repair and a similar connective tissue ingrowth and macrophage response as we observed has been described in these applications [199-201].

In addition to connective tissue deposition around the silicone cuffs, we observed a thin layer of CD68+ macrophages at the biotic/abiotic interface. Likewise, we observed CD68+ cells surrounding, and within, the mesh grids. It is important to note that while the CD68+ layer associated with the silicone group was thin, the CD68+ layer associated with the mesh cuffs was thick and extended through the entire thickness of the mesh material. Given the fact that activated macrophages in the peripheral nervous system secrete proinflammatory cytokines [65, 128, 202], the inflammatory footprint of the

mesh cuffs was therefore likely much greater than that of the silicone cuffs. Additionally, while the CD68 reaction around gold cuffs coated with parylene appeared somewhat reduced compared with the uncoated gold mesh group, it did not appear that this difference was significant. It has recently been shown by our lab that a Parylene-C coating reduces microglia, the resident brain macrophage, attachment *in vitro* and *in vivo* [167, 203]. Therefore, since we observed no large difference in the macrophage response to the gold with parylene mesh group compared with the gold mesh group, we hypothesize that the macrophage reaction around the mesh cuffs is due to cuff design rather than the material at the interface.

We had initially hypothesized that the mesh cuffs would result in fewer morphometric changes in the underlying nerve than silicone cuffs, due to the fact that the mesh cuffs would allow connective tissue growth through the cuff which would mitigate any compression injury in the nerve due to connective tissue deposition at the biotic/abiotic interface. However, we found that morphometric changes appeared to be exacerbated in the cuff groups, rather than mitigated. This exacerbation was particularly evident in fiber packing and fiber diameter distribution measurements. Since it is highly unlikely that the mesh cuffs created a compression injury due to connective tissue deposition, these results must be attributed to other phenomenon. One potential factor could be nerve constriction at the time of initial implantation due to the cuff itself, although care was taken to avoid placing the cuff on too tightly. A more likely factor is the extensive inflammatory reaction observed around the mesh cuffs when compared to the silicone cuffs. The diffusion of cytokines from inflammatory cells into the nerve

could lead to the recruitment and activation of macrophages and Schwann Cells within the fascicular space, leading to nerve degeneration.

We also observed in this study that the animals in the gold mesh cohort showed morphometric changes in fiber count and fiber diameter distributions in the contralateral nerve compared to control animals. This observation supports the findings of previous researchers that unilateral implantation or manipulation can lead to contralateral changes [169, 187]. However, the cause of these changes remains unknown. Previous researchers have shown that unilateral implantation of a nerve cuff electrode, or even simply unilaterally transecting the nerve, is sufficient to cause increases in contralateral nerve proinflammatory cytokine levels [128, 183], suggesting that if the degree of inflammation around a nerve cuff is great enough, contralateral changes could be induced by increased proinflammatory cytokine levels within the nerve. Alternatively, contralateral changes could be due to nerve atrophy due to sedentary lifestyles if the animal develops deficiencies in the implanted nerve which would restrict or make movement uncomfortable. However, we observed no qualitative difference in animal behavior between groups, suggesting that animal behavior is an unlikely cause for such changes.

Conclusion

This study finds that nerve cuffs are associated with a persistent inflammatory response which is exacerbated in mesh cuff designs. This foreign body reaction also induces changes in morphometric parameters which are again exacerbated in the mesh cuff groups. It is therefore plausible that the degree of inflammation strongly influences morphometric changes which occur in the underlying nerve. Based on this interpretation,

efforts should continue to be made to reduce the inflammatory footprint of these devices to increase their efficacy in neuroprosthetic applications. Finally, we observed that in our animal cohort which exhibited the greatest degree of change in morphometric parameters, that some parameters in the contralateral nerve were also affected. This suggests that the use of contralateral nerves as internal controls is inappropriate as unilateral implantation can lead to contralateral change.

CHAPTER 5

SUMMARY, CONCLUSIONS, AND FUTURE WORK

Summary and Conclusions

Microelectrodes which interface with the PNS offer the potential for use in neuroprosthetic devices, such as prosthetic limbs. However, as reviewed in Chapter 1, these electrodes elicit a foreign body reaction which may negatively affect device performance. In order to find ways to mitigate such a response, a basic understanding of the extent of this reaction must first be obtained. Specifically, the foreign body response to the chronic implantation of axially penetrating arrays has not been well studied either qualitatively or quantitatively. Further, although the response to nerve cuffs has been relatively well studied, the mast majority of these studies have used only one class of devices, namely solid silicone cuffs. Therefore, proposed alterations in cuff design to improve biocompatibility, such as mesh designs which may allow cytokines to diffuse away from the nerve, or different material compositions, such as the use of electrically shielding materials, is not well understood.

In Chapter 2, morphometric parameters from cat sciatic nerves implanted with USEAs from 13-350 days were quantified and compared with contralateral, nonimplanted nerves. Additionally, sections from the implant site, as well as proximal to the implant but still encapsulated by the silicone containment cuff, were assessed for

inflammation using IHC. Our results indicated that the chronic implantation of these devices causes a persistent inflammatory reaction with the pathological hallmark being the presence of activated macrophages. This inflammatory reaction was present at the interface of the nerve with the encapsulating cuff, as well as at base of the microelectrode array. The presence of activated macrophages continued down the electrode tines in the epineurial space, but became more diffuse in the endoneurial space. Quantitative data suggested that the chronic implantation of these electrodes, along with their accompanying encapsulation cuffs, was sufficient to decrease fiber packing values in the implanted nerves, as well as shift fiber diameter distributions toward smaller diameter fibers. However, no statistical differences were detected in fascicle area, fiber count, fiber density, or g-ratio distributions. These data suggest that, although ongoing efforts should be made to reduce the inflammatory footprint of these devices, a large number of presumptively viable fibers can be supported in implanted nerves.

In analyzing the results from Chapter 2, the question arose of whether the differences in morphometric parameters that were observed could be due to natural differences in these parameters based on nerve location. Therefore, in Chapter 3, we sought to evaluate these parameters in naïve nerves from both cats and rats to determine the influence of nerve location and animal age on morphometric data. In rats, the side of the animal from which the nerve was taken did not significantly alter morphometric parameters except for g-ratio values which were different between left and right nerves for both age groups studied. Animal age, however, did significantly alter a number of morphometric parameters including fascicle area and fiber packing, which were larger in older rats, and fiber density, which was lower in older rats. Additionally, fiber diameter

distributions were significantly different between the two age groups tested in rats, with the slightly older group showing a shift in the distribution towards larger diameter fibers. The cat nerves that we collected also revealed some significant differences between parameters based on nerve location. Fascicle areas were significantly larger at locations closer to the bifurcation into the tibial and peroneal branches, while fiber packing values were significantly larger in the right nerves compared with the left. Additionally, right nerves showed significantly different fiber diameter distributions than the left nerves, with the right nerves having a larger proportion of large diameter fibers and a smaller proportion of small diameter fibers. These data suggest that, when evaluating morphometric parameters, the use on nonaged-matched control animals or the use of the contralateral nerve as an internal control (a method employed frequently in the literature, particularly in cat models) is inappropriate.

Since we had found significant differences in fiber packing between implanted (generally the left nerve) and contralateral nerves in Chapter 2, as well as significant shifts in implanted nerve fiber diameter distributions, we decided to normalize our data from Chapter 2 with the data collected in Chapter 3 to see if significant and nonsignificant differences in the parameters we tested held true. While we continued to see no significant differences in fiber counts and densities, we did reveal a significant difference in fascicle areas where none previously existed. We found that, after normalization, sections proximal to the implant showed a significant increase in total fascicle area compared with contralateral nerves. Additionally, we found that mean g-ratio values, which were not significantly different in Chapter 2, became significantly different between distal sections and contralateral sections after normalization, with distal

sections having a higher g-ratio value (thinner myelination). In contrast to this new significance, we found that normalization of our data from Chapter 2 eliminated any significant differences in fiber packing values. We also found that normalization did not change significant differences found in fiber diameter distributions.

In Chapter 2, we found that the silicone encapsulation cuff used to maintain the position of the electrode array appeared to cause an inflammatory reaction on its own. In order to better understand the tissue reaction to these silicone cuffs, as well as investigate the reaction surrounding porous cuffs which could allow proinflammatory cytokines to diffuse away from the nerve, we evaluated rat sciatic nerves which were implanted with nerve cuffs for 2 months. We found that solid silicone cuffs elicited a persistent inflammatory response at the material interface, but that the inflammatory response to gold mesh or gold coated with parylene mesh cuffs elicited a much larger response. We propose that this greater response has to do with device architecture which allows the deposition of connective tissue in between mesh grids. This large volume of connective tissue can then be infiltrated with inflammatory cells, whereas with the solid silicone cuffs which directly abutted the nerve, only a very small volume exists between the nerve and the cuff for inflammatory cell infiltration. We also found that the implantation of these cuff devices was sufficient to alter morphometric parameters in the underlying nerve. Specifically, we found that fiber counts, fiber densities, fiber packing, mean g-ratio values, and fiber diameter distributions were significantly altered after cuff implantation. Solid silicone cuffs seemed to exhibit the least severe changes, while the gold mesh cuffs seemed to elicit the largest changes. We also observed that in the gold mesh group, fiber diameter distributions from the contralateral nerve were significantly

different from control nerves, suggesting that ipsilateral implantation or manipulation of a nerve may be sufficient to cause morphometric changes on the contralateral side. Whether these changes are due to some systemic inflammatory response or changes in animal behavior are not clear, but again underscore that the use of contralateral nerves as internal controls is not appropriate. This work suggests that, although nerve cuffs have been used successfully in clinical applications for long periods of time, continued efforts should be made to reduce the inflammatory footprint of these devices. This is particularly important when cuffs are used as containment devices for other electrodes, as the cuff could exacerbate the response to the electrode itself.

Future Work

The Influence of Peripheral Nerve Implantation on Hippocampal Neurogenesis

As outlined in this dissertation, the implantation of nerve cuffs and/or penetrating electrodes causes a persistent inflammatory response and alters morphometric parameters in the underlying nerve. However, it is less clear what systemic effects the implantation of such devices might have.

It has been previously shown that a single peripheral injection of bacterial lipopolysaccharide (LPS), which induces systemic inflammation, is sufficient to decrease hippocampal neurogenesis after 1 week [204]. It has also been shown in our lab that the implantation of microelectrodes or hollow fiber membranes in the cortex, away from the hippocampus, is sufficient to reduce neurogenesis [205]. We have shown here that a persistent inflammatory response is associated with the implantation of peripheral nerve electrodes and nerve cuffs. However, it is not clear if the degree of inflammation around

these devices, which are implanted in the PNS rather than the CNS, is sufficient to cause a decrease in hippocampal neurogenesis. It has been previously shown by others that the peripheral implantation of a sieve electrode is sufficient to alter the expression of calcium-binding proteins in the cortex, but markers for inflammation and neurogenesis were not investigated [145].

In order to begin to investigate whether the implantation of peripheral nerve electrodes or nerve cuffs is sufficient to alter hippocampal neurogenesis, brains from animals used in Chapter 4 of this work have been harvested and horizontally sectioned. Markers for cellular proliferation and immature neurons will be applied to every 10^{th} section through the entire hippocampus and counted as described previously [205]. Counts from implanted animals will be compared to age-matched nonimplanted animals housed in the same facility. This work is currently underway.

Naturally-Derived Cellular Material for Use as Nerve Cuffs

As outlined in this dissertation, nerve cuffs are commonly used in peripheral nerve electrode applications. However, devices currently used in these applications elicit a chronic foreign body response which can alter the morphometric composition of the underlying nerve. The use of natural, cell-derived materials as nerve cuffs could mitigate this response and improve the biocompatibility of implanted systems.

Our lab has recently developed a technique for harvesting extracellular matrix (ECM) from populations of living cells [206]. Briefly, cells are seeded onto polyurethane foams, created through a phase-inversion process, and allowed to grow for 3 weeks. Following the growth period, cell-seeded scaffolds are rinsed in the same solvent used during the polymer scaffold manufacturing process to dissolve away the polymer from

the cellular material. Following removal of the polymer, the remaining cellular material is rinsed in water and lyophilized. Cellular components may optionally be removed during this process, leaving just ECM.

In order to begin to access the potential use of this process in creating cellular material which may be used as a nerve cuff, we have cultured and harvested material from rat dermal fibroblasts. Harvested cellular material was of sufficient quantity to allow for handling and wrapping of an excised rat sciatic nerve (Figure 5-1:A). We have also begun experiments to evaluate the *in vivo* tissue response of this material by implanting harvested cellular material around the sciatic nerve in SD rats (Figure 5-1:B-C). Following the implantation period, nerves will be examined as in Chapter 4 of this work to determine the potential efficacy of using cell-based materials in nerve cuff applications.

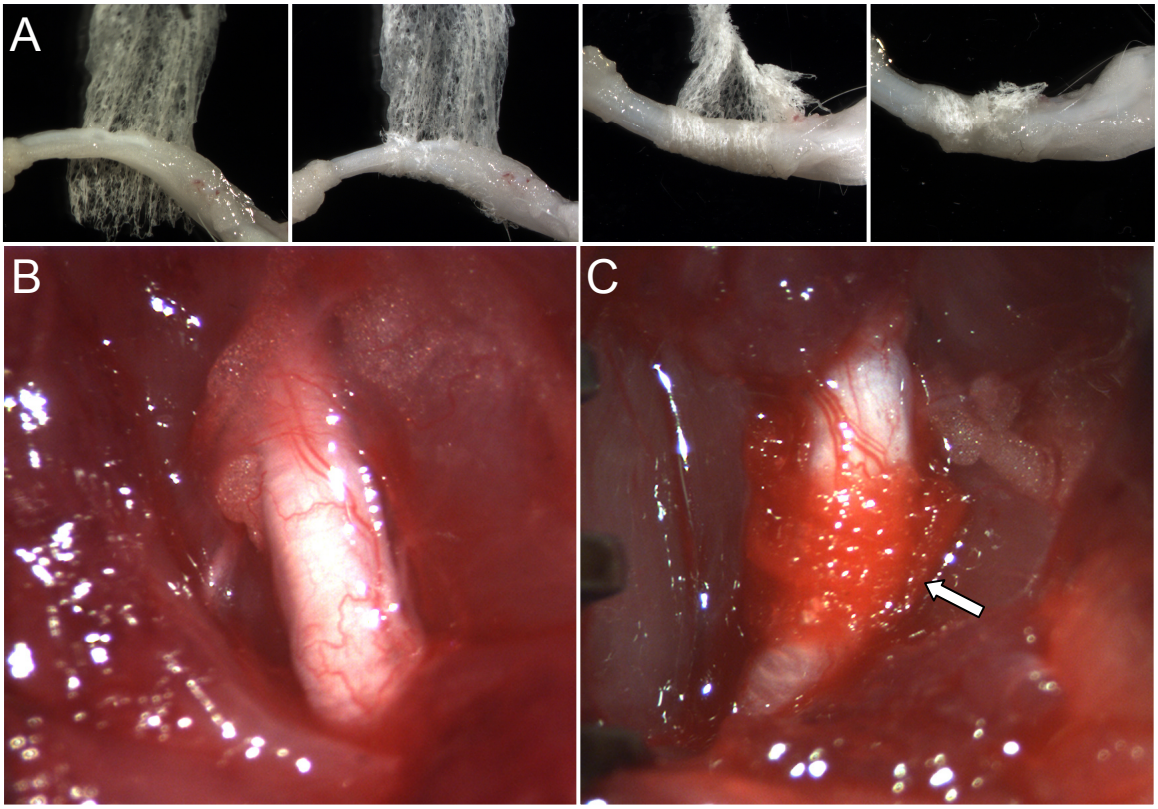

Figure 5-1: Cell-derived materials as nerve cuffs. **A)** Sequence of pictures showing unfixed rat dermal fibroblast material being wrapped around an explanted rat sciatic nerve, demonstrating the feasibility of using such material as an *in* vivo cuff. **B-C)** *In situ* images of rat sciatic nerves used for *in vivo* biocompatibility testing. **B)** A sciatic nerve prior to implantation. The sciatic nerve is easily isolated and can be separated from the surrounding tissue to allow wrapping of the nerve with cell-derived material. **C)** A representative image of a sciatic nerve that has been wrapped with rat dermal fibroblast-derived material (arrow). Lyophilized material is quickly wetting during implantation and sticks to the nerve.

APPENDIX

In Chapter 2 of this dissertation, morphometric parameters in cat sciatic nerves implanted with USEAs were discussed. In evaluating these parameters, since no changes over time were statistically observed, animals were grouped together and implanted nerves were compared with contralateral nerves. However, in order to better understand the possible correlation, if any, between electrode functionality and these parameters, a case-by-case evaluation needs to be undertaken. To this end, we have compiled information from each animal, including total implantation time, time from implantation to recording failure, and time from implantation to stimulation failure, as well as the reason for device failure, if known, as presented in Table A-1.

As seen from Table A-1, successful recordings from the implanted nerve for the duration of the implant were only obtained in one animal, F06-079. Successful stimulation of the nerve for the duration of the implant was achieved in five animals. Unfortunately, it is difficult to draw conclusions about the ability of the electrode itself to function as the reason for device failure was primarily attributed to connector and wire failure. Therefore, the electrode array itself might have maintained the ability to function had the other components of the device not failed. Thus, a comparison of histological outcomes in animals where successful recording or stimulation was accomplished throughout the duration of the implant compared with those animals where recording and stimulation failed prior to sacrifice, might be misleading when trying to draw conclusions

Table A-1: Outline of animal implantation duration and functional device lifetime.

Animal	Implantation Duration (Days)	Time to Last Successful Recording (Days)	Time to Last Successful Stimulation (Days)	Reason for Failure
F06-027	13	7	13	Failed Connector
F06-026	15	11	15	Failed Connector
F06-079	36	35	None	Infection at Connector
F07-020	40	16	40	Unknown
F06-078	43	28	4	Connector Partially Detached
F07-023	95	18	0	Wire Breakage
F06-041	104	83	12	Failed Connector
F07-018	154	85	85	Wire Breakage
F07-019	161	42	161	Unknown
F06-053	182	12	12	Unknown
F06-002	350	None	350	Failed Connector

about whether morphometric parameters affect electrode performance. Nonetheless, parameters from nerves distal to the implant in animals with successful recoding or stimulation throughout the duration of the implant have been averaged and compared with those from animals without successful recording or stimulation, as presented in Table A-2.

As seen in Table A-2, parameters from animals with and without functional recording or stimulation throughout the duration of the implant exhibit similar values. However, in order to detect whether any significant differences existed, t-tests were conducted between these groups. No significant differences in parameters were detected between nerves from animals where successful recording or stimulation was achieved for the duration of the implant and those where it was not. As previously mentioned, this does not necessarily mean that morphometric parameters have no affect on electrode function as it is not clear whether the electrode arrays from the animals which did not maintain device functionality were still intact. Further studies should be conducted to investigate the possible influence of morphometric parameters on electrode function.

Table A-2: Average ±SEM of morphometric parameters grouped by device functionality.

Parameter	**Values from Animals with Functioning Devices**	**Values from Animals with Nonfunctioning Devices**
Total Fascicle Area (mm^2)	3.09 ±0.40	3.42 ±0.36
Total Fiber Count	18274 ±1880	19925 ±1100
Fiber Density (fibers/mm^2)	6166 ±827	5986 ±591
Fiber Packing	50.9% ±6.7%	41.5% ±6.0%
Mean g-ratio	0.56 ±0.01	0.56 ±0.02

REFERENCES

1. Greenfield S, Brostoff S, Eylar EH, Morell P. Protein composition of myelin of the peripheral nervous system. J Neurochem. 1973;20(4):1207-1216.

2. Wolfgram F, Kotorii K. The composition of the myelin proteins of the peripheral nervous system. J Neurochem. 1968;15(11):1291-1295.

3. Hofteig JH, Vo PN, Yates AJ, Leon KS. Peripheral nerve phospholipid composition: development in normal nerve and age-dependent changes in Wallerian degenerated nerve. J Neurochem. 1982;39(2):401-408.

4. Fullerton PM, Gilliatt RW, Lascelles RG, Morgan-Hughes JA. The relationship between fibre diameter and internodal length in chronic neuropathy. Journal of Physiology. 1965:26-28.

5. Friede RL, Beuche W. A new approach toward analyzing peripheral nerve fiber populations. I. Variance in sheath thickness corresponds to different geometric proportions of the internodes. J Neuropathol Exp Neurol. 1985;44(1):60-72.

6. Vizoso AD, Young JZ. Internode length and fibre diameter in developing and regenerating nerves. J Anat. 1948;82(Pts 1-2):110-134.

7. Ranvier LA. Contributions al'histologie et a la physiologie des nerf peripheriques. Comptes Rendus de l'Academie Sciences. 1871.

8. Helmholtz H. On the rate of transmission of the nerve impulse. Monatsber Preuss Akad Wiss Berl. 1850.

9. Sato A, Sato Y, Suzuki H. Aging effects on conduction velocities of myelinated and unmyelinated fibers of peripheral nerves. Neurosci Lett. 1985;53(1):15-20.

10. Krarup C, Buchthal F. Conduction studies in peripheral nerve. Neurobehav Toxicol Teratol. 1985;7(4):319-323.

11. Hursh JB. Conduction velocity and diameter of nerve fibers. Am J Physiol. 1939;127:131-139.

12. Fugleholm K, Schmalbruch H, Krarup C. Early peripheral nerve regeneration after crushing, sectioning, and freeze studied by implanted electrodes in the cat. J Neurosci. 1994;14(5 Pt 1):2659-2673.

13. Waxman SG. Determinants of conduction velocity in myelinated nerve fibers. Muscle Nerve. 1980;3(2):141-150.

14. Remak R. Observationes anatomicae et microscopicae de systematis nervosi structura. Berlin; 1838.

15. Tuckett IL. On the Structure and Degeneration of Non-Medullated Nerve Fibres. J Physiol. 1896;19(4):i1-311.

16. Gasser HS. Unmedullated fibers originating in dorsal root ganglia. J Gen Physiol. 1950;33(6):651-690.

17. Gasser HS. Properties of dorsal root unmedullated fibers on the two sides of the ganglion. J Gen Physiol. 1955;38(5):709-728.

18. Grundfest H, Gasser HS. Properties of mammalian nerve fibers of slowest conduction. Am J Physiol. 1938;123:307-318.

19. Thomas PK, Jones DG. The cellular response to nerve injury. II. Regeneration of the perineurium after nerve section. J Anat. 1967;101(Pt 1):45-55.

20. Radek A, Thomas PK, King RH. Perineurial differentiation in interchange grafts of rat peripheral nerve and spinal root. J Anat. 1986;147:207-217.

21. Thomas PK. The connective tissue of peripheral nerve: an electron microscope study. J Anat. 1963;97:35-44.

22. Schroder JM. Altered ratio between axon diameter and myelin sheath thickness in regenerated nerve fibers. Brain Res. 1972;45(1):49-65.

23. Waxman SG. Conduction in myelinated, unmyelinated, and demyelinated fibers. Arch Neurol. 1977;34(10):585-589.

24. Murinson BB, Archer DR, Li Y, Griffin JW. Degeneration of myelinated efferent fibers prompts mitosis in Remak Schwann cells of uninjured C-fiber afferents. J Neurosci. 2005;25(5):1179-1187.

25. Kristensson K, Olsson Y. The perineurium as a diffusion barrier to protein tracers. Acta Neuropathol. 1971;17(2):127-138.

26. Waggener JD, Bunn SM, Beggs J. The diffusion of ferritin within the peripheral nerve sheath: an electron microscopy study. J Neuropathol Exp Neurol. 1965;24(3):430-443.

27. Olsson Y, Kristensson K. The perineurium as a diffusion barrier to protein tracers following trauma to nerves. Acta Neuropathol. 1973;23(2):105-111.

28. Myers RR, Heckman HM, Powell HC. Endoneurial fluid is hypertonic. Results of microanalysis and its significance in neuropathy. J Neuropathol Exp Neurol. 1983;42(3):217-224.

29. Luque EH, Angulo E, Montes GS. A histochemical and electron microscopic study on the collagen of nerves in the domestic fowl. J Anat. 1983;137 (Pt 1):171-176.

30. Shellswell GB, Restall DJ, Duance VC, Bailey AJ. Identification and differential distribution of collagen types in the central and peripheral nervous systems. FEBS Lett. 1979;106(2):305-308.

31. Junqueira LC, Montes GS, Krisztan RM. The collagen of the vertebrate peripheral nervous system. Cell Tissue Res. 1979;202(3):453-460.

32. Bennett D. An anatomical and histological study of the sciatic nerve, relating to peripheral nerve injuries in the dog and cat. J Small Anim Pract. 1976;17(6):379-386.

33. Schmalbruch H. Fiber composition of the rat sciatic nerve. Anat Rec. 1986;215(1):71-81.

34. Lago N, Ceballos D, Rodriguez FJ, Stieglitz T, Navarro X. Long term assessment of axonal regeneration through polyimide regenerative electrodes to interface the peripheral nerve. Biomaterials. 2005;26(14):2021-2031.

35. Ceballos D, Valero-Cabre A, Valderrama E, Schuttler M, Stieglitz T, Navarro X. Morphologic and functional evaluation of peripheral nerve fibers regenerated through polyimide sieve electrodes over long-term implantation. J Biomed Mater Res. 2002;60(4):517-528.

36. Jenq CB, Coggeshall RE. Long-term patterns of axon regeneration in the sciatic nerve and its tributaries. Brain Res. 1985;345(1):34-44.

37. Jenq CB, Coggeshall RE. Numbers of regenerating axons in parent and tributary peripheral nerves in the rat. Brain Res. 1985;326(1):27-40.

38. Jenq CB, Chung K, Coggeshall RE. Postnatal loss of axons in normal rat sciatic nerve. J Comp Neurol. 1986;244(4):445-450.

39. Lago N, Yoshida K, Koch KP, Navarro X. Assessment of biocompatibility of chronically implanted polyimide and platinum intrafascicular electrodes. IEEE Trans Biomed Eng. 2007;54(2):281-290.

40. Rafiuddin Ahmed M, Jayakumar R. Peripheral nerve regeneration in RGD peptide incorporated collagen tubes. Brain Res. 2003;993(1-2):208-216.

41. Rodriguez FJ, Ceballos D, Schuttler M, Valero A, Valderrama E, Stieglitz T, et al. Polyimide cuff electrodes for peripheral nerve stimulation. J Neurosci Methods. 2000;98(2):105-118.

42. Leventhal DK, Cohen M, Durand DM. Chronic histological effects of the flat interface nerve electrode. J Neural Eng. 2006;3(2):102-113.

43. Romero E, Denef JF, Delbeke J, Robert A, Veraart C. Neural morphological effects of long-term implantation of the self-sizing spiral cuff nerve electrode. Med Biol Eng Comput. 2001;39(1):90-100.

44. Sladjana UZ, Ivan JD, Bratislav SD. Microanatomical structure of the human sciatic nerve. Surg Radiol Anat. 2008;30(8):619-626.

45. Waller A. Experiments on the section of the glossopharyngeal and hypoglossal nerves of the frog, and observations of the alterations produced thereby in the structure of their primitive fibres. Philosophical Transactions of the Royal Society of London. 1850;140:423-429.

46. Williams PL, Hall SM. Prolonged in vivo observations of normal peripheral nerve fibres and their acute reactions to crush and deliberate trauma. J Anat. 1971;108(Pt 3):397-408.

47. Schlaepfer WW, Bunge RP. Effects of calcium ion concentration on the degeneration of amputated axons in tissue culture. J Cell Biol. 1973;59(2 Pt 1):456-470.

48. Ballin RH, Thomas PK. Changes at the nodes of ranvier during wallerian degeneration: an electron microscope study. Acta Neuropathol. 1969;14(3):237-249.

49. Liu HM, Yang LH, Yang YJ. Schwann cell properties: 3. C-fos expression, bFGF production, phagocytosis and proliferation during Wallerian degeneration. J Neuropathol Exp Neurol. 1995;54(4):487-496.

50. Cravioto H. Wallerian degeneration: ultrastructural and histochemical studies. Bull Los Angeles Neurol Soc. 1969;34(4):233-253.

51. Morris JH, Hudson AR, Weddell G. A study of degeneration and regeneration in the divided rat sciatic nerve based on electron microscopy. I. The traumatic degeneration

of myelin in the proximal stump of the divided nerve. Z Zellforsch Mikrosk Anat. 1972;124(1):76-102.

52. Pellegrino RG, Politis MJ, Ritchie JM, Spencer PS. Events in degenerating cat peripheral nerve: induction of Schwann cell S phase and its relation to nerve fibre degeneration. J Neurocytol. 1986;15(1):17-28.

53. Witzel C, Rohde C, Brushart TM. Pathway sampling by regenerating peripheral axons. J Comp Neurol. 2005;485(3):183-190.

54. Brushart TM. Motor axons preferentially reinnervate motor pathways. J Neurosci. 1993;13(6):2730-2738.

55. Jenq CB, Coggeshall RE. Regeneration of axons in tributary nerves. Brain Res. 1984;310(1):107-121.

56. Evans DH, Murray JG. A study of regeneration in a motor nerve with a unimodal fiber diameter distribution. Anat Rec. 1956;126(3):311-333.

57. Shawe GD. On the number of branches formed by regenerating nerve-fibres. Br J Surg. 1955;42(175):474-488.

58. Goodrum JF, Earnhardt T, Goines N, Bouldin TW. Fate of myelin lipids during degeneration and regeneration of peripheral nerve: an autoradiographic study. J Neurosci. 1994;14(1):357-367.

59. Griffin JW, George R, Ho T. Macrophage systems in peripheral nerves. A review. J Neuropathol Exp Neurol. 1993;52(6):553-560.

60. Stoll G, Griffin JW, Li CY, Trapp BD. Wallerian degeneration in the peripheral nervous system: participation of both Schwann cells and macrophages in myelin degradation. J Neurocytol. 1989;18(5):671-683.

61. Fernandez-Valle C, Bunge RP, Bunge MB. Schwann cells degrade myelin and proliferate in the absence of macrophages: evidence from in vitro studies of Wallerian degeneration. J Neurocytol. 1995;24(9):667-679.

62. Stoll G, Jander S, Myers RR. Degeneration and regeneration of the peripheral nervous system: from Augustus Waller's observations to neuroinflammation. J Peripher Nerv Syst. 2002;7(1):13-27.

63. Clemence A, Mirsky R, Jessen KR. Non-myelin-forming Schwann cells proliferate rapidly during Wallerian degeneration in the rat sciatic nerve. J Neurocytol. 1989;18(2):185-192.

64. Abercrombie M, Johnson ML. Quantitative histology of Wallerian degeneration: I. Nuclear population in rabbit sciatic nerve. J Anat. 1946;80(Pt 1):37-50.

65. Stoll G, Muller HW. Nerve injury, axonal degeneration and neural regeneration: basic insights. Brain Pathol. 1999;9(2):313-325.

66. Heumann R, Korsching S, Bandtlow C, Thoenen H. Changes of nerve growth factor synthesis in nonneuronal cells in response to sciatic nerve transection. J Cell Biol. 1987;104(6):1623-1631.

67. Acheson A, Barker PA, Alderson RF, Miller FD, Murphy RA. Detection of brain-derived neurotrophic factor-like activity in fibroblasts and Schwann cells: inhibition by antibodies to NGF. Neuron. 1991;7(2):265-275.

68. Friedman B, Scherer SS, Rudge JS, Helgren M, Morrisey D, McClain J, et al. Regulation of ciliary neurotrophic factor expression in myelin-related Schwann cells in vivo. Neuron. 1992;9(2):295-305.

69. Curtis R, Scherer SS, Somogyi R, Adryan KM, Ip NY, Zhu Y, et al. Retrograde axonal transport of LIF is increased by peripheral nerve injury: correlation with increased LIF expression in distal nerve. Neuron. 1994;12(1):191-204.

70. Ip NY, Yancopoulos GD. The neurotrophins and CNTF: two families of collaborative neurotrophic factors. Annu Rev Neurosci. 1996;19:491-515.

71. Dinarello CA. The biological properties of interleukin-1. Eur Cytokine Netw. 1994;5(6):517-531.

72. Lindholm D, Heumann R, Hengerer B, Thoenen H. Interleukin 1 increases stability and transcription of mRNA encoding nerve growth factor in cultured rat fibroblasts. J Biol Chem. 1988;263(31):16348-16351.

73. Bolin LM, Verity AN, Silver JE, Shooter EM, Abrams JS. Interleukin-6 production by Schwann cells and induction in sciatic nerve injury. J Neurochem. 1995;64(2):850-858.

74. Reichert F, Levitzky R, Rotshenker S. Interleukin 6 in intact and injured mouse peripheral nerves. Eur J Neurosci. 1996;8(3):530-535.

75. Ishihara K, Hirano T. IL-6 in autoimmune disease and chronic inflammatory proliferative disease. Cytokine Growth Factor Rev. 2002;13(4-5):357-368.

76. Moore KW, de Waal Malefyt R, Coffman RL, O'Garra A. Interleukin-10 and the interleukin-10 receptor. Annu Rev Immunol. 2001;19:683-765.

77. Oldfors A. Macrophages in peripheral nerves. An ultrastructural and enzyme histochemical study on rats. Acta Neuropathol. 1980;49(1):43-49.

78. Bruck W, Huitinga I, Dijkstra CD. Liposome-mediated monocyte depletion during wallerian degeneration defines the role of hematogenous phagocytes in myelin removal. J Neurosci Res. 1996;46(4):477-484.

79. Vass K, Hickey WF, Schmidt RE, Lassmann H. Bone marrow-derived elements in the peripheral nervous system. An immunohistochemical and ultrastructural investigation in chimeric rats. Lab Invest. 1993;69(3):275-282.

80. Hirata K, Mitoma H, Ueno N, He JW, Kawabuchi M. Differential response of macrophage subpopulations to myelin degradation in the injured rat sciatic nerve. J Neurocytol. 1999;28(8):685-695.

81. Beuche W, Friede RL. The role of non-resident cells in Wallerian degeneration. J Neurocytol. 1984;13(5):767-796.

82. Bendszus M, Stoll G. Caught in the act: in vivo mapping of macrophage infiltration in nerve injury by magnetic resonance imaging. J Neurosci. 2003;23(34):10892-10896.

83. Omura T, Omura K, Sano M, Sawada T, Hasegawa T, Nagano A. Spatiotemporal quantification of recruit and resident macrophages after crush nerve injury utilizing immunohistochemistry. Brain Res. 2005;1057(1-2):29-36.

84. Monaco S, Gehrmann J, Raivich G, Kreutzberg GW. MHC-positive, ramified macrophages in the normal and injured rat peripheral nervous system. J Neurocytol. 1992;21(9):623-634.

85. Williams PL, Hall SM. Chronic Wallerian degeneration--an in vivo and ultrastructural study. J Anat. 1971;109(Pt 3):487-503.

86. Dinarello CA. IL-18: A TH1-inducing, proinflammatory cytokine and new member of the IL-1 family. J Allergy Clin Immunol. 1999;103(1 Pt 1):11-24.

87. Trinchieri G. Interleukin-12: a proinflammatory cytokine with immunoregulatory functions that bridge innate resistance and antigen-specific adaptive immunity. Annu Rev Immunol. 1995;13:251-276.

88. Gillen C, Jander S, Stoll G. Sequential expression of mRNA for proinflammatory cytokines and interleukin-10 in the rat peripheral nervous system: comparison between immune-mediated demyelination and Wallerian degeneration. J Neurosci Res. 1998;51(4):489-496.

89. Stoll G, Jung S, Jander S, van der Meide P, Hartung HP. Tumor necrosis factor-alpha in immune-mediated demyelination and Wallerian degeneration of the rat peripheral nervous system. J Neuroimmunol. 1993;45(1-2):175-182.

90. Boehm U, Klamp T, Groot M, Howard JC. Cellular responses to interferon-gamma. Annu Rev Immunol. 1997;15:749-795.

91. Weerasuriya A, Rapoport SI, Taylor RE. Perineurial permeability increases during Wallerian degeneration. Brain Res. 1980;192(2):581-585.

92. Podhajsky RJ, Myers RR. The vascular response to nerve crush: relationship to Wallerian degeneration and regeneration. Brain Res. 1993;623(1):117-123.

93. Sparrow JR, Kiernan JA. Endoneurial vascular permeability in degenerating and regenerating peripheral nerves. Acta Neuropathol. 1981;53(3):181-188.

94. Weerasuriya A. Patterns of change in endoneurial capillary permeability and vascular space during Wallerian degeneration. Brain Res. 1988;445(1):181-187.

95. Kim JH, Manuelidis EE, Glen WW, Kaneyuki T. Diaphragm pacing: histopathological changes in the phrenic nerve following long-term electrical stimulation. J Thorac Cardiovasc Surg. 1976;72(4):602-608.

96. Mayr W, Bijak M, Girsch W, Holle J, Lanmuller H, Thoma H, et al. Multichannel stimulation of phrenic nerves by epineural electrodes. Clinical experience and future developments. Asaio J. 1993;39(3):M729-735.

97. Glenn WW, Phelps ML. Diaphragm pacing by electrical stimulation of the phrenic nerve. Neurosurgery. 1985;17(6):974-984.

98. Flageole H, Adolph VR, Davis GM, Laberge JM, Nguyen LT, Guttman FM. Diaphragmatic pacing in children with congenital central alveolar hypoventilation syndrome. Surgery. 1995;118(1):25-28.

99. Brindley GS, Polkey CE, Rushton DN, Cardozo L. Sacral anterior root stimulators for bladder control in paraplegia: the first 50 cases. J Neurol Neurosurg Psychiatry. 1986;49(10):1104-1114.

100. Oerlemans DJ, van Kerrebroeck PE. Sacral nerve stimulation for neuromodulation of the lower urinary tract. Neurourol Urodyn. 2008;27(1):28-33.

101. Sutherland SE, Lavers A, Carlson A, Holtz C, Kesha J, Siegel SW. Sacral nerve stimulation for voiding dysfunction: one institution's 11-year experience. Neurourol Urodyn. 2007;26(1):19-28; discussion 36.

102. McNeal DR, Waters R, Reswick J. Experience with implanted electrodes. Neurosurgery. 1977;1(2):228-229.

103. Lyons GM, Sinkjaer T, Burridge JH, Wilcox DJ. A review of portable FES-based neural orthoses for the correction of drop foot. IEEE Trans Neural Syst Rehabil Eng. 2002;10(4):260-279.

104. Wilder RP, Wind TC, Jones EV, Crider BE, Edlich RF. Functional electrical stimulation for a dropped foot. J Long Term Eff Med Implants. 2002;12(3):149-159.

105. Owings MF, Kozak LJ. Ambulatory and inpatient procedures in the United States, 1996. Vital Health Stat 13. 1998;(139):1-119.

106. Branner A, Stein RB, Normann RA. Selective stimulation of cat sciatic nerve using an array of varying-length microelectrodes. J Neurophysiol. 2001;85(4):1585-1594.

107. Kim YH, Lee C, Ahn KM, Lee M, Kim YJ. Robust and real-time monitoring of nerve regeneration using implantable flexible microelectrode array. Biosens Bioelectron. 2009;24(7):1883-1887.

108. Ziegler-Graham K, MacKenzie EJ, Ephraim PL, Travison TG, Brookmeyer R. Estimating the prevalence of limb loss in the United States: 2005 to 2050. Arch Phys Med Rehabil. 2008;89(3):422-429.

109. Stansbury LG, Lalliss SJ, Branstetter JG, Bagg MR, Holcomb JB. Amputations in U.S. military personnel in the current conflicts in Afghanistan and Iraq. J Orthop Trauma. 2008;22(1):43-46.

110. Stinner DJ, Burns TC, Kirk KL, Ficke JR. Return to duty rate of amputee soldiers in the current conflicts in Afghanistan and Iraq. J Trauma. 2010;68(6):1476-1479.

111. Williams D. Objectivity in the evaluation of biological safety of medical devices and biomaterials. Med Device Technol. 1991;2(1):44-48.

112. Whittenberger JL, Sarnoff SJ, Hardenbergh E. Electrophrenic respiration. Ii. its use in man. J Clin Invest. 1949;28(1):124-128.

113. Waters RL, McNeal D, Perry J. Experimental correction of footdrop by electrical stimulation of the peroneal nerve. J Bone Joint Surg Am. 1975;57(8):1047-1054.

114. Picaza JA, Hunter SE, Cannon BW. Pain suppression by peripheral nerve stimulation. Chronic effects of implanted devices. Appl Neurophysiol. 1977;40(2-4):223-234.

115. Stein RB, Nichols TR, Jhamandas J, Davis L, Charles D. Stable long-term recordings from cat peripheral nerves. Brain Res. 1977;128(1):21-38.

116. Rosenkranz D, Fenzl G, Holle J, Lack W, Losert U, Thoma H. Influence of long-term low direct current on rat ischiadic nerves. Appl Neurophysiol. 1986;49(1-2):42-52.

117. Krarup C, Loeb GE. Conduction studies in peripheral cat nerve using implanted electrodes: I. Methods and findings in controls. Muscle Nerve. 1988;11(9):922-932.

118. Naples GG, Mortimer JT, Scheiner A, Sweeney JD. A spiral nerve cuff electrode for peripheral nerve stimulation. IEEE Trans Biomed Eng. 1988;35(11):905-916.

119. Agnew WF, McCreery DB, Yuen TG, Bullara LA. Histologic and physiologic evaluation of electrically stimulated peripheral nerve: considerations for the selection of parameters. Ann Biomed Eng. 1989;17(1):39-60.

120. Jellema T, Teepen JL. A miniaturized cuff electrode for electrical stimulation of peripheral nerves in the freely moving rat. Brain Res Bull. 1995;37(5):551-554.

121. Walter JS, McLane J, Cai W, Khan T, Cogan S. Evaluation of a thin-film peripheral nerve cuff electrode. J Spinal Cord Med. 1995;18(1):28-32.

122. Loeb GE, Peck RA. Cuff electrodes for chronic stimulation and recording of peripheral nerve activity. J Neurosci Methods. 1996;64(1):95-103.

123. Larsen JO, Thomsen M, Haugland M, Sinkjaer T. Degeneration and regeneration in rabbit peripheral nerve with long-term nerve cuff electrode implant: a stereological study of myelinated and unmyelinated axons. Acta Neuropathol (Berl). 1998;96(4):365-378.

124. Agnew WF, McCreery DB, Yuen TG, Bullara LA. Evolution and resolution of stimulation-induced axonal injury in peripheral nerve. Muscle Nerve. 1999;22(10):1393-1402.

125. Grill WM, Mortimer JT. Neural and connective tissue response to long-term implantation of multiple contact nerve cuff electrodes. J Biomed Mater Res. 2000;50(2):215-226.

126. Tyler DJ, Durand DM. Chronic response of the rat sciatic nerve to the flat interface nerve electrode. Ann Biomed Eng. 2003;31(6):633-642.

127. Vince V, Brelen ME, Delbeke J, Colin IM. Anti-TNF-alpha reduces the inflammatory reaction associated with cuff electrode implantation around the sciatic nerve. J Neuroimmunol. 2005;165(1-2):121-128.

128. Vince V, Thil MA, Gerard AC, Veraart C, Delbeke J, Colin IM. Cuff electrode implantation around the sciatic nerve is associated with an upregulation of TNF-alpha and TGF-beta 1. J Neuroimmunol. 2005;159(1-2):75-86.

129. Thil MA, Duy DT, Colin IM, Delbeke J. Time course of tissue remodelling and electrophysiology in the rat sciatic nerve after spiral cuff electrode implantation. J Neuroimmunol. 2007;185(1-2):103-114.

130. Marks AF. Bullfrog nerve regeneration into porous implants. Anat Rec. 1969;163:226.

131. Bowman BR, Erickson RC, 2nd. Acute and chronic implantation of coiled wire intraneural electrodes during cyclical electrical stimulation. Ann Biomed Eng. 1985;13(1):75-93.

132. Malagodi MS, Horch KW, Schoenberg AA. An intrafascicular electrode for recording of action potentials in peripheral nerves. Ann Biomed Eng. 1989;17(4):397-410.

133. Lefurge T, Goodall E, Horch K, Stensaas L, Schoenberg A. Chronically implanted intrafascicular recording electrodes. Ann Biomed Eng. 1991;19(2):197-207.

134. Tyler DJ, Durand DM. A slowly penetrating interfascicular nerve electrode for selective activation of peripheral nerves. IEEE Trans Rehabil Eng. 1997;5(1):51-61.

135. Malmstrom JA, McNaughton TG, Horch KW. Recording properties and biocompatibility of chronically implanted polymer-based intrafascicular electrodes. Ann Biomed Eng. 1998;26(6):1055-1064.

136. Lawrence SM, Larsen JO, Horch KW, Riso R, Sinkjaer T. Long-term biocompatibility of implanted polymer-based intrafascicular electrodes. J Biomed Mater Res. 2002;63(5):501-506.

137. Zheng X, Zhang J, Chen T, Chen Z. Recording and stimulating properties of chronically implanted longitudinal intrafascicular electrodes in peripheral fascicles in an animal model. Microsurgery. 2008;28(3):203-209.

138. Edell DJ, Churchill JN, Gourley IM. Biocompatibility of a silicon based peripheral nerve electrode. Biomater Med Devices Artif Organs. 1982;10(2):103-122.

139. Kovacs GT, Storment CW, Halks-Miller M, Belczynski CR, Jr., Della Santina CC, Lewis ER, et al. Silicon-substrate microelectrode arrays for parallel recording of neural activity in peripheral and cranial nerves. IEEE Trans Biomed Eng. 1994;41(6):567-577.

140. Navarro X, Calvet S, Rodriguez FJ, Stieglitz T, Blau C, Buti M, et al. Stimulation and recording from regenerated peripheral nerves through polyimide sieve electrodes. J Peripher Nerv Syst. 1998;3(2):91-101.

141. Klinge PM, Vafa MA, Brinker T, Brandis A, Walter GF, Stieglitz T, et al. Immunohistochemical characterization of axonal sprouting and reactive tissue changes after long-term implantation of a polyimide sieve electrode to the transected adult rat sciatic nerve. Biomaterials. 2001;22(17):2333-2343.

142. Ramachandran A, Schuettler M, Lago N, Doerge T, Koch KP, Navarro X, et al. Design, in vitro and in vivo assessment of a multi-channel sieve electrode with integrated multiplexer. J Neural Eng. 2006;3(2):114-124.

143. Lago N, Udina E, Ramachandran A, Navarro X. Neurobiological assessment of regenerative electrodes for bidirectional interfacing injured peripheral nerves. IEEE Trans Biomed Eng. 2007;54(6 Pt 1):1129-1137.

144. Castro J, Negredo P, Avendano C. Fiber composition of the rat sciatic nerve and its modification during regeneration through a sieve electrode. Brain Res. 2008;1190:65-77.

145. Panetsos F, Avendano C, Negredo P, Castro J, Bonacasa V. Neural prostheses: electrophysiological and histological evaluation of central nervous system alterations due to long-term implants of sieve electrodes to peripheral nerves in cats. IEEE Trans Neural Syst Rehabil Eng. 2008;16(3):223-232.

146. Branner A, Normann RA. A multielectrode array for intrafascicular recording and stimulation in sciatic nerve of cats. Brain Res Bull. 2000;51(4):293-306.

147. Branner A, Stein RB, Fernandez E, Aoyagi Y, Normann RA. Long-term stimulation and recording with a penetrating microelectrode array in cat sciatic nerve. IEEE Trans Biomed Eng. 2004;51(1):146-157.

148. Garde K, Keefer E, Botterman B, Galvan P, Romero MI. Early interfaced neural activity from chronic amputated nerves. Front Neuroengineering. 2009;2:5.

149. Rousche PJ, Normann RA. Chronic recording capability of the Utah Intracortical Electrode Array in cat sensory cortex. J Neurosci Methods. 1998;82(1):1-15.

150. Schmidt S, Horch K, Normann R. Biocompatibility of silicon-based electrode arrays implanted in feline cortical tissue. J Biomed Mater Res. 1993;27(11):1393-1399.

151. Rousche PJ, Normann RA. A method for pneumatically inserting an array of penetrating electrodes into cortical tissue. Ann Biomed Eng. 1992;20(4):413-422.

152. Normann RA, Maynard EM, Rousche PJ, Warren DJ. A neural interface for a cortical vision prosthesis. Vision Res. 1999;39(15):2577-2587.

153. Maynard EM, Fernandez E, Normann RA. A technique to prevent dural adhesions to chronically implanted microelectrode arrays. J Neurosci Methods. 2000;97(2):93-101.

154. Campbell PK, Normann RA, Horch KW, Stensaas SS. A chronic intracortical electrode array: preliminary results. J Biomed Mater Res. 1989;23(A2 Suppl):245-259.

155. Middlebrooks JC, Bierer JA, Snyder RL. Cochlear implants: the view from the brain. Curr Opin Neurobiol. 2005;15(4):488-493.

156. Benabid AL, Chabardes S, Mitrofanis J, Pollak P. Deep brain stimulation of the subthalamic nucleus for the treatment of Parkinson's disease. Lancet Neurol. 2009;8(1):67-81.

157. Benabid AL. Deep brain stimulation for Parkinson's disease. Curr Opin Neurobiol. 2003;13(6):696-706.

158. Agnew WF, McCreery DB. Considerations for safety with chronically implanted nerve electrodes. Epilepsia. 1990;31 Suppl 2:S27-32.

159. Biran R, Martin DC, Tresco PA. Neuronal cell loss accompanies the brain tissue response to chronically implanted silicon microelectrode arrays. Exp Neurol. 2005;195(1):115-126.

160. Bouldin TW, Earnhardt TS, Goines ND. Restoration of blood-nerve barrier in neuropathy is associated with axonal regeneration and remyelination. J Neuropathol Exp Neurol. 1991;50(6):719-728.

161. Gray M, Palispis W, Popovich PG, van Rooijen N, Gupta R. Macrophage depletion alters the blood-nerve barrier without affecting Schwann cell function after neural injury. J Neurosci Res. 2007;85(4):766-777.

162. Del Bigio MR. Biological reactions to cerebrospinal fluid shunt devices: a review of the cellular pathology. Neurosurgery. 1998;42(2):319-325; discussion 325-316.

163. Chou KL, Forman MS, Trojanowski JQ, Hurtig HI, Baltuch GH. Subthalamic nucleus deep brain stimulation in a patient with levodopa-responsive multiple system atrophy. Case report. J Neurosurg. 2004;100(3):553-556.

164. Nielsen MS, Bjarkam CR, Sorensen JC, Bojsen-Moller M, Sunde NA, Ostergaard K. Chronic subthalamic high-frequency deep brain stimulation in Parkinson's disease--a histopathological study. Eur J Neurol. 2007;14(2):132-138.

165. Pilitsis JG, Chu Y, Kordower J, Bergen DC, Cochran EJ, Bakay RA. Postmortem study of deep brain stimulation of the anterior thalamus: case report. Neurosurgery. 2008;62(2):E530-532; discussion E532.

166. Szarowski DH, Andersen MD, Retterer S, Spence AJ, Isaacson M, Craighead HG, et al. Brain responses to micro-machined silicon devices. Brain Res. 2003;983(1-2):23-35.

167. Leung BK, Biran R, Underwood CJ, Tresco PA. Characterization of microglial attachment and cytokine release on biomaterials of differing surface chemistry. Biomaterials. 2008;29(23):3289-3297.

168. Winslow BD, Tresco PA. Quantitative analysis of the tissue response to chronically implanted microwire electrodes in rat cortex. Biomaterials. 2010;31(7):1558-1567.

169. Greenman MJ. Studies on the regeneration of the peroneal nerve of the albina rat: number and sectional areas of fibers: area relation to axis of sheath. J Comp Neurol. 1913;23:479-513.

170. Biran R, Martin DC, Tresco PA. The brain tissue response to implanted silicon microelectrode arrays is increased when the device is tethered to the skull. J Biomed Mater Res A. 2007;82(1):169-178.

171. Spataro L, Dilgen J, Retterer S, Spence AJ, Isaacson M, Turner JN, et al. Dexamethasone treatment reduces astroglia responses to inserted neuroprosthetic devices in rat neocortex. Exp Neurol. 2005;194(2):289-300.

172. Zhong Y, Bellamkonda RV. Dexamethasone-coated neural probes elicit attenuated inflammatory response and neuronal loss compared to uncoated neural probes. Brain Res. 2007;1148:15-27.

173. Collias JC, Manuelidis EE. Histopathological changes produced by implanted electrodes in cat brains: comparison with histopathological changes in human and experimental puncture wounds. J Neurosurg. 1957;14(3):302-328.

174. Akers JM, Peckham PH, Keith MW, Merritt K. Tissue response to chronically stimulated implanted epimysial and intramuscular electrodes. IEEE Trans Rehabil Eng. 1997;5(2):207-220.

175. Cameron T, Liinamaa TL, Loeb GE, Richmond FJ. Long-term biocompatibility of a miniature stimulator implanted in feline hind limb muscles. IEEE Trans Biomed Eng. 1998;45(8):1024-1035.

176. Romero E, Cuisenaire O, Denef JF, Delbeke J, Macq B, Veraart C. Automatic morphometry of nerve histological sections. J Neurosci Methods. 2000;97(2):111-122.

177. Gillespie MJ, Stein RB. The relationship between axon diameter, myelin thickness and conduction velocity during atrophy of mammalian peripheral nerves. Brain Res. 1983;259(1):41-56.

178. Strain RE, Olson WH. Selective damage of large diameter peripheral nerve fibers by compression: an application of Laplace's law. Exp Neurol. 1975;47(1):68-80.

179. Korthals JK, Korthals MA, Wisniewski HM. Progression of regeneration after nerve infarction. Brain Res. 1991;552(1):41-46.

180. Gutmann E, Sanders FK. Recovery of fibre numbers and diameters in the regeneration of peripheral nerves. J Physiol (Lond). 1943;101:489-518.

181. Mazzer PY, Barbieri CH, Mazzer N, Fazan VP. Morphologic and morphometric evaluation of experimental acute crush injuries of the sciatic nerve of rats. J Neurosci Methods. 2008;173(2):249-258.

182. Krarup C, Loeb GE, Pezeshkpour GH. Conduction studies in peripheral cat nerve using implanted electrodes: II. The effects of prolonged constriction on regeneration of crushed nerve fibers. Muscle Nerve. 1988;11(9):933-944.

183. Ruohonen S, Jagodi M, Khademi M, Taskinen HS, Ojala P, Olsson T, et al. Contralateral non-operated nerve to transected rat sciatic nerve shows increased expression of IL-1beta, TGF-beta1, TNF-alpha, and IL-10. J Neuroimmunol. 2002;132(1-2):11-17.

184. Vince V, Thil MA, Veraart C, Colin IM, Delbeke J. Biocompatibility of platinum-metallized silicone rubber: in vivo and in vitro evaluation. J Biomater Sci Polym Ed. 2004;15(2):173-188.

185. Hoffer JA, Loeb GE, Pratt CA. Single unit conduction velocities from averaged nerve cuff electrode records in freely moving cats. J Neurosci Methods. 1981;4(3):211-225.

186. Koltzenburg M, Wall PD, McMahon SB. Does the right side know what the left is doing? Trends Neurosci. 1999;22(3):122-127.

187. Tamaki K. The effect of unilateral section of the peroneal nerve of the albino rat on the number of myelinated fibres in the intact nerve of the opposite side. Anat Rec. 1933;181(3):267-286.

188. Muglia U, Vita G, Laura R, Mammola CL, Germana G. Morphometric comparison between contralateral sciatic nerves in the male and female rabbit. Anat Histol Embryol. 1997;26(2):147-150.

189. Adhami H, Sawatzky KH, Hornung J. Morphometric studies on the relationship between myelin sheath and axon area in the sciatic nerve of adult rats. Anat Anz. 1976;140(1-2):52-61.

190. Le Beau JM, Ellisman MH, Powell HC. Ultrastructural and morphometric analysis of long-term peripheral nerve regeneration through silicone tubes. J Neurocytol. 1988;17(2):161-172.

191. Koller R, Girsch W, Liegl C, Gruber H, Holle J, Losert U, et al. Long-term results of nervous tissue alterations caused by epineurial electrode application: an experimental study in rat sciatic nerve. Pacing Clin Electrophysiol. 1992;15(1):108-115.

192. De Angelis C, Scarfo C, Falcinelli M, Perna E, Reda E, Ramacci MT, et al. Acetyl-L-carnitine prevents age-dependent structural alterations in rat peripheral nerves and promotes regeneration following sciatic nerve injury in young and senescent rats. Exp Neurol. 1994;128(1):103-114.

193. Di Benedetto G, Zura G, Mazzucchelli R, Santinelli A, Scarpelli M, Bertani A. Nerve regeneration through a combined autologous conduit (vein plus acellular muscle grafts). Biomaterials. 1998;19(1-3):173-181.

194. Prodanov D, Feirabend HK. Morphometric analysis of the fiber populations of the rat sciatic nerve, its spinal roots, and its major branches. J Comp Neurol. 2007;503(1):85-100.

195. Seymour JP, Kipke DR. Neural probe design for reduced tissue encapsulation in CNS. Biomaterials. 2007;28(25):3594-3607.

196. Dyck PJ, Karnes J, Sparks M, Low PA. The morphometric composition of myelinated fibres by nerve, level and species related to nerve microenvironment and ischaemia. Electroencephalogr Clin Neurophysiol Suppl. 1982;36:39-55.

197. Tan U, Kutlu N. The distribution of paw preference in right-, left-, and mixed pawed male and female cats: the role of a female right-shift factor in handedness. Int J Neurosci. 1991;59(4):219-229.

198. Yuen TG, Agnew WF, Bullara LA. Histopathological evaluation of dog sacral nerve after chronic electrical stimulation for micturition. Neurosurgery. 1984;14(4):449-455.

199. Klinge U, Klosterhalfen B, Muller M, Schumpelick V. Foreign body reaction to meshes used for the repair of abdominal wall hernias. Eur J Surg. 1999;165(7):665-673.

200. Bellon JM, Bujan J, Contreras L, Hernando A. Integration of biomaterials implanted into abdominal wall: process of scar formation and macrophage response. Biomaterials. 1995;16(5):381-387.

201. Rosch R, Junge K, Schachtrupp A, Klinge U, Klosterhalfen B, Schumpelick V. Mesh implants in hernia repair. Inflammatory cell response in a rat model. Eur Surg Res. 2003;35(3):161-166.

202. Kiefer R, Kieseier BC, Stoll G, Hartung HP. The role of macrophages in immune-mediated damage to the peripheral nervous system. Prog Neurobiol. 2001;64(2):109-127.

203. Winslow BD, Christensen MB, Yang WK, Solzbacher F, Tresco PA. A comparison of the tissue response to chronically implanted Parylene-C-coated and uncoated planar silicon microelectrode arrays in rat cortex. Biomaterials. 2010;31(35):9163-9172.

204. Monje ML, Toda H, Palmer TD. Inflammatory blockade restores adult hippocampal neurogenesis. Science. 2003;302(5651):1760-1765.

205. Winslow BD, Merriam ME, Perlin GE, Wise KD, Tresco PA. Chronic microelectrode implantation is accompanied by decreased neurogenesis in the dentate gyrus. 39th Annual Meeting, Society for Neuroscience; 2009 October 17-21; Chicago, Illinois; 2009.

206. Wolchok JC, Tresco PA. The isolation of cell derived extracellular matrix constructs using sacrificial open-cell foams. Biomaterials. 2010;31(36):9595-9603.